DOE/NASA/0106-1
NASA CR-165,170
GARRETT 31-3653

NASA-CR-165170
19810012429

ANALYTICAL DESIGN OF AN ADVANCED RADIAL TURBINE

Gerold D. Large, David G. Finger, and Charles G. Linder
Garrett Turbine Engine Company
A Division of the Garrett Corporation

February 1981

Prepared for
NATIONAL AERONAUTICS AND SPACE ADMINISTRATION
Lewis Research Center
Under Contract DEN3-106

for
U.S. DEPARTMENT OF ENERGY,
CONSERVATION AND SOLAR ENERGY
Office of Transportation Programs

NOTICE

Errata
7-6-81

ERRATA

NASA Contractor Report 165170
DOE/NASA/0106-1
GARRETT 31-3653

ANALYTICAL DESIGN OF AN ADVANCED RADIAL TURBINE

Gerold D. Large, David G. Finger, and Charles G. Linder
February 1981

The Contractor Report number on the cover should be 165170 instead of 16570.

DOE/NASA/0106-1
NASA CR-165170
Garrett 31-3653

ANALYTICAL DESIGN OF AN ADVANCED RADIAL TURBINE

G.D. Large, D.G. Finger and C.G. Linder
Garrett Turbine Engine Company
A Division of the Garrett Corporation

February 1981

Prepared for
National Aeronautics and Space Administration
Lewis Research Center
Cleveland Ohio 44135
Under Contract DEN3-106

for
U.S. DEPARTMENT OF ENERGY, CONSERVATION AND SOLAR ENERGY
Office of Transportation Programs
Division of Automotive Technology Development
Washington, D.C. 20545
Under Interagency Agreement DEAI 01-77CS51040

This Page Intentionally Left Blank

TABLE OF CONTENTS

		Page
1.0	SUMMARY	1
1.1	Identification of Program	1
1.2	Objective	1
1.3	Summary of Major Results	1
2.0	INTRODUCTION	3
2.1	Background	3
2.2	Related Work	3
2.3	Scope/Purpose	10
3.0	DISCUSSION OF RESULTS	11
3.1	Single-Shaft Engine Cycle Selection	11
3.2	Configuration Definition	11
3.3	Optimization Study Parameter Range	11
3.4	Aerodynamic Performance Correlations for Parametric Study	15
3.5	Projected 1983-1985 Performance Improvements	31
3.6	Preliminary Stator and Rotor Geometry	32
3.7	Parametric Study Results	33
3.8	Stator and Rotor Solidity Studies	55
3.9	Parametric Study for Two-Dimensional Mechanical Analysis	60
3.10	Parametric Study of Detail Aerodynamic Analysis	77
4.0	DETAIL ROTOR AERODYNAMIC AND MECHANICAL DESIGN	86
4.1	Aerodynamic Detail Design	86
4.2	Detailed Mechanical Design	91
5.0	OFF-DESIGN PERFORMANCE EVALUATION	110
6.0	CONCLUSIONS	114

ATTACHMENTS:

Appendix A.	Abbreviations and Symbols	117
Appendix B.	Deswirl Vane Loss Model	123
Appendix C.	Rotor Flow Path and Blade Geometry for β_B = 0, 10, and 20°	131
REFERENCES		145

TABLE OF CONTENTS (Contd)

TABLES:

		Page
I.	Ceramic Radial Inflow Turbine Reference Cycle Requirements	12
II.	Parameter Range for Optimization Study	14
III.	Performance and Nondimensional Geometry for Selected Diffuser Configuration	23
IV.	Selected Configurations for Detail Aerodynamic and Mechanical Design	87
V.	Optimum Configuration Derived from Parametric Study and 3-D Mechanical Analysis	95
VI.	Stress and Cumulative Probability of Success Summary at 95,000 rpm	108

LIST OF ILLUSTRATIONS:

1.	Optimum Tip Speed as a Function of Stage Work and Blade Number	4
2.	Effect of Rotor Tip Speed on Attainable Turbine Efficiency	6
3.	Illustration of Swirl Effect on Rotor Downstream Ducting (ref. 2)	8
4.	Turbine System Optimization Technique	9
5.	Definition of Radial Turbine System for Parametric Study	13
6.	Specific Speed Correlation for Radial Turbines	16
7.	Reynolds Number Correlation for Radial Turbines	18
8.	Summary of Radial Turbine Rotor Clearance Effects on Total Stage Efficiency	20
9.	Exhaust Diffuser Configuration Used in Parametric Study	22
10.	Diffuser Duct Loss Data	24

TABLE OF CONTENTS (Contd)

LIST OF ILLUSTRATIONS (Contd):

		Page
11.	Deswirl Vane Loss Characteristics (ref. 3) Using Arbitrary Air-Foil Shapes	25
12.	Representative Rotor Exit Efficiency Characteristics for Radial Turbines	28
13.	Preliminary Correlation for Radial Turbine Reaction	30
14.	Turbine System Parametric Study, N = 80,000 rpm, $\beta_B = 0°$	35
15.	Turbine System Parametric Study, N = 80,000 rpm, $\beta_B = 10°$	36
16.	Turbine System Parametric Study, N = 80,000 rpm $\beta_B = 20°$	37
17.	Turbine System Parametric Study, N = 95,000 rpm, $\beta_B = 0°$	38
18.	Turbine System Parametric Study, N = 95,000 rpm, $\beta_B = 10°$	39
19.	Turbine System Parametric Study, N = 95,000 rpm, $\beta_B = 20°$	40
20.	Turbine System Parametric Study, N = 110,000 rpm, $\beta_B = 0°$	41
21.	Turbine System Parametric Study, N = 110,000 rpm, $\beta_B = 10°$	42
22.	Turbine System Parametric Study, N = 110,000 rpm, $\beta_B = 20°$	43
23.	Effects of Rotor Exit Area and Radius Ratio on Turbine System Efficiency, N = 95,000 rpm, $\beta_B = 0°$	45
24.	Turbine Vector Diagram and System Parameters Along Individual Tip Speed Envelopes, N = 80,000 rpm, $\beta_B = 0°$	46
25.	Turbine Vector Diagram and System Parameters Along Individual Tip Speed Envelopes, N = 80,000 rpm, $\beta_B = 0°$ (Contd)	47

LIST OF ILLUSTRATIONS (Contd):

		Page
26.	Peak System Efficiency for N = 80,000 rpm	49
27.	Peak System Efficiency for N = 95,000 rpm	50
28.	Peak System Efficiency for N = 110,000 rpm	51
29.	Peak System Efficiency for N = 95,000 rpm with Deswirl Vanes	52
30.	Tip Speed Envelope with Reaction and Deswirl Vane Effects	53
31.	Characteristic Rotor Flow Path Configurations for Selected Parametric Study Rotational Speeds	54
32.	Stator Solidity Study, N = 95,000 rpm, $\beta_B = 0°$	56
33.	Rotor Solidity Study, Axial Length = 4.8 cm (1.9 in.)	57
34.	Rotor Solidity Study, Axial Length = 4.3 cm (1.7 in.)	58
35.	Rotor Solidity Study, Axial Length = 3.8 cm (1.5 in.)	59
36.	Typical Two-Dimensional Finite Element Model	62
37.	Tangential Thickness and Maximum Principal Stresses	63
38.	Campbell Diagram for 80,000-rpm Design	64
39.	Normalized Deflections (Modes 1 and 2)	65
40.	Normalized Deflections (Modes 3 and 4)	66
41.	Tangential Thicknesses and Maximum Principal Stresses	67
42.	Campbell Diagram for 95,000-rpm Case With 58.1 cm^2 (9.0 $in.^2$) Exit Area	68
43.	Tangential Thicknesses and Maximum Principal Stresses	69
44.	Campbell Diagram for 95,000-rpm Case with 45.2 cm^2 (7 $in.^2$) Exit Area	70

LIST OF ILLUSTRATIONS (Contd)

		Page
45.	Normalized Deflections (Modes 1 and 2)	71
46.	Normalized Deflections (Modes 3 and 4)	72
47.	Tangential Thicknesses and Maximum Principal Stresses	73
48.	Campbell Diagram for 110,000-rpm Case	74
49.	Effect of Speed on Maximum Principal Disk Stress	75
50.	Maximum Disk Stress Versus Number of Blades	76
51.	Tangential Thicknesses and Maximum Principal Stresses	78
52.	Tangential Thicknesses and Maximum Principal Stresses	79
53.	Maximum Disk Stress Versus Tip Speed, A_E = 45.2 cm^2 (7 $in.^2$), N = 95,000 rpm, N_B = 12	80
54.	Effect of Rotor Exit Hub Blockage on Rotor Loss	81
55.	Effect of Rotor Exit Hub Blockage and Blade Number on System Efficiency	82
56.	Effects of Reaction, Rotor Exit Area, and Blockage on System Efficiency	83
57.	Effect of Reaction, Blockage, and Exit Annular Area on Tip Speed Characteristics	85
58.	Final Rotor Flow Path Configurations	89
59.	Rotor Blade Angle Distribution Versus Percent Meridional Distance	90
60.	Velocity Distributions	92
61.	Typical Three-Dimensional Finite Element Model	94
62.	Maximum Principal Stresses	96
63.	Maximum Principal Stresses	98

LIST OF ILLUSTRATIONS: (Contd)

		Page
64.	Blade Shape, Original Thickness (Rake = 0)	99
65.	Blade Shape, Original Thickness (Rake = -30)	100
66.	Maximum Principal Stresses, Original Thickness	101
67.	Blade Shape, Modified Thickness	102
68.	Maximum Principal Stresses, Modified Thickness (1)	103
69.	Maximum Principal Stresses, Modified Thickness (2)	104
70.	Maximum Principal Stresses, Modified Thickness (3)	105
71.	Maximum Principal Stresses, Original Thickness	106
72.	Maximum Principal Stresses, Modified Thickness (3)	107
73.	Maximum Power Design-Point Selection for Off-Design Performance Evaluation	111
74.	Off-Design Performance Characteristics as a Function of Design-Point Exit Swirl (from NASA-DOE Advanced Gas Turbine Power-Train System Development Program)	112
75.	Equivalent Conical Angle Correlation of Diffusing Cascade Data (ref. 3)	126
76.	Deswirl Equivalent Area Ratio for Maximum Diffusion Efficiency (ref. 3)	128

1.0 SUMMARY

1.1 Identification of Program

This is the final report for the Analytical Design of an Advanced Radial Turbine study program under NASA Contract DEN3-106, to define an optimum ceramic radial inflow, single-stage turbine system, for an advanced automotive gas turbine engine. The turbine study program is based on an advanced gas turbine cycle, 100.67-kW (135-shp) engine for use in a 1588-kg (3500-lb) automobile, with a specific fuel consumption of 0.227 kg/kW-hr (0.373 lb/hp-hr).

Utilization of high turbine cycle temperatures of 1370°C (2500°F) and ceramic materials are prime features of this study.

1.2 Objective

The program objective is to investigate the effects of tip speed, non-radial rotor blading, inducer-to-exducer work split, and deswirl vanes on the system efficiency and mechanical reliability of a single-stage, ceramic, radial turbine designed to meet the performance requirements of an advanced automotive gas turbine cycle.

1.3 Summary of Major Results

Analysis results indicate that, based on projected 1983 aerodynamic performance and ceramic material properties, radial blade rotor configurations with a tip speed of 701 m/sec (2300 fps) are feasible and satisfy the goals of 87.0-percent system efficiency and 0.9999 cumulative probability of success mechanically.

Nonradial blade rotor configurations allow rotor inducer tip speed to be reduced for equivalent performance. However, the inherent higher blade stress associated with this type of configuration requires a drastic increase in blade thickness to restore reasonable cumulative probability of success (CPS) values for the ceramic material blade. The required increase in blade material thickness, in turn, results in higher disk loadings and reduced CPS values for the wheel. Therefore, from aerodynamic, mechanical, and off-design considerations, the radial-blade rotor appears to offer the lowest overall risk

and is the optimum configuration considered in this study. This design includes the following:

Shaft speed	95,000 rpm
Inducer tip speed	701 m/sec (2300 fps)
Rotor inlet blade angle	0 degrees
Rotor blade number	12 to 14
Rotor exit swirl	-10 degrees
Rotor exit critical velocity ratio	0.449
Rotor exducer-to-inducer tip radius ratio	0.632

2.0 INTRODUCTION

2.1 Background

The need for more efficient use of available fuel supplies has led to increased interest in gas turbine engines for automotive applications. Both government and industry have conducted studies to determine optimum cycle parameters and mechanical configurations. A high-temperature, regenerated, single-shaft engine has created considerable interest for automotive application due to economy, cost, packageability, and driveability. In a current NASA-DOE contract design study effort for an improved gas turbine engine, a single-stage radial turbine has emerged as the leading candidate compared to a single- or multi-stage axial turbine.

The single-stage radial inflow turbine has attributes particularly suited to this size engine because of ruggedness, lower sensitivity to tip clearance, and higher stage work levels when compared to axial turbines.

For a single-shaft automotive application, a single-stage radial turbine must effectively cope with the basic requirement of high-stage work levels at maximum power and still maintain acceptable performance over the entire automotive duty cycle to achieve significant reductions in fuel consumption. However, by reducing fuel consumption on the order of 30 to 50 percent, the gas turbine will offer a distinct advantage in fuel economy over current spark-ignition engines and provide an automotive engine that is adaptable to a wide range of alternate fuels.

2.2 Related Work

For a single-shaft configuration, studies conducted to date show that work levels from 419 to 512 kJ/kg (180 to 220 Btu/lb) are required at maximum power for the radial turbine. Numerous experimental studies conducted at AiResearch have shown that maximum radial turbine performance correlates well with the centrifugal compressor slip factor developed by Stanitz (ref. 1). That is, peak radial turbine performance occurs at a rotor inlet work coefficient (rotor inlet tangential velocity/rotor inlet tip speed) that is consistent with the slip factor criteria developed by Stanitz. On this basis, a relationship between stage work and inducer tip speed can be derived for maximum radial turbine efficiency.

This relationship is presented in Figure 1 for zero exit swirl and for a range of inducer blade numbers. At the expected maximum power work levels, tip speeds between 671 and 762 m/sec (2200 and 2500 fps) would be required to achieve peak radial

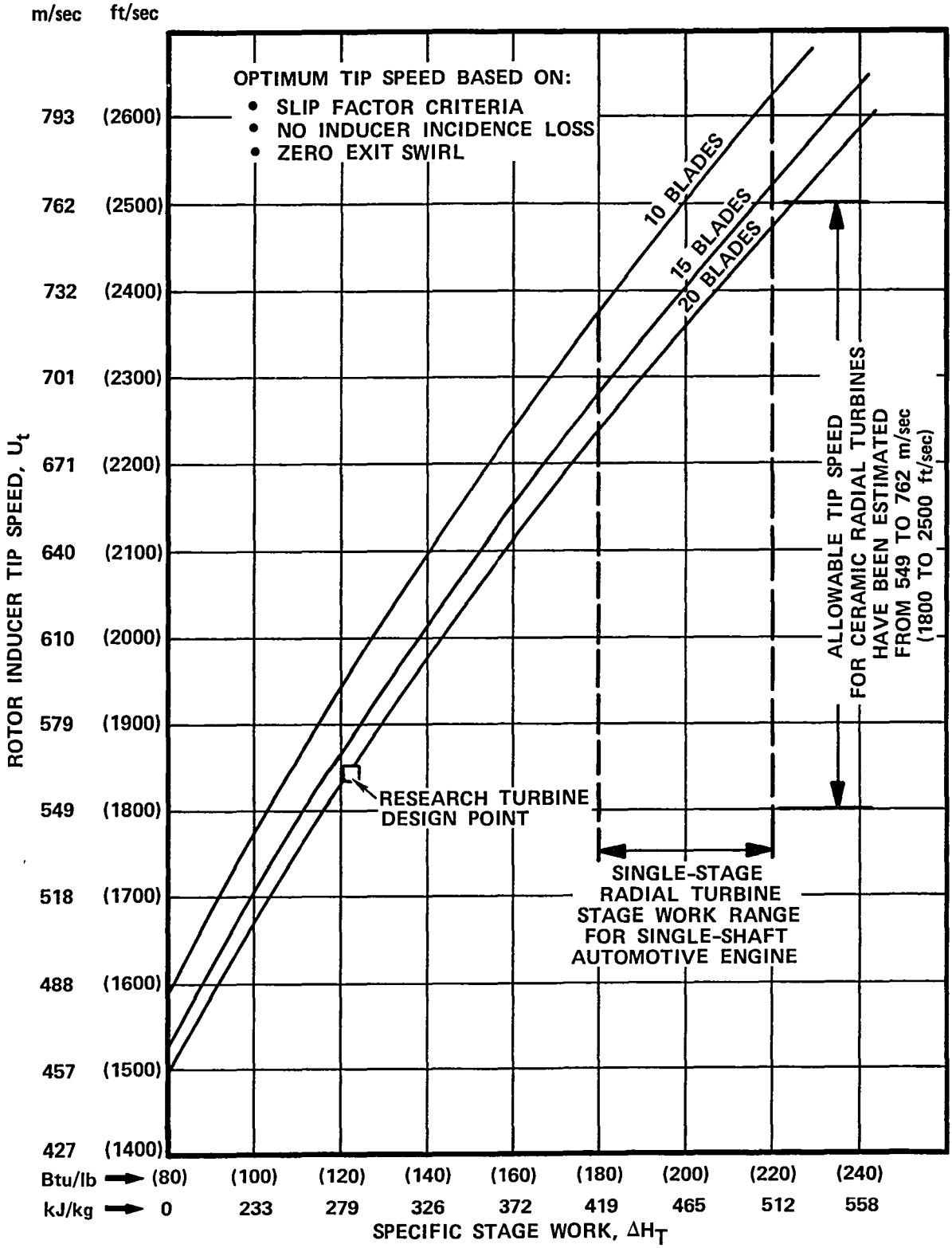

Figure 1. Optimum Tip Speed as a Function of Stage Work and Blade Number.

turbine performance. Cycle studies indicate that high turbine inlet temperatures [1370°C (2500°F)] also will be required to achieve the fuel reduction goals. Ceramic materials have received considerable attention for this application because they eliminate the need for turbine cooling and the critical materials required for metal turbines, as well as having the potential for low cost. However, at the start of the program, the mechanical properties of ceramic materials were in a period of such rapid improvement that an accurate estimate of maximum allowable tip speed of a radial turbine was not possible.

If tip speeds from 549 to 610 m/sec (1800 to 2000 fps) were required to satisfy the material properties, severe tip speed limitations would exist relative to the optimum tip speed required to achieve maximum performance (Figure 1). The impact of tip speed limitations on radial turbine performance is illustrated in Figure 2. Results from a research turbine test program (designed with optimum tip speed) indicate that peak efficiency was achieved at the design point. However, increasing or decreasing tip speed from the design point results in a severe performance penalty.

The radial turbine performance characteristics, shown in Figure 2, raise a number of questions:

- What are the physical phenomena that cause the rapid decrease in performance at higher or lower than optimum rotor inducer tip speeds?
- Once the physical phenomena are established, what design technique would tend to minimize the effect and reestablish maximum performance at nonoptimum tip speeds?
- What technique would tend to optimize turbine performance not only at maximum power but throughout the entire duty cycle range?

These underlying questions formed the basis for arriving at a radial turbine design technique that would optimize radial turbine performance for the entire duty cycle of a single-shaft automotive gas turbine engine.

First, assume that the effects of lower or higher than optimum tip speed are attributed to rotor inlet incidence loss, and then, that the incidence penalty is directly proportional to the difference in kinetic energy between the optimum inlet work coefficient and that actually implied by the rotor inlet vector diagram. Figure 2 shows that, with these assumptions, the predicted and measured decrement in turbine efficiency are in good agreement (considering that the effect of stator loss and rotor reaction are also present under these conditions). Given this correlation between nonoptimum rotor tip speed and rotor

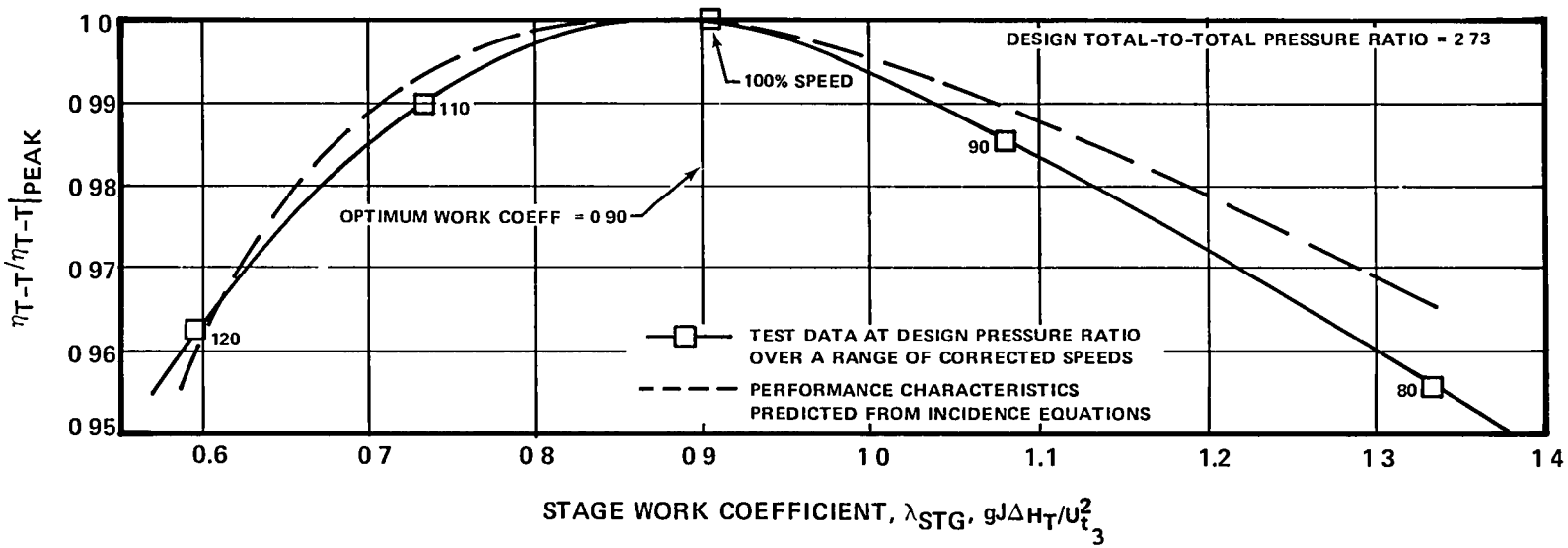

Figure 2. Effect of Rotor Tip Speed on Attainable Turbine Efficiency.

inlet incidence loss, what design technique would minimize these effects? Two approaches appear to be feasible: First, the rotor inducer-to-exducer work split could be adjusted to the point that optimum rotor inlet conditions would be reestablished (i.e., high negative rotor exit swirl). Second, the rotor inlet blade angle could be adjusted to reestablish optimum rotor inlet conditions with a 90-degree radial inlet flow configuration.

Adjusting the inducer-to-exducer work split should be beneficial for all types of rotor blading as long as a limitation on tip speed or blade angle exists. Unfortunately, numerous experimental studies indicate that the turbine downstream ducting is relatively sensitive to rotor exit swirl, and that the magnitude of duct loss is highly dependent on the type of geometry utilized. For example, Figure 3 illustrates the loss characteristics as a function of inlet swirl for an interstage duct and exhaust diffuser. Although Dovzhik's data (ref. 2) are for uniform inlet conditions, rig test results with the actual rotor inlet conditions show the same basic characteristics. Unpublished AiResearch results for radial diffusers indicate that this type of exhaust duct could be the least sensitive to inlet swirl; however, additional analyses and experimental studies are required to further define the design techniques. With the assumption that the turbine exit ducting loss is a function of swirl, the duct loss characteristics must be included in the optimization process for tip speed-limited radial rotor designs. Even if optimum tip speed and zero exit swirl are achieved for a given design point, the wide range of operating conditions experienced by the single-shaft turbine would still result in relatively high rotor exit swirl during the normal duty cycle.

A turbine system optimization technique based on combining the performance characteristics of the turbine stage and exhaust duct is illustrated in Figure 4. At the corrected work level shown, a tip speed of 781 m/sec (2562.0 fps) would be required to achieve optimum rotor inlet conditions and zero exit swirl. However, with an allowable tip speed of 610 m/sec (2000 fps), zero exit swirl would occur at a rotor inlet work coefficient of 1.37. Although the exhaust duct loss would be minimized under these conditions, Figure 4 shows that stage efficiency rapidly decreases as this level of inlet work coefficient is approached. By combining the performance characteristics of the turbine stage and exhaust duct, the rotor inlet incidence effects are minimized, and system efficiency is improved by 4.0 points.

Figure 4 was based on conventional radial element rotor blades. Further improvement in system efficiency is expected with three-dimensional (nonradial) blades. AiResearch has

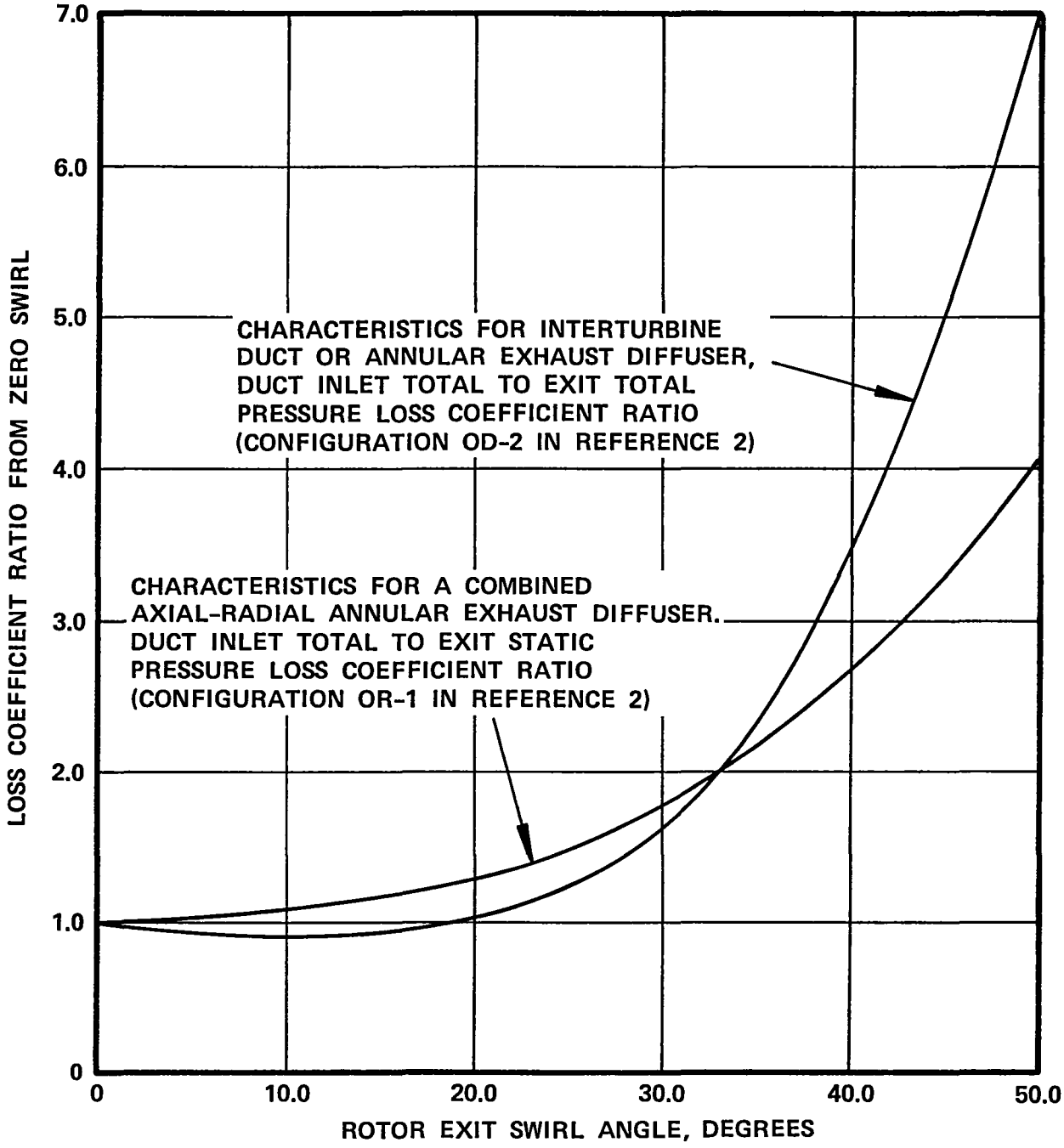

Figure 3. Illustration of Swirl Effect on Rotor Downstream Ducting (ref. 2).

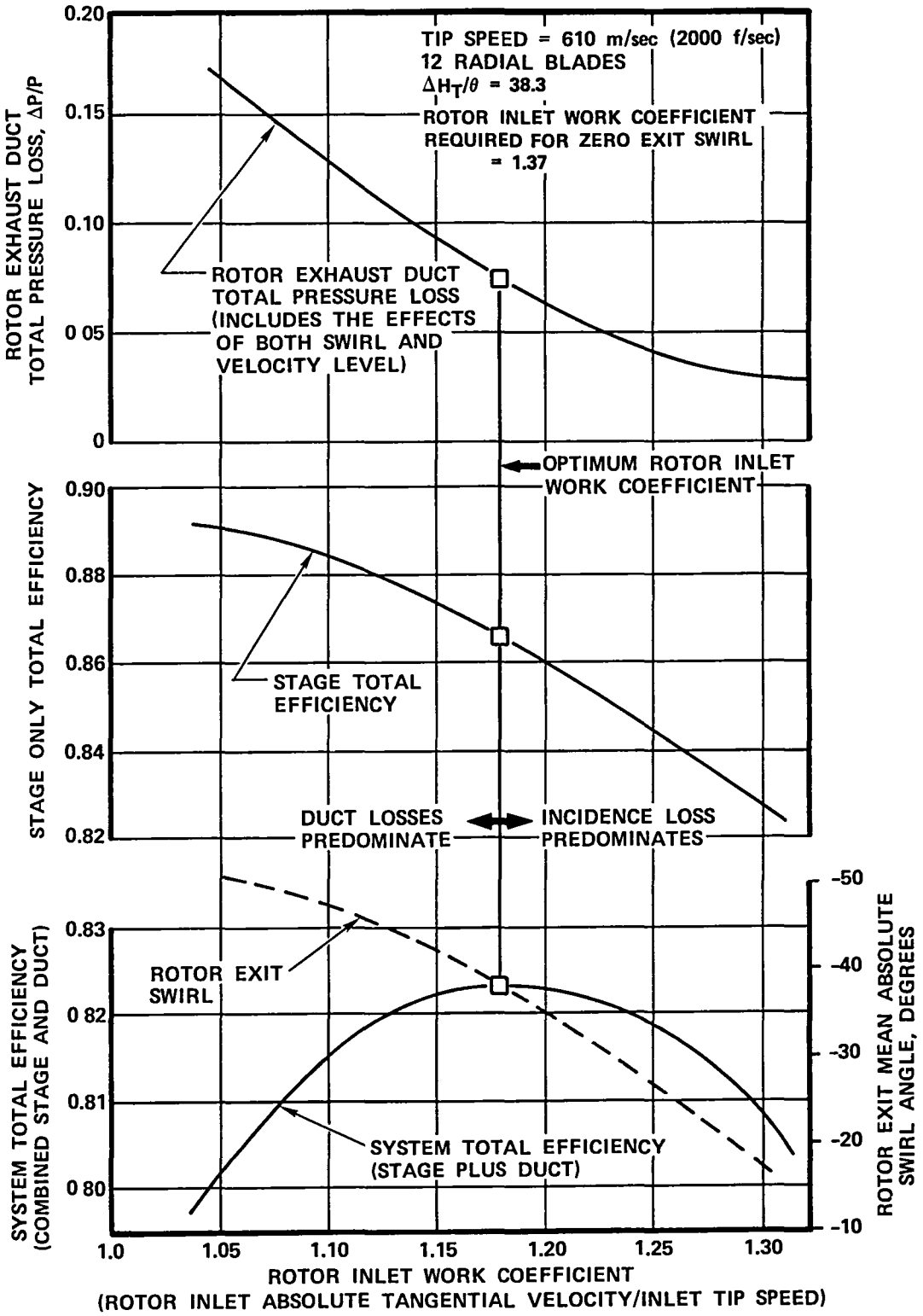

Figure 4. Turbine System Optimization Technique.

investigated the aerodynamic and mechanical feasibility of nonradial rotors, and the results indicate the following:

- With careful control of the rotor blade turning distributed through the rotor, rig test results show that the increase in performance is in good agreement with that predicted from a decrease in inducer incidence loss

- Minimized rotor blade bending stress requires extensive rotor blade thickness optimization and blade restacking. At the present time, 20 degrees of rotor inlet blade angle appears to be the upper limit in terms of rotor mechanical design

The recent study conducted on deswirl vanes by Mitchell and Soileau (ref. 3) indicates that duct losses could be significantly reduced for high exit swirl and Mach number turbine designs. Therefore, deswirl vanes will be included in the system optimization.

2.3 Scope/Purpose

The program objective was to investigate the performance potential of a high-work, ceramic, single-stage, radial turbine with radial and nonradial rotor blading, with and without deswirl vanes, based on a system optimization approach applicable to a single-shaft automotive engine. This was accomplished with a parametric study by examination of the aerodynamic and mechanical effects of the following parameters:

- A range of shaft speeds to evaluate rotor size effects

- A range of inducer tip speeds to determine the effects on efficiency and mechanical integrity

- A range of rotor inlet blade angles to determine the effects on inducer blade loading and the impact on rotor inducer blade stresses

- A range of rotor inducer-to-exducer work splits to determine the effects of rotor exit Mach number and exit swirl on exhaust diffuser losses

- A range of rotor inducer tip-to-exducer tip radius ratios for each value of shaft and tip speed

- An examination of blade number effects

To evaluate turbine performance effects only, all cycle parameters, with the exception of radial turbine efficiency and exhaust duct pressure loss, were held constant for the analysis.

3.0 DISCUSSION OF RESULTS

3.1 Single-Shaft Engine Cycle Selection

The maximum power point cycle selected for the advanced radial turbine is representative of operating conditions projected for a gas turbine automotive engine produced in the mid-1980s for a 1588-kg (3500-lb) automobile.

The engine specific fuel consumption (SFC) is 0.1965 kg/kW-hr (0.323 lb/hp-hr), and the net power is 101 kW (135 hp). The turbine system design requirements and performance goals at this condition are presented in Table I. Station nomenclature used in Table I is defined in Figure 5.

3.2 Configuration Definition

The selected system configuration consists of a turbine inlet scroll, radial stage and downstream axial exhaust diffuser (with and without deswirl vanes). Alternate turbine inlet and exhaust configurations are possible; indeed, further automobile engine analysis may indicate these are required. However, the primary objective of this program is to evaluate the performance potential of a ceramic radial turbine through use of a system optimization procedure that could be used to evaluate modifications that may be required by further automobile engine analysis.

The effect of selecting either a scroll or an annular inlet is expected to be small for the present program since, in either case, the objective is to maintain a relatively low Mach number. Therefore, pressure loss with either type of inlet would be expected on the order of 1/2 to 1 percent. The type of exhaust diffuser configuration selected is more significant due to the difference in the levels of losses expected from an axial or a radial diffuser. Since the type of exhaust diffuser selected for the analysis will limit the generality of the results, both at the selected maximum power design point and off-design conditions, the selection will be based on available diffuser data with actual radial rotor exit conditions imposed. The selected exhaust duct configuration shown schematically in Figure 5 is a conical diffuser and is the type normally used for small auxiliary power units (APUs). Detailed test results are available for this type of diffuser.

3.3 Optimization Study Parameter Range

The design parameters evaluated in the optimization study, and the associated range, are presented in Table II. The lower limit of turbine shaft speed (80,000 rpm) corresponds to the lowest specific speed at which peak efficiency could be maintained, based on available data. The upper limit of shaft speed

TABLE I. CERAMIC RADIAL INFLOW TURBINE REFERENCE CYCLE REQUIREMENTS

Parameters	Units	Requirements
Turbine Operating Life	hr	3500
Turbine Design Reliability		0.9999
Turbine Scroll Inlet Total Temperature	°C (°F)	1370 (2500)
Cycle Pressure Ratio		5:1
Scroll Inlet Total Pressure	kN/m^2 (psia)	478 (69.331)
Rotor Exit Total Pressure	kN/m^2 (psia)	116 (16.8)
Mass Flow, w	kg/sec (lb/sec)	373 (0.823)
Specific Stage Work, $\Delta H_T\|_{1-4}$	kJ/kg (Btu/lb)	509 (218.73)
Stage Total-to-Total Pressure Ratio, $P_{R_{T-T}}\|_{1-4}$		4.087
Stage Inlet Corrected Flow, $w\sqrt{\theta}/\delta\|_1$	kg/sec (lb/sec)	0.191 (0.421)
Stage Corrected Work, $\Delta H_T/\theta\|_{1-4}$	kJ/kg (Btu/lb)	89.162 (38.333)
Stage Total-to-Total Efficiency, $\eta_{T-T}\|_{1-4}$		0.897*
Scroll Total Pressure Loss, $\Delta P/P\|_{0-1}$		0.01*
Exhaust Diffuser Total Pressure Loss, $\Delta P/P\|_{4-6}$ (with or without deswirl vanes		0.04*
System Total-to-Total Efficiency $\eta_{T-T}\|_{0-6}$		0.870**

*Varies in parametric study
**Goal from parametric study

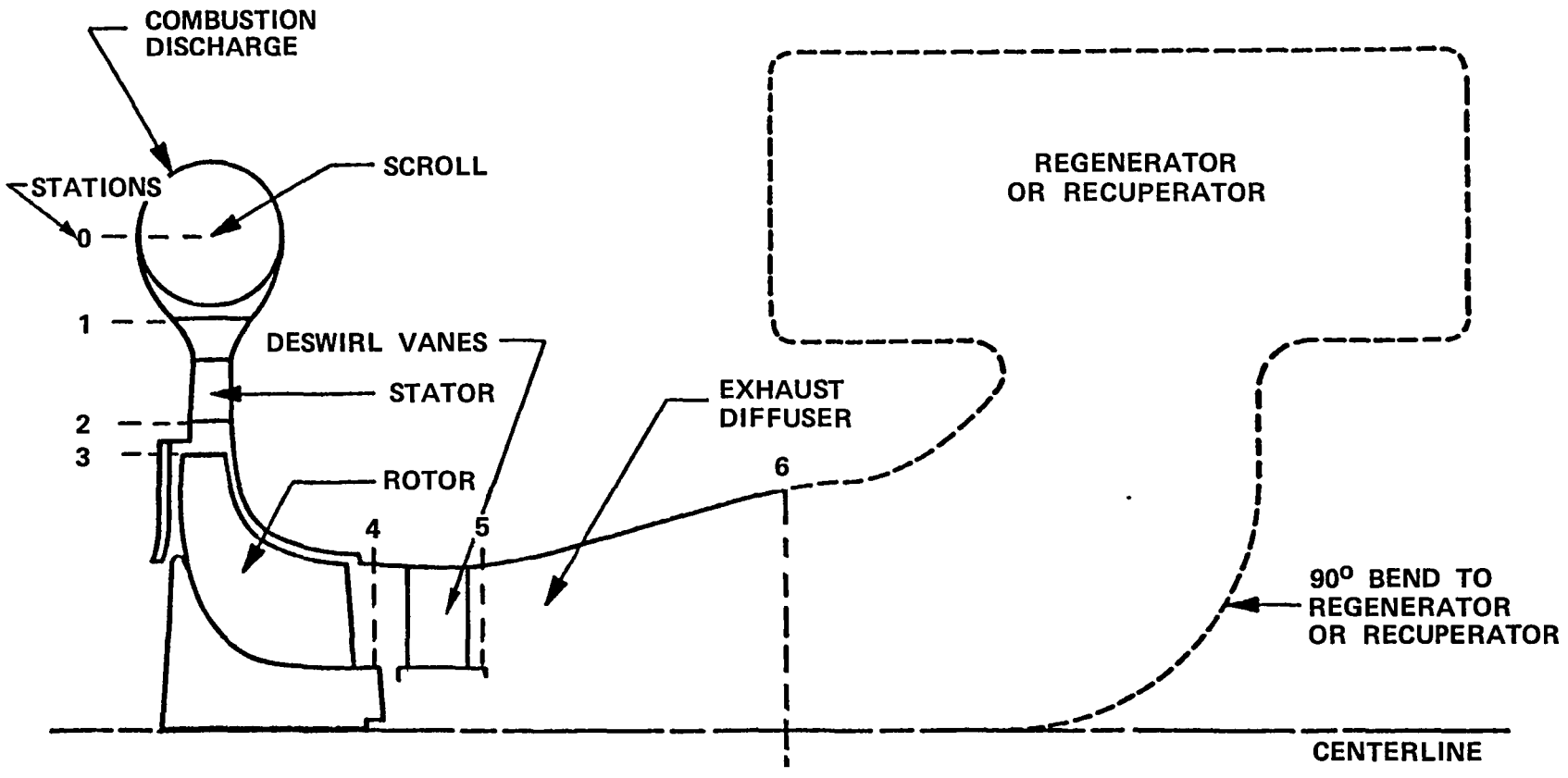

NOTE:
TURBINE SYSTEM PERFORMANCE FOR PARAMETRIC STURY
IS DEFINED FROM SCROLL INLET (COMBUSTION DISCHARGE)
TO EXHAUST DIFFUSER EXIT PLANES.

Figure 5. Definition of Radial Turbine System for Parametric Study.

TABLE II. PARAMETER RANGE FOR OPTIMIZATION STUDY

Parameters	Units	Range
Rotational Speed, N	rpm	80,000 to 110,000
Inducer Tip Speed, U_{t_3}	m/sec (fps)	792 (2600) (optimum with 10 blades)
		753 (2470) (optimum with 20 blades)
		549 (1800) (lower limit)
Inducer Blade Angle, β_B	deg	0 to 20
Rotor Exit Swirl, α	deg	0 to -50*
Rotor Exit Absolute Critical Velocity Ratio, V/A_{cr}		0.30 to 0.60*
Rotor Blade Number, N_B		10 to 16
Rotor Exducer-to-Inducer Radius Ratio, R_{T_4}/R_{T_3}		Minimum based on 50% rotor exit hub blockage, maximum of 0.80
Axial Shroud Clearance (Ca)	cm (in.)	0.0254 (0.010) (constant)
Radial Shroud Clearance (Cr)		0.0254 (0.010) (constant)
Rotor Backface Clearance (Cb)		0.0508 (0.020) (constant)

*Estimated; absolute range will result from the rotor exit work coefficient and annular area imposed.

(110,000 rpm) is based on maintaining acceptable single-stage centrifugal compressor design characteristics. Higher speeds are possible; however, this would involve a compressor performance trade-off (due to the increasing inducer tip Mach number, which is considered beyond the scope of the current program). The range of selected shaft speeds is indicated on the specific speed curve in Figure 6.

3.4 Aerodynamic Performance Correlations for Parametric Study

The initial parametric study was based on a one-dimensional aerodynamic performance evaluation model for the turbine scroll, stage and axial exhaust diffuser system. Correlations for the scroll and exhaust diffuser were incorporated into an existing radial turbine design program to arrive at a system performance for the range of parameters presented in Table II and based on the selected cycle conditions shown in Table I. The correlations and methods utilized for the parametric study are:

- Scroll Loss: The pressure loss in a turbine scroll is primarily a result of turning the flow and wall friction. Rogo (ref. 4) presented a method for predicting the turning loss for a turbine scroll based on a mass averaged dynamic head within the scroll. Eckert (ref. 5) developed a technique for predicting the friction loss for a compressor scroll. A technique for predicting total turbine scroll loss has been derived from the work of Eckert and Rogo in terms of a scroll inlet Mach number, scroll inlet diameter (a) at the tongue, scroll inside radius (r_o), and friction resistance coefficient ($\bar{\lambda}$), as follows:

$$\frac{\Delta P}{P_{TOTAL}} = \frac{q}{P_{INLET}}\left(\frac{a}{r_o c}\right)0.266 + \frac{2\pi\lambda}{a}\left(r_o + \frac{a}{3}\right)$$

where:

$$c = \ln\left(\frac{r_o + a}{r_o}\right)$$

$$\bar{\lambda}_R = \frac{1}{[0.8686 \ln\left(\frac{a}{4}\right) + 1.74]^2} \quad \text{(Rough)}$$

$$\bar{\lambda}_S = \frac{0.316}{\bar{Re}^{1/4}} \quad \text{(Smooth)}$$

and $$\bar{Re} = \frac{D_H V_U}{\nu}$$

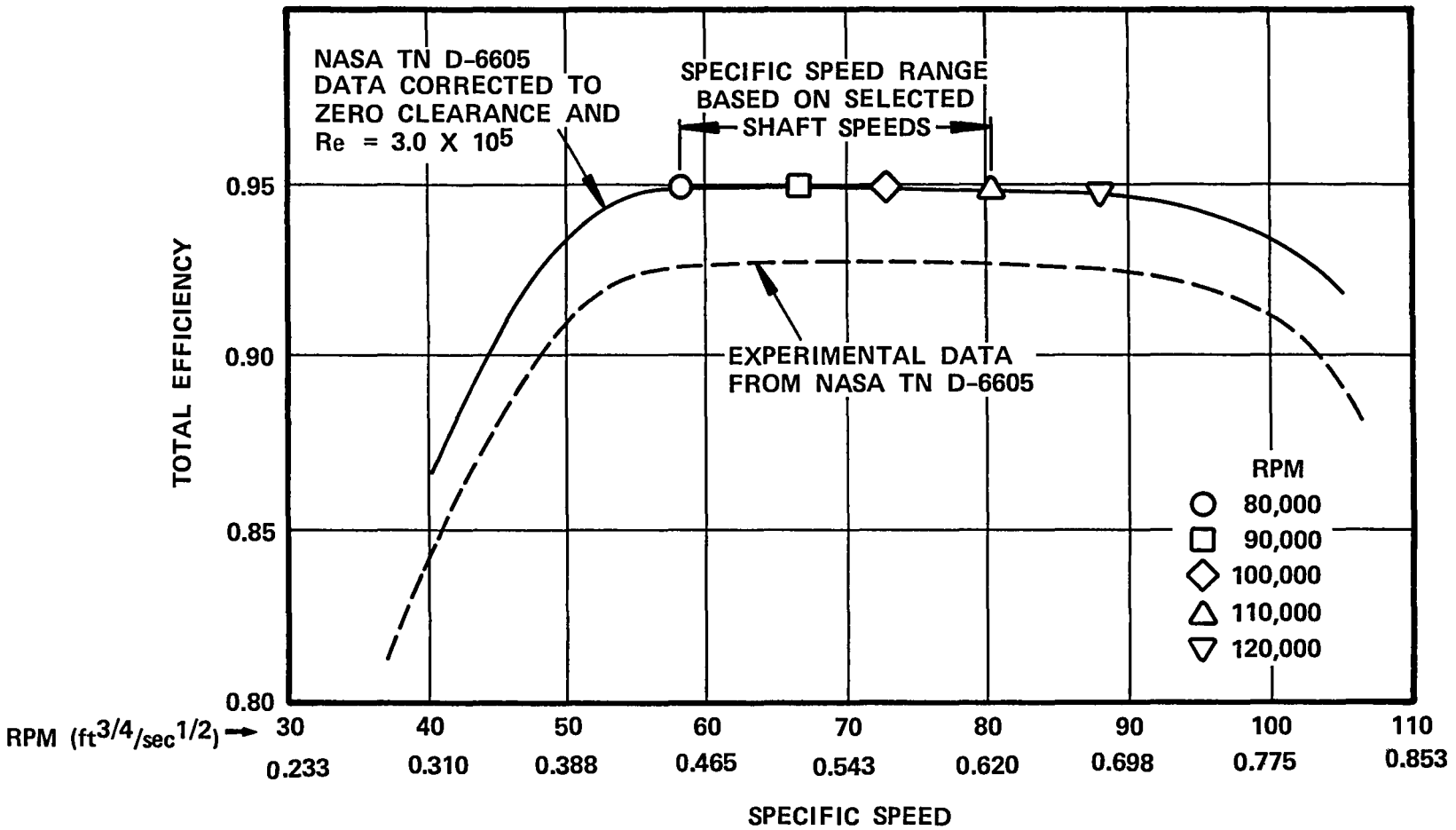

Figure 6. Specific Speed Correlation for Radial Turbines.

The loss predicted from the preceding equation would be the minimum loss that would be expected for a scroll of circular cross section and design, using the continuity and radial equilibrium scroll design equations.

- Maximum attainable (base) efficiency is established from specific speed correlations based on NASA (ref. 6) and AiResearch data. The NASA correlation is presented in Figure 6.

- Base efficiency is then corrected for Reynolds number effects based on results from NASA (ref. 7) and AiResearch data. The correlation is presented in Figure 7.

- Rotor inlet incidence loss is calculated for a specified rotor inlet work coefficient from the following relationships:

  In general,

$$\lambda_{3,i} = \text{S.F.} \frac{\left(U_{t_3} + V_{R_3} \tan \beta_B\right)}{U_{t_3}}$$

  For radial blades,

$$\lambda_{3,i} = \text{S.F.} = 1 - \frac{2}{N_B} \text{ (Stanitz Slip Factor)}$$

$$\lambda_{3,act} = \frac{Vu_3}{U_{t_3}}$$

$$\lambda_{STG} = \lambda_{3,act} - \left(\frac{R_{4M}}{R_{T_3}}\right)^2 \lambda_{4,M} = gJ\left(\Delta H_T\Big|_{0-4} \Big/ U_{t_3}^2\right)$$

$$\eta_i = \frac{1}{1 + \left(\frac{\eta_{base}}{2\lambda_{STG}}\right)\left(\lambda_{3,act} - \lambda_{3,i}\right)^2}$$

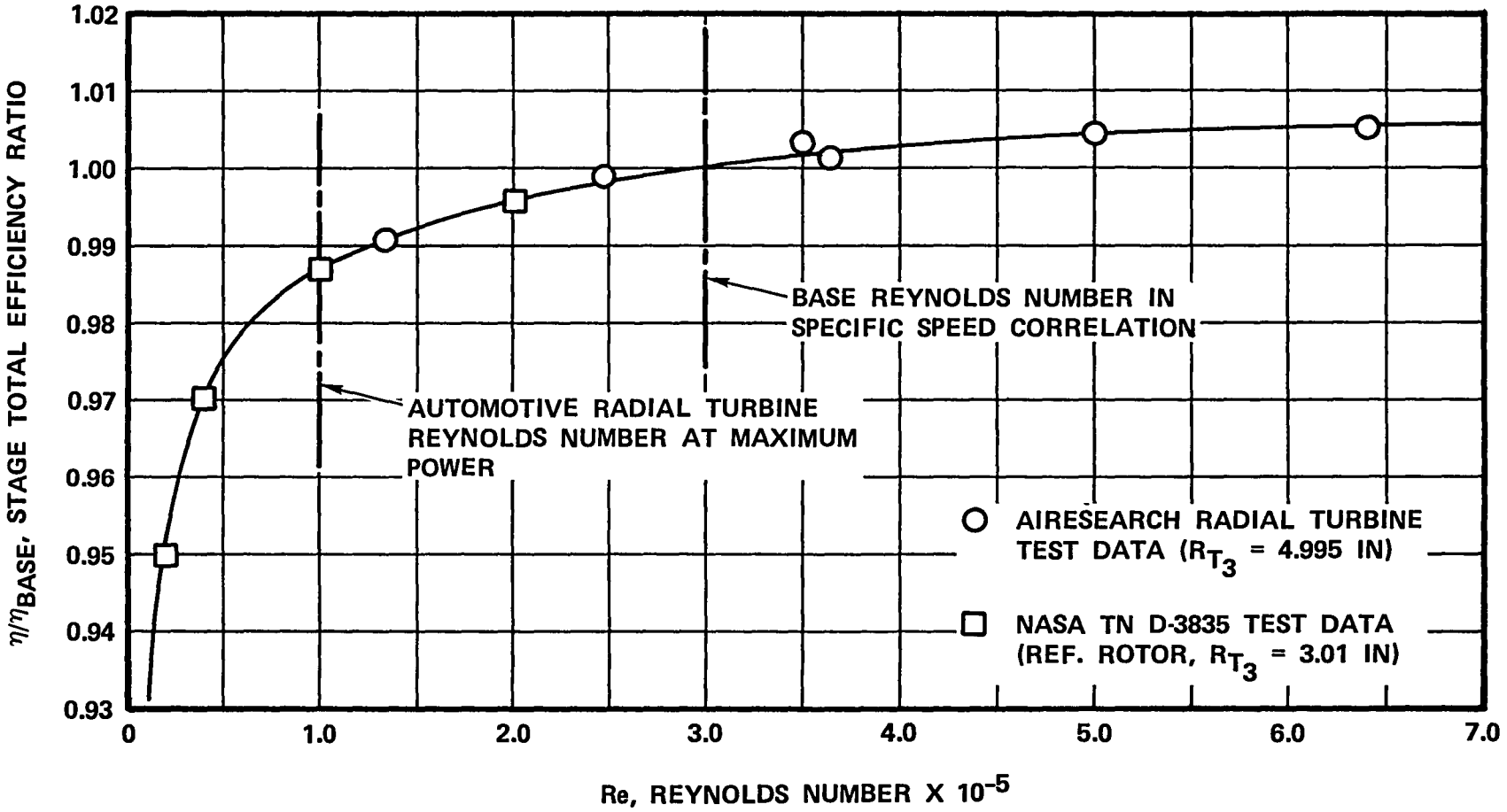

Figure 7. Reynolds Number Correlation for Radial Turbines.

where:

U_{t_3} = Rotor inducer tip speed

V_{R_3} = Rotor inlet absolute radial velocity

Vu_3 = Rotor inlet absolute tangential velocity

R_{T_3} = Rotor inlet tip radius

R_{4M} = Rotor exit mean radius

ΔH_T = Stage total specific work

$\lambda_{3,i}$ = Rotor inlet work coefficient for zero incidence loss

$\lambda_{3,act}$ = Rotor inlet work coefficient from vector diagram for a specific tip speed and inducer-to-exducer work split

λ_{STG} = Stage work coefficient

$\lambda_{4,M}$ = Rotor exit mean work coefficient

η_i = Stage total efficiency with incidence loss

β_{base} = Stage total efficiency before incidence loss

β_B = Rotor inlet blade angle

V_R = Rotor inlet radial velocity

S.F. = Slip factor for radial blades, $1 - (2/N_B)$

N_B = Number of rotor blades

- The effect of rotor shroud clearance is based on correlations derived from references 8 and 9 and on AiResearch test results. The performance penalties are a function of both axial (Ca) and radial (Cr) clearance. The experimental data from references 8 and 9 are presented in Figures 8a and 8b. Additional rotor clearance effects are present with rotor scallops. The performance effects as a function of backface clearance recently have been evaluated for the Model GTP305-2 turbine (ref. 10) and are presented in Figure 8. The size and scallop depth of this turbine are similar to the turbine considered in this study.

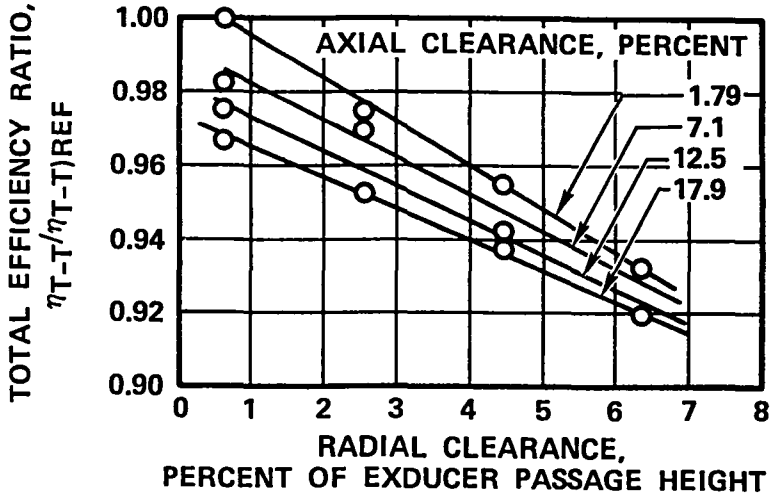

(A) Summary of Radial and Axial Clearance Effects on Total Stage Efficiency (Ref. 8)

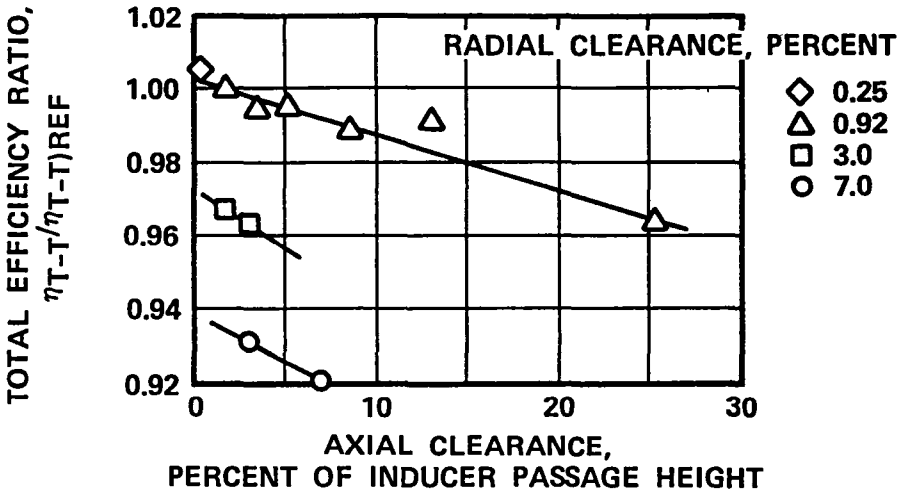

(B) Summary of Radial and Axial Clearance Effects on Total Stage Efficiency at Design Equivalent Values of Speed and Pressure Ratio (Ref. 9)

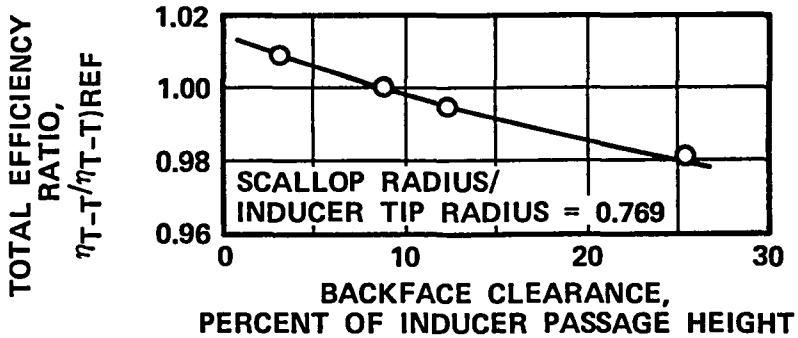

(C) Effect of Rotor Backface Clearance on Stage Total Efficiency at Design Conditions (Ref. 10)

Figure 8. Summary of Radial Turbine Rotor Clearance Effects on Total Stage Efficiency.

In addition, the results of a 1978 AiResearch-sponsored radial turbine research program investigated the effects of scallop depth on radial turbine performance. These data will be used to supplement the correlation derived from the Model GTP305-2 turbine.

- The performance effects of blade number are based on the Models GTCP305-1, GTCP36-4, and published Pratt and Whitney data (ref. 11). The resultant change in turbine efficiency represents the effect of increased blade loading as the blade number is reduced for a given work requirement.

- Disk friction losses along the rotor backface are estimated based on the results of the investigation conducted in reference 12. This work is fully described in reference 13. Note, however, that disk friction is based on a full rotor backface disk. The effect of rotor scallops on rotor disk friction is currently not available.

- The exhaust diffuser loss correlation was based on the Model GTC36-200 configuration shown in Figure 9a. The annular inlet to the diffuser is followed by a rotor exit hub dump, a constant area section, and a conical diffuser section. The constant area section downstream from the rotor exit dump allows the flow to mix and stabilize, prior to the rapid diffusion near the diffuser exit. The net result is a linear static pressure rise along the diffuser shroud from rotor exit to diffuser exit.

  The non-dimensionalized diffuser geometry and performance potential of this system is presented in Table III. The loss characteristics of the Model GTC36-200 exhaust diffuser as a function of inlet swirl are presented in Figure 10. Although a number of data points at high corrected speed or low-pressure ratios result in relatively low loss levels, the predominant characteristic is at a high loss level, as shown.

  The lower loss levels would be equivalent to lower diffuser inlet blockage levels, which is consistent with diffuser test data. However, for the high work and pressure ratio levels of this program, the higher loss level is considered realistic. The minimum loss coefficient ($\bar{\omega}_{min}$) derived from Figure 10 is 0.30.

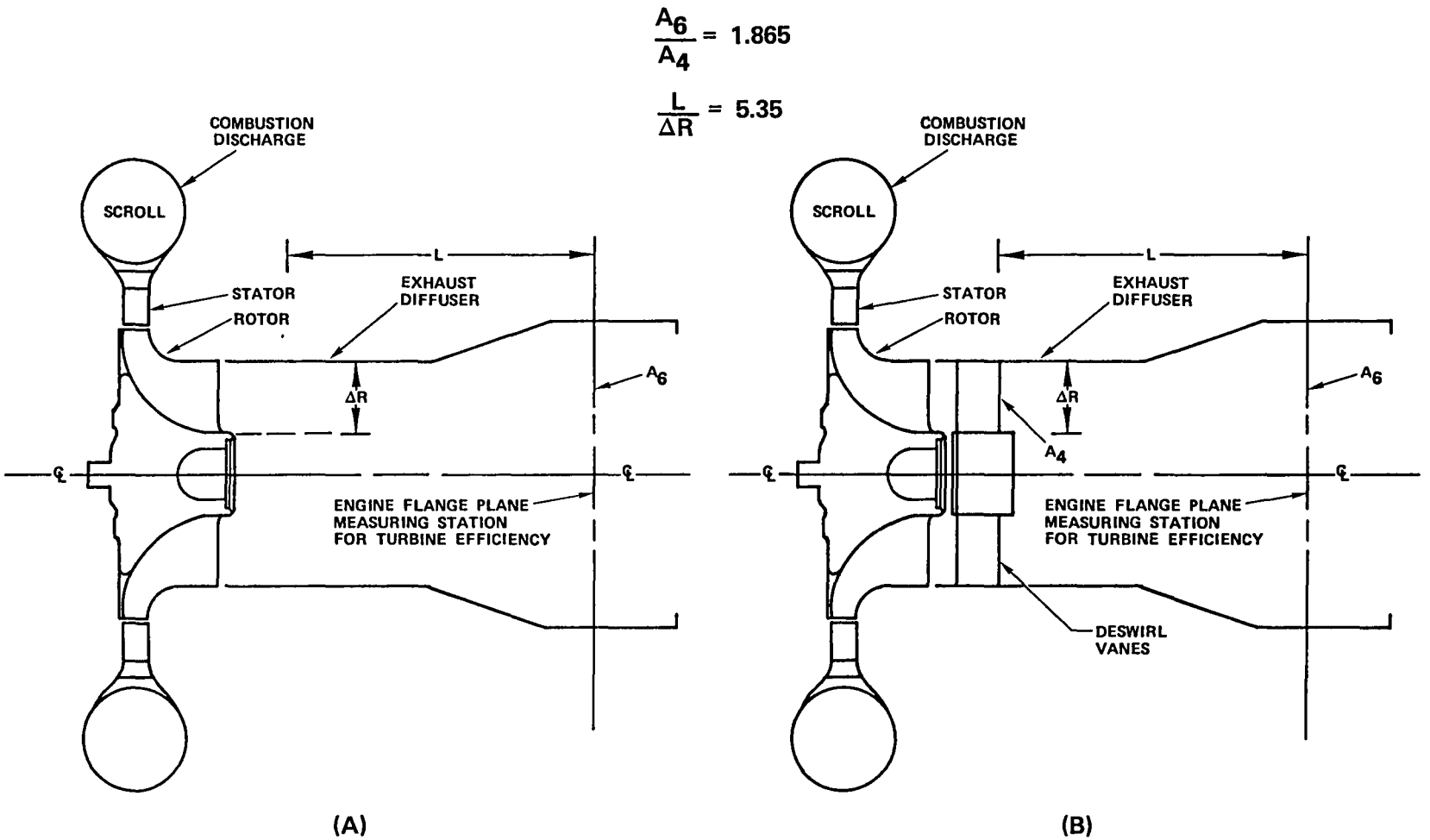

RADIAL TURBINE SYSTEM PERFORMANCE FOR PARAMETRIC STUDY IS DEFINED FROM SCROLL INLET (COMBUSTION DISCHARGE) TO EXHAUST DIFFUSER EXIT PLANES (A) WITHOUT DESWIRL VANES' (B) WITH DESWIRL VANES.

Figure 9. Exhaust Diffuser Configuration Used in Parametric Study.

TABLE III. PERFORMANCE AND NONDIMENSIONAL GEOMETRY FOR SELECTED DIFFUSER CONDIFURATION

Parameters	Value
Exit Area/Inlet Area	1.865
$L/\Delta R$ $\frac{\text{Diffuser Length}}{\text{Inlet Height}}$	5.35
Static Pressure Recovery at Design Conditions, R_D	0.468*
Maximum Static Pressure Recovery	0.60**
Diffuser Inlet Critical Velocity Ratio at Design-Point, V/A_{Cr}	0.463
Average Diffuser Inlet Swirl at Design-Point (α), deg	-3.0

*100-percent corrected speed, $P_{R_{T-T}}\Big|_{1-4} = 4.07$

**110-percent corrected speed, $P_{R_{T-T}}\Big|_{1-4} = 3.85$

$P_{R_{T\text{-}DE}}$ = 2.0 TO 5.3

$\bar{\omega}_{MIN}$ = 0.30

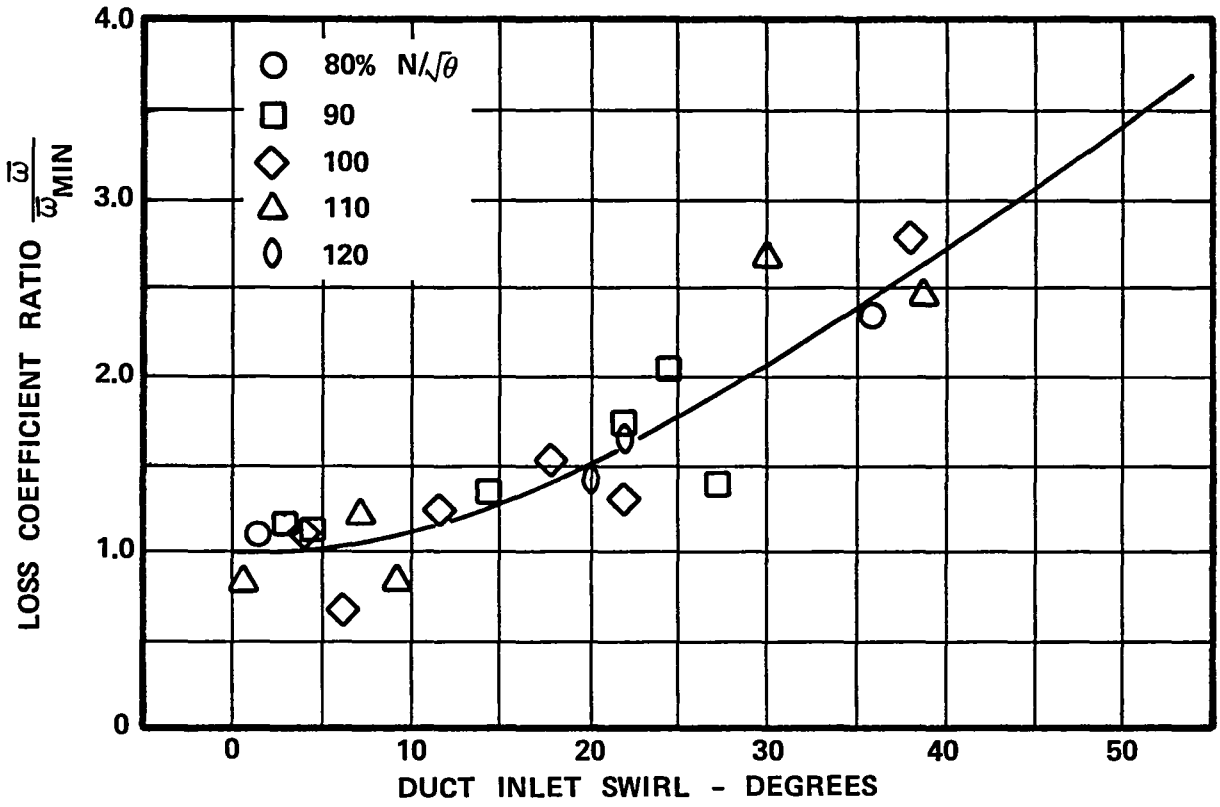

Figure 10. Diffuser Duct Loss Data.

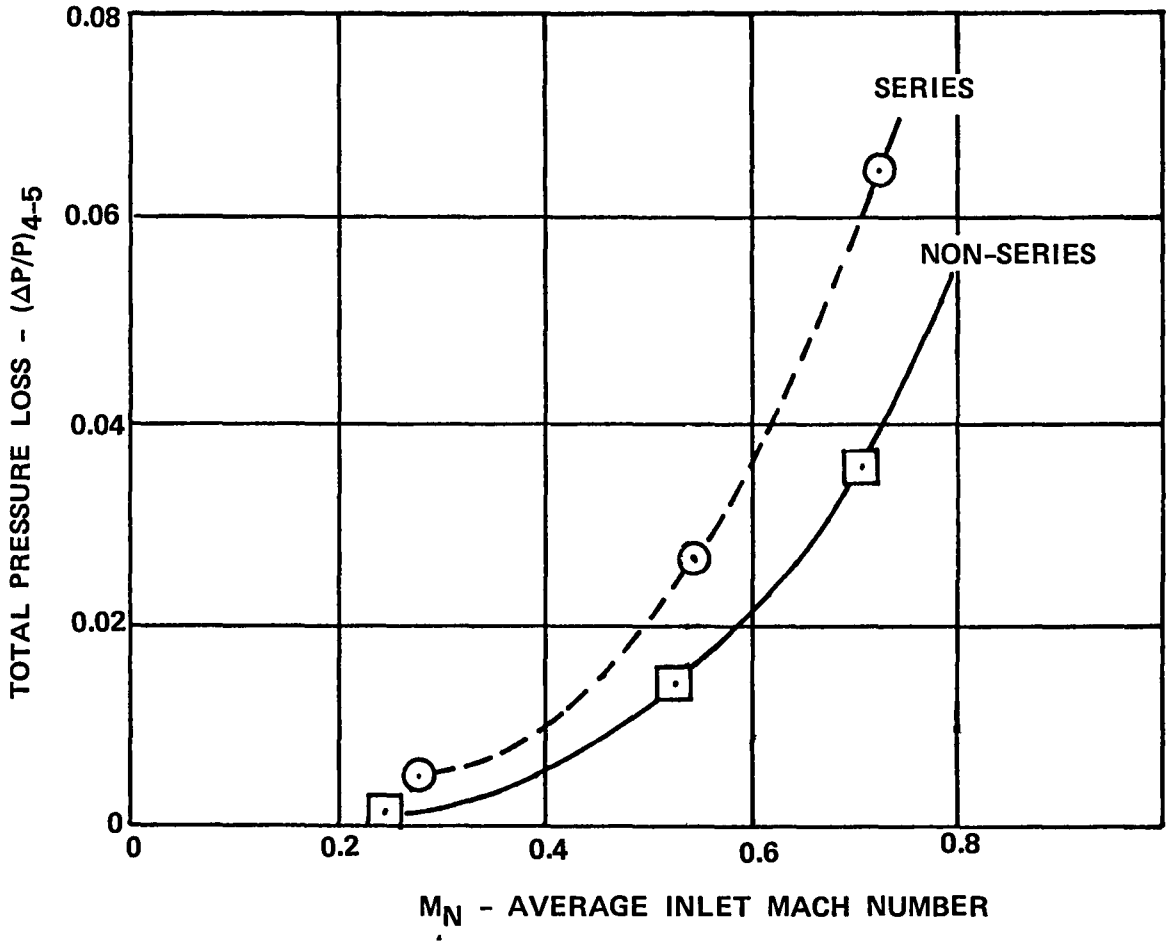

Figure 11. Deswirl Vane Loss Characteristics (ref. 3) Using Arbitrary Air-Foil Shapes.

- When a rotor exit deswirl vane is used, the diffuser non-dimensionalized parameters shown in Table III will be applied at the deswirl vane exit. The losses required for the deswirl vane to reestablish axial flow are based on the performance potential achievable with arbitrary airfoil shapes indicated in Figure 11. The test data shown are based on the work of Pratt and Whitney (ref. 3). The deswirl vane geometry (solidity, aspect ratio) and diffusion limits will be derived from current axial compressor vane technology. A detailed description of the model used in the parametric study is presented in Appendix B.

The above correlations represent the majority of the design data available to the radial turbine designer. The current state-of-the-art for radial turbine design is a result of two major factors. First, the number of design variables associated with the radial turbine are increased significantly compared to the axial turbine. For example, rotor clearance effects are a function of rotor inducer blade width, exducer blade height, backface seal clearance, scallop depth and scallop saddle configuration. As a result, extensive (and expensive) rig test programs are required to arrive at meaningful correlations, which tend to restrict the dissemination of radial turbine data. Secondly, the flow field in the radial turbine is highly three-dimensional, radial stators are usually in the very low aspect ratio region, and the relative vorticity complicates rotor inlet and exit flow predictions.

Nevertheless, experience gained from axial turbine designs has shown that the effects of rotor exit blockage and stage reaction should not be ignored during the turbine design process. The effects of rotor blockage on overall radial turbine performance do not appear to be available in the open literature. The rotor exit hub blockage of AiResearch turbines used for specific speed correlation is on the order of 30 percent, and under this condition, excellent performance levels are still achieved. However, for the automotive engine, turbine rotor weight and inertia will have a significant influence on engine acceleration and subsequent driveability; for this reason, a minimized rotor exit hub radius (lower rotor exducer hub-to-inducer radius ratio) is desirable. The resultant increase in rotor exit blade height would reduce the sensitivity to rotor radial clearance.

Under these conditions, an order of magnitude effect for rotor trailing edge blockage is necessary to arrive at a rational tradeoff. Analytical analysis in terms of evaluating boundary layer characteristics along the rotor meridional streamlines is considered ineffective at the present time, due to highly three-dimensional flow characteristics in the rotor. The problem is further compounded by the local inducer flow separation associated with the highly loaded designs. Even if this

approach were pursued, the time required to analyze a large number of solutions on this basis would be prohibitive. Therefore, a simplified approach is taken, whereby the relative effects of rotor exit blockage are calculated, based on the compressible mixing loss due to the rotor trailing edge thickness and local relative velocity. The total pressure loss calculated in this manner is compared with the loss calculated for an existing reference design, and the difference in calculated loss is used to penalize the higher blockage designs. The model will be based on modifying Stewart's (ref. 14) compressible mixing loss equations to account for trailing edge thickness alone.

The basis for this model is a result of numerous observations of test result that indicate the boundary layer thickness in the rotor exit hub region is small. For example, Figure 12 shows the local efficiency of the selected reference turbine derived from rotor exit survey data. As indicated, the efficiency is relatively constant at 95.5 percent up to approximately 40 percent of the blade height and then decreases rapidly above this point. The implication from rotor powder traces and predicted hub velocity distributions is that high secondary flow generated at the rotor inducer region propagates to the rotor exit shroud region. The flow along the hub line then experiences high acceleration downstream from the rotor inducer region at a relatively low loading level. The net result is that the losses in the hub region are extremely low and account for the high efficiencies measured.

On this basis, then, a calculated mixing loss due to the trailing edge thickness alone would be expected to provide a realistic estimate of the effects of increased blockage in this region. However, even with this simplified approach, the calculation procedure becomes fairly complex in order to arrive at an estimated performance decrement for rotor exit blockage. For example, the rotor exit flow path dimensions, specified exit work coefficient, and continuity must be solved to satisfy the radial equilibrium equation inside the rotor trailing edge. However, a radial thickness distribution is required that satisfies both the maximum tip thickness and maximum allowable blade stress with a radial distribution of blade angle (usually radial blades in this region). Then, the calculated radial relative velocity in conjunction with the established radial thickness distribution can be utilized to calculate a relative total pressure loss from hub to tip based on blade blockage alone.

Since this type of analysis could not be achieved with the one-dimensional performance model available for the parametric study and the effect of rotor blockage should not be ignored, the following procedure was adopted:

- First, the one-dimensional model was used to establish peak performance characteristics for a range of tip speeds and rotational speeds.

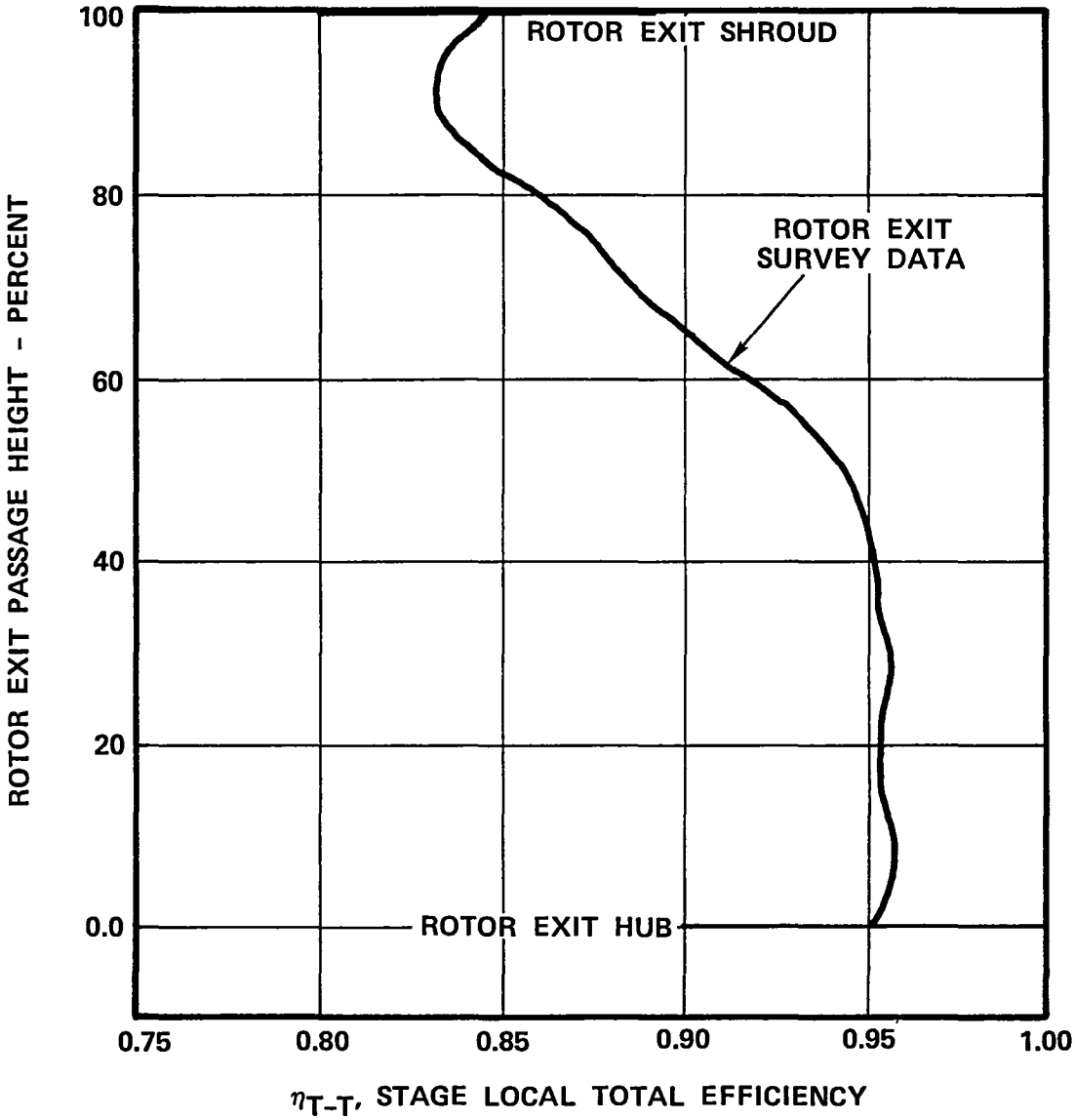

Figure 12. Representative Rotor Exit Efficiency Characteristics for Radial Turbines.

- Viable configurations were examined mechanically with two-dimensional finite element methods that established rotor blade thickness satisfying the maximum allowable blade stress. A separate computer program being developed was utilized to solve the radial equilibrium equation with the specified blade thickness, and an estimated rotor exit blockage performance decrement was calculated.

The effect of stage reaction is expected to increase directly with increasing work coefficient. However, isolating this effect with highly loaded radial turbines is complicated by rotor inducer incidence and stator loss, which will change as inducer-to-exducer work split is adjusted to increase stage reaction. If a systematic procedure is used to extract known losses at tested off-design points, a relative rotor reaction effect should evolve. This approach has been applied to the Model GTP36-51 and 1976 research radial turbine test data to derive a preliminary correlation of stage reaction on radial turbine performance. Figure 13 shows results as desirable mean-line reactions of 50 to 60 percent. The stage reaction shown in Figure 13 is defined in the usual manner by the ratio of static enthalpy across the rotor, relative to total stage work:

$$R_{STG} = \frac{\Delta h}{\Delta H_T}$$

In terms of a stage work coefficient and relative velocity, the stage reaction can be expressed as:

$$R_{STG} = \frac{1}{2\lambda_{STG}} - \frac{\left(R_{4M}/R_{T_3}\right)^2}{2\lambda_{STG}} + \frac{W_{4M}^2 - W_3^2}{2\lambda_{STG}\, U_{t_3}^2}$$

The effect of stage reaction was incorporated in the performance model and the results of the parametric study will be presented with and without these effects.

An additional effect that cannot be accounted for is rotor shroud curvature. The shroud curvature, as a function of rotor size and exducer tip-to-exducer tip radius ratio, increased with increasing radius ratio and resulted in higher velocity peaks and subsequent diffusion on the suction surface shroud streamline, as the radius ratio approached 1.0. Therefore, if the parametric study indicates that high radius ratio designs are more favorable, this effect would not become evident until the detail rotor flow solution was in progress. To minimize this occurrence, the radius ratio was limited to 0.80.

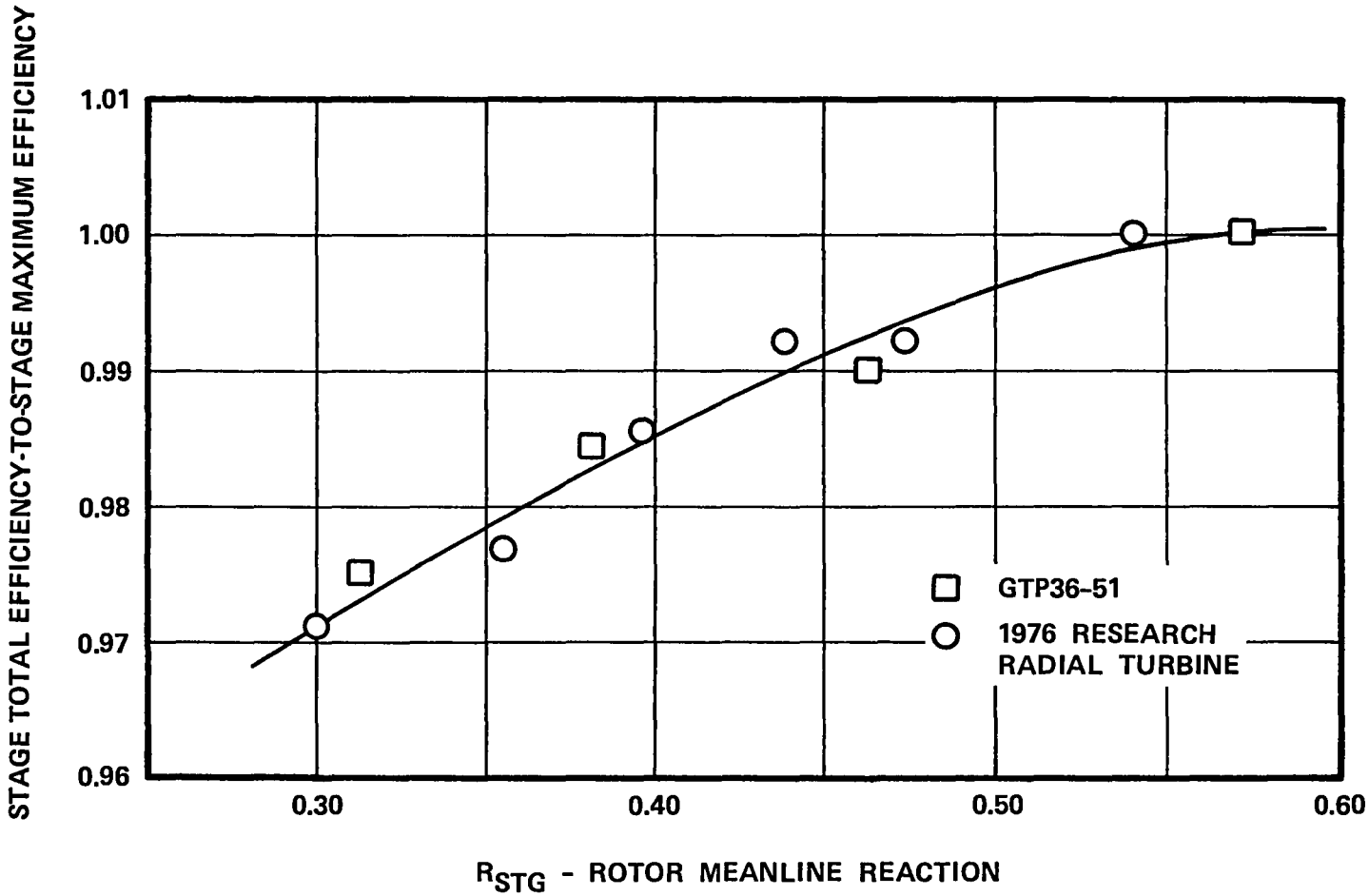

Figure 13. Preliminary Correlation for Radial Turbine Reaction.

3.5 Projected 1983-1985 Performance Improvements

The previously discussed performance model is based on current 1979 technology. However, as indicated in Table I, the high-stage work and performance level required by the turbine to achieve a 50-percent reduction in fuel consumption is aggressive and will require significant improvements in turbine efficiency. With the smaller size associated with the automotive application, both stator aspect ratio and rotor tip clearance penalties will tend to restrict the attainable efficiency level, even if optimum tip speed is achieved.

Historically, radial nozzle designs have been based on constant section profiles with parallel end-walls. These conditions, coupled with the favorable nozzle inlet-to-exit area ratio, result in a theoretically high-acceleration two-dimensional nozzle. However, in practice, the nozzle aspect ratio is extremely low compared with an axial turbine, and the rotor shroud curvature imposes cross-passage static pressure gradients at the stator exit and transforms the highly accelerating two-dimensional flow to a complex three-dimensional flow field.

Indications that the stator is not the low-loss two-dimensional device originally expected are implied from flow visualization techniques (powder traces) and from an inability to match radial turbine off-design test data utilizing techniques similar to reference 15, unless stator loss coefficients are increased significantly. Powder traces from a 0.30 aspect ratio radial nozzle showed that secondary flow accumulations covered approximately 90 percent of the passage in the trailing edge suction surface region. Even with constant section profiles and parallel end-walls, secondary flows would be expected due to the end-wall pressure-to-suction static pressure gradients that result from the high turning. In addition, studies conducted by Langston (ref. 16) and Gaugler (ref. 17) show that blade-to-blade secondary flows are further compounded by the so-called horseshoe vortex generated at the nozzle leading edge.

The concept of stator end-wall contouring and non-free vortex work distributions has been widely utilized in axial turbine designs over the past few years with excellent success. Since the effect of end-wall contouring is to reduce the blade-to-blade static pressure gradient (loading) at the nozzle end-walls, this concept will apply to radial nozzles also. Indeed, the benefits may be more pronounced with radial nozzles since the aspect ratios are significantly lower compared with axial nozzles. Therefore, in 1978 the potential benefits of end-wall contouring were investigated for radial stators with a compressible 3-D viscous flow analysis computer program developed by AiResearch under USAF Contract (F33615-76-C-2110). The study was conducted as part of the TARADCOM advanced radial turbine program (ref. 18). Five different end-wall configurations were

examined (including a parallel wall baseline case) and compared on a predicted total loss basis. The analytical results showed that total pressure loss is reduced by 50 percent with end-wall contouring. Additional analytical and experimental effort is required to identify the true potential of the concept and also evaluate the performance potential of combining both the end-wall contouring and three-dimensional vane profile (non-free vortex type) concepts. However, on the basis of preliminary analysis, a 1.0-point improvement in turbine performance is considered feasible.

Although the sensitivity to rotor shroud clearance is reduced compared with axial turbines, scaling the allowable running clearance with the reduced size of the automotive turbine may not be possible. In addition, the rotor scallop introduces a third clearance effect that is a function of both backface seal clearance scallop depth and scallop saddle configuration.

Under these conditions, the estimated clearances shown in Table II will result in relatively high performance decrements. If higher engine running clearances are required due to shaft dynamics or differential thermo growth, then attainable radial turbine performance will be appreciably effected. Therefore, the concept of clearance treatment to minimize clearance effects will be considered for this application.

Dejc (ref. 19) has shown reductions of approximately 50 percent in clearance loss on axial turbine stages through the use of circumferential grooves in the rotor shroud. Although this concept does not appear to have been applied to a radial turbine configuration, the clearance phenomena are basically the same. The shroud and backface seal surface treatment is considered viable for this application. Based on a 35-percent shroud and backface clearance loss reductions, a 1.35-point increase in performance is considered feasible. The total improvement predicted for both stator loss reduction and rotor clearance effects is 2.35 points for the 1983-1985 time frame.

Performance levels of the turbine inlet scroll, exhaust diffuser and deswirl vanes will be maintained at current 1979 predicted levels. This does not imply that the performance potential of these components cannot be improved, but except for the deswirl vane, less research effort has been devoted to these components. In addition, the configurations ultimately adapted for this size shaft engine may differ from the representative configurations used in the parametric study.

3.6 Preliminary Stator and Rotor Geometry

The radial turbine stator preliminary geometry was established with the one-dimensional performance model. For a given stator trailing edge thickness of 0.030 in. (from ceramic considerations) and a trailing edge blockage of 10.0 percent (which

is consistent with the geometries used in the specific speed correlation), the stator vane number and radial chord were established from a radial nozzle loading coefficient. The loading coefficient was based on the Zweiffel loading concept applied specifically to the radial nozzle geometry.

The rotor inlet and exit radii and blade height were established with the one-dimensional performance model. The rotor flow path and axial length were evaluated from a meanline loading distribution through the rotor over a range of meridional flow shapes and axial lengths. The entire blade height through the rotor was treated as a stream tube and the continuity equations, with an estimated rotor blade angle distribution, determine the rotor mean-line relative velocity distribution. The condition of zero absolute vorticity was used to arrive at a blade-to-blade loading.

3.7 Parametric Study Results

A one-dimensional performance evaluation model for the turbine scroll, stage, and exhaust diffuser system was first established by modifying an existing radial turbine design program to account for the scroll and duct losses and projected 1985 performance improvements. The computer program calculates geometric and vector diagram quantities at the stator inlet, stator exit, rotor inlet and rotor exit mean-line stations. Due to the number of variables required to define the turbine flow path, the input to the program consisted of both free and fixed parameters. The free parameters were:

- Rotational speed (N) = 80,000, 95,000 and 110,000 rpm
- Rotor inducer tip speed (U_{t_3}) = 549, 610, 701, and 782 m/sec (1800, 2000, 2300, and 2565 fps)
- Rotor inlet blade angle (β_B) = 0, 10, and 20 degrees
- Inducer tip-to-exducer tip radius ratio, 0.80 maximum
- Rotor exit annular area = 45.2 to 58.1 cm^2 (7.0 to 9.0 $in.^2$)
- Rotor inducer work coefficient (which establishes an inducer-to-exducer work split, rotor exit swirl, and Mach number)
- With and without deswirl vane
- With and without predicted reaction effects

Fixed parameters used in the basic parametric study were:

- Rotor blade number, set at 12 (The combined effects of rotor blade number and rotor exit blockage were examined for specific cases but are not included in the basic parametric curves)
- Stator exit vane angle (defined at the rotor inlet radii) was set at 72 degrees
- A stator loading parameter was fixed
- The vane trailing edge thickness was fixed at 0.076 cm (0.030 in.)
- Rotor clearances were set at 0.020, 0.020, and 0.010 for rotor backface, axial, and radial, respectively
- The vane trailing edge blockage was set at 10 percent, which was considered the maximum allowable for the specific speed correlation to be valid
- The conditions of stator blockage, trailing edge thickness and loading criteria then set the stator vane number
- The cycle conditions, except for efficiency and duct loss, were fixed

Results of the basic parametric study are presented in Figures 14 through 22. The basic characteristics of the aerodynamic study are summarized below:

- For a specified tip speed, the parametric study shows that an optimum system efficiency is obtained for all rotational speeds, both types of blading, with and without deswirl vanes
- Rotor reaction significantly affects both the efficiency level and optimum inlet work coefficient at lower tip speed levels
- Peak efficiency increases uniformly with increasing rotor inlet blade angle except at high tip speeds when rotor inlet incidence is eliminated
- The level of tip speed required to achieve the system efficiency goal is relatively high [579 to 701 m/sec (1900 to 2300 fps)]
- The turbine efficiency level increases with rotational speed; however, when the effect of rotor exit hub blockage is considered, this effect is reduced

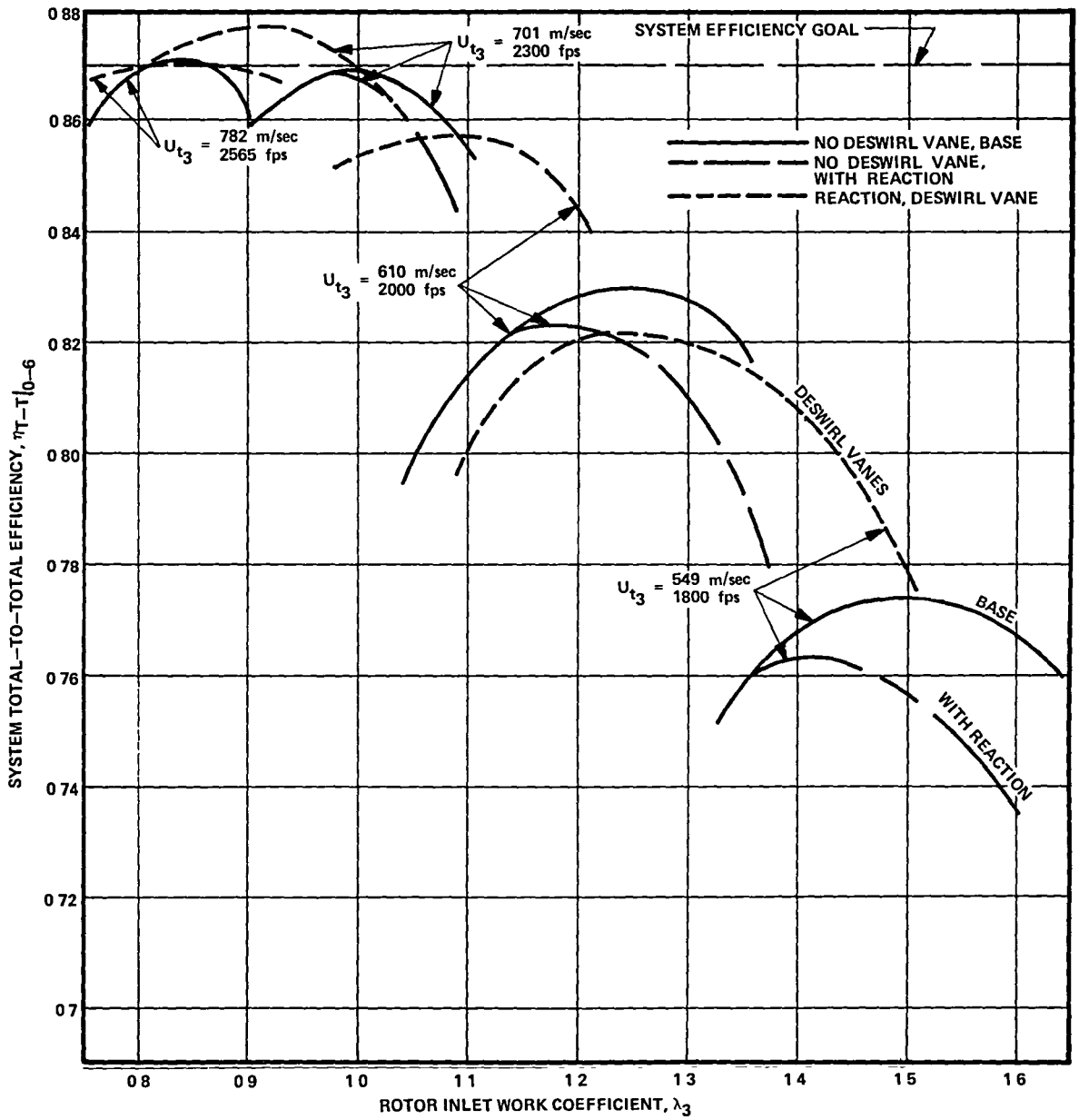

Figure 14. Turbine System Parametric Study, N = 80,000 rpm, $\beta_B = 0°$.

- N = 80,000 RPM
- β_B = 10°
- NO DESWIRL VANE
- N_B = 12

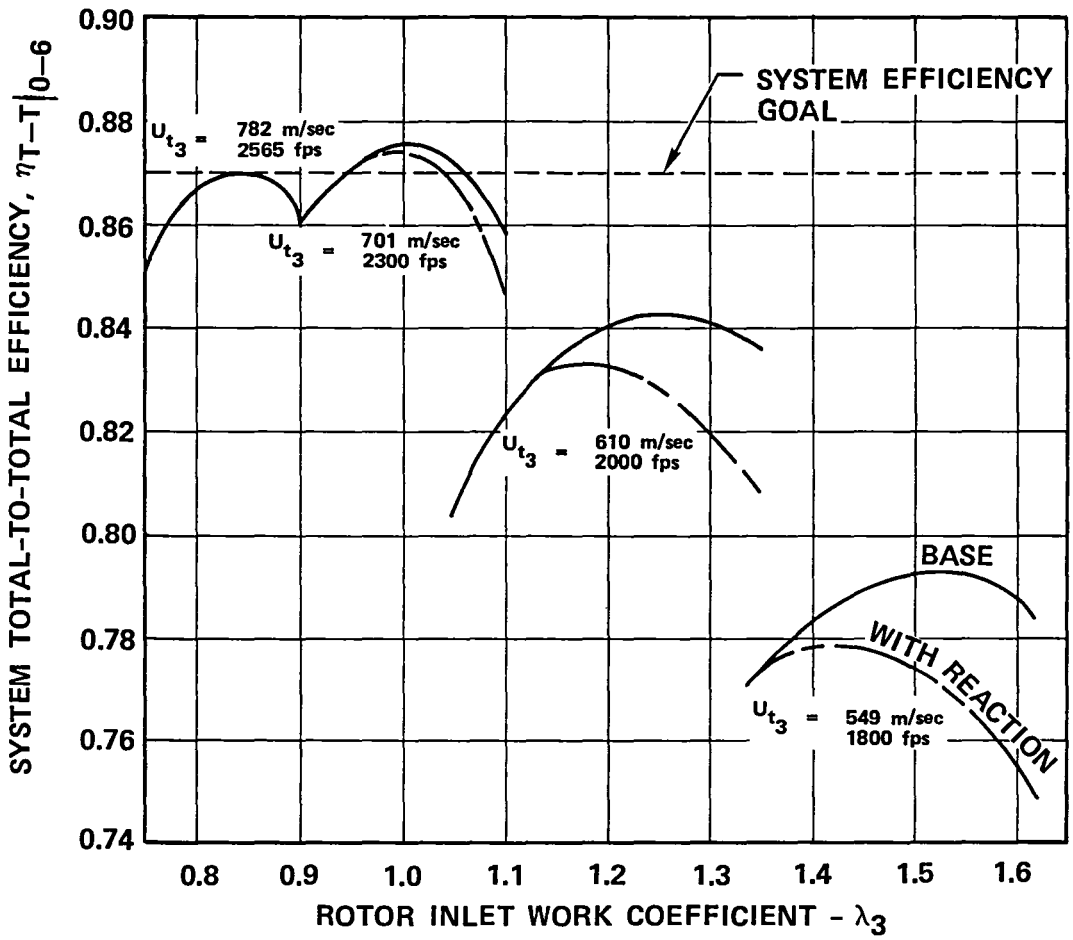

Figure 15. Turbine System Parametric Study, N = 80,000 rpm, β_B = 10°.

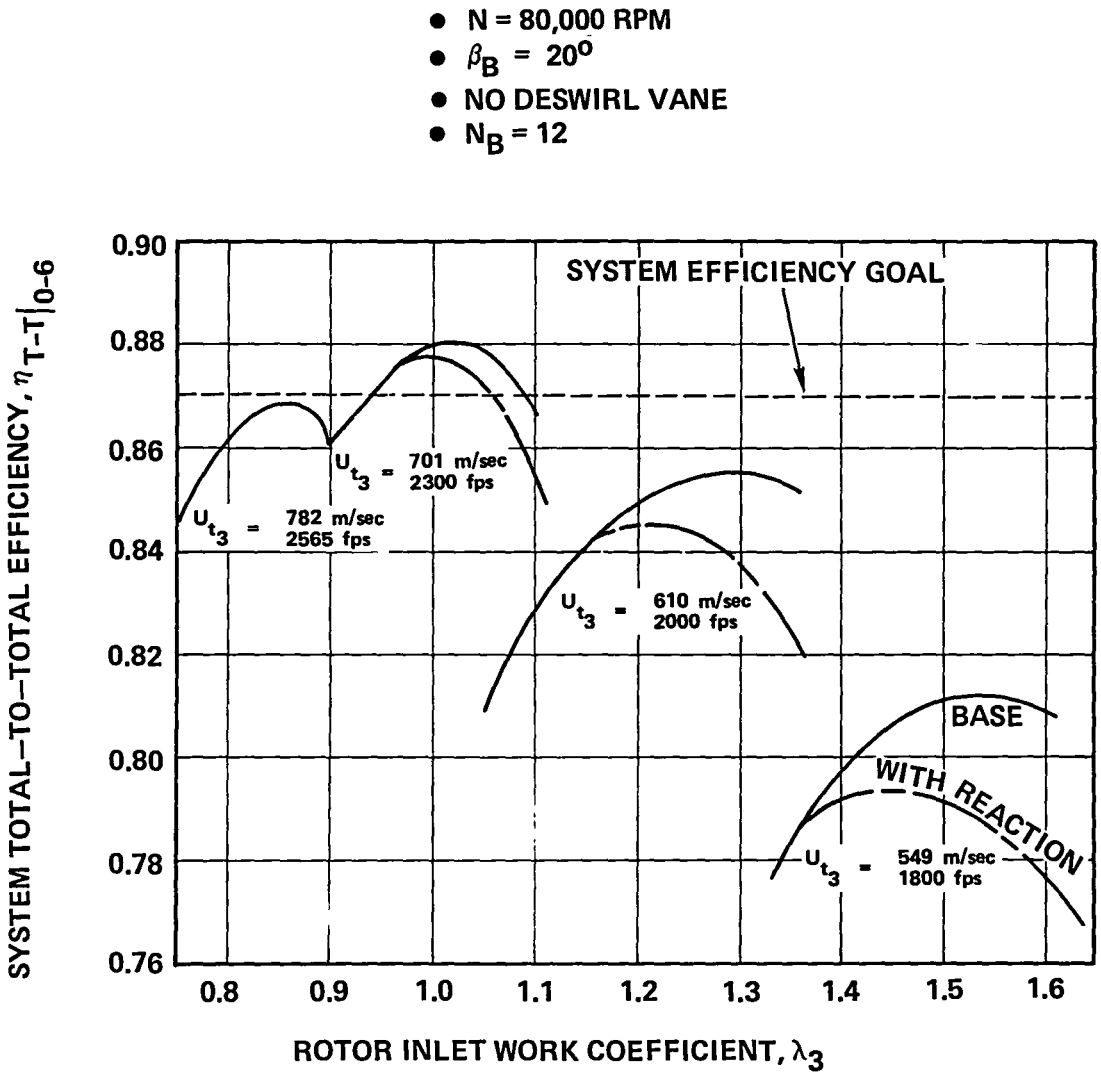

Figure 16. Turbine System Parametric Study, N = 80,000 rpm, β_B = 20°.

N = 95,000 RPM
$\beta_B = 0^o$
$N_B = 12$

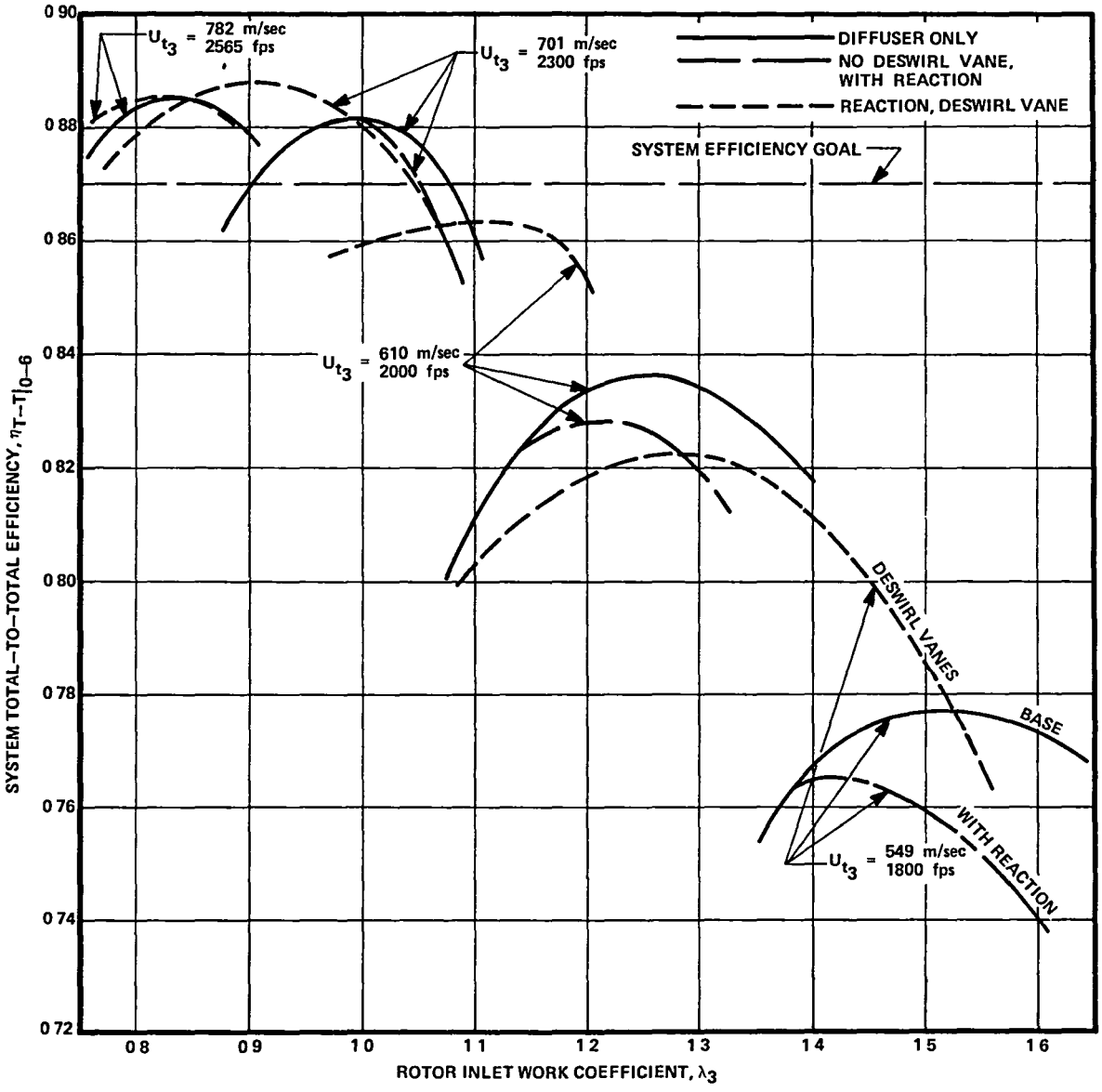

Figure 17. Turbine System Parametric Study, N = 95,000 rpm, $\beta_B = 0°$.

- N = 95,000 RPM
- β_B = 10°
- N_B = 12

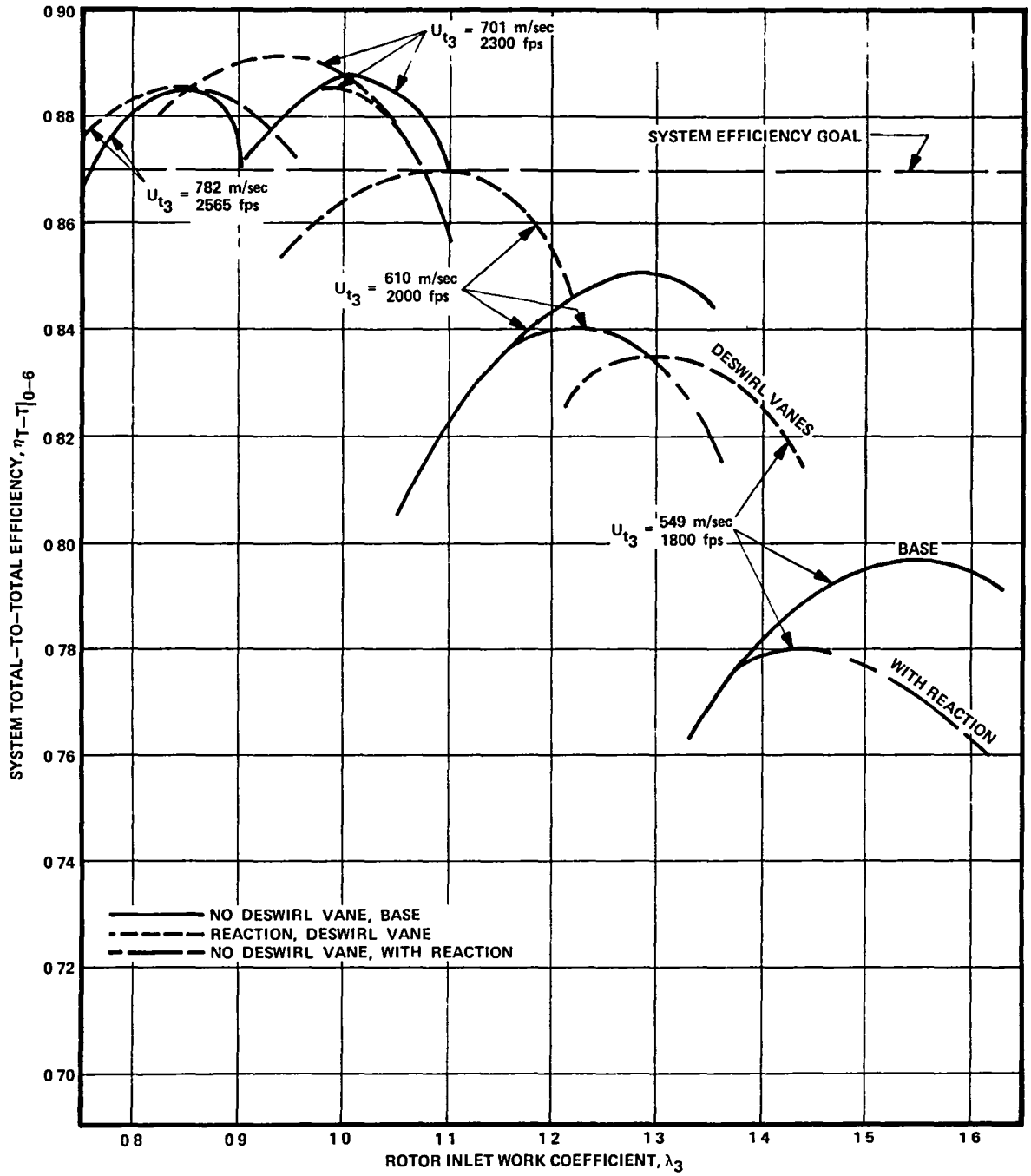

Figure 18. Turbine System Parametric Study, N = 95,000 rpm, β_B = 10°.

- N = 95,000 RPM
- $\beta_B = 20^o$
- $N_B = 12$

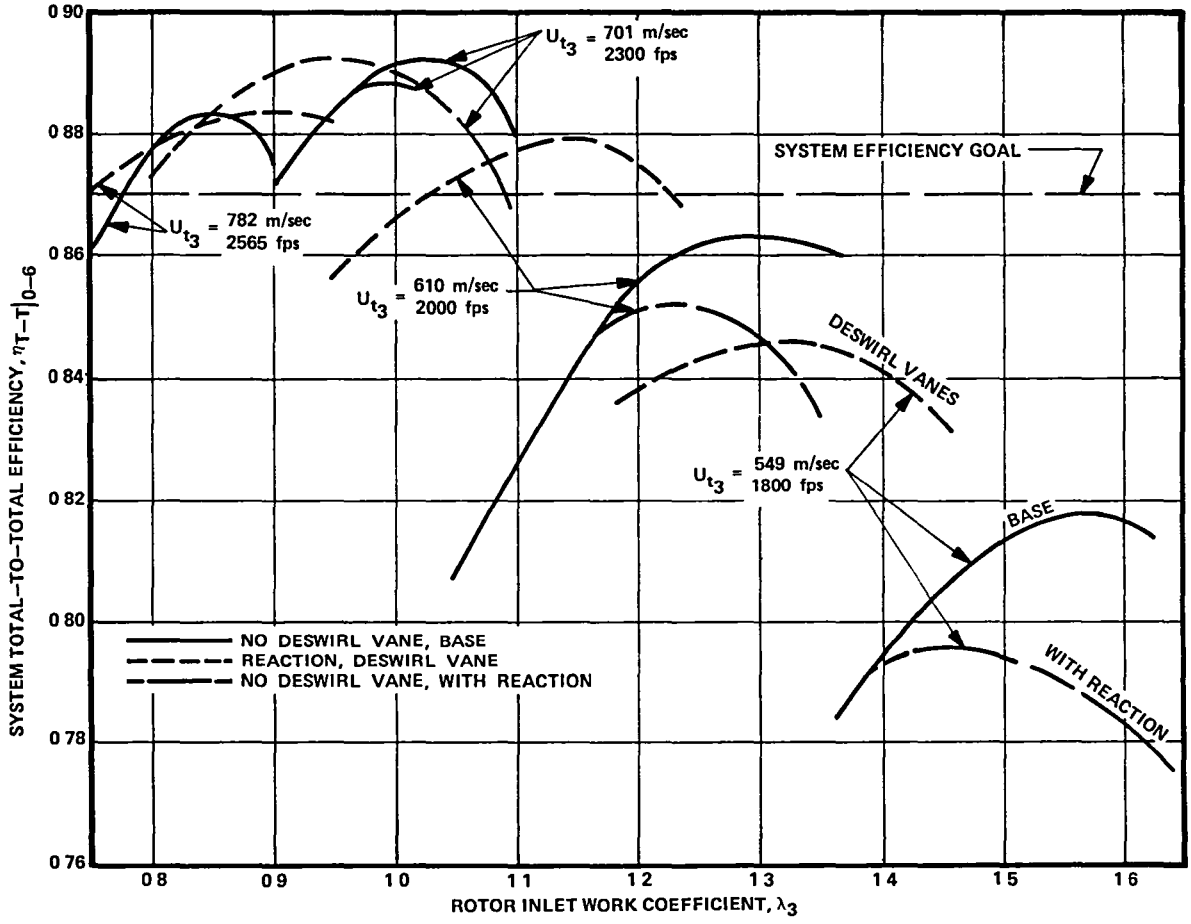

Figure 19. Turbine System Parametric Study, N = 95,000 $\beta_B = 20°$.

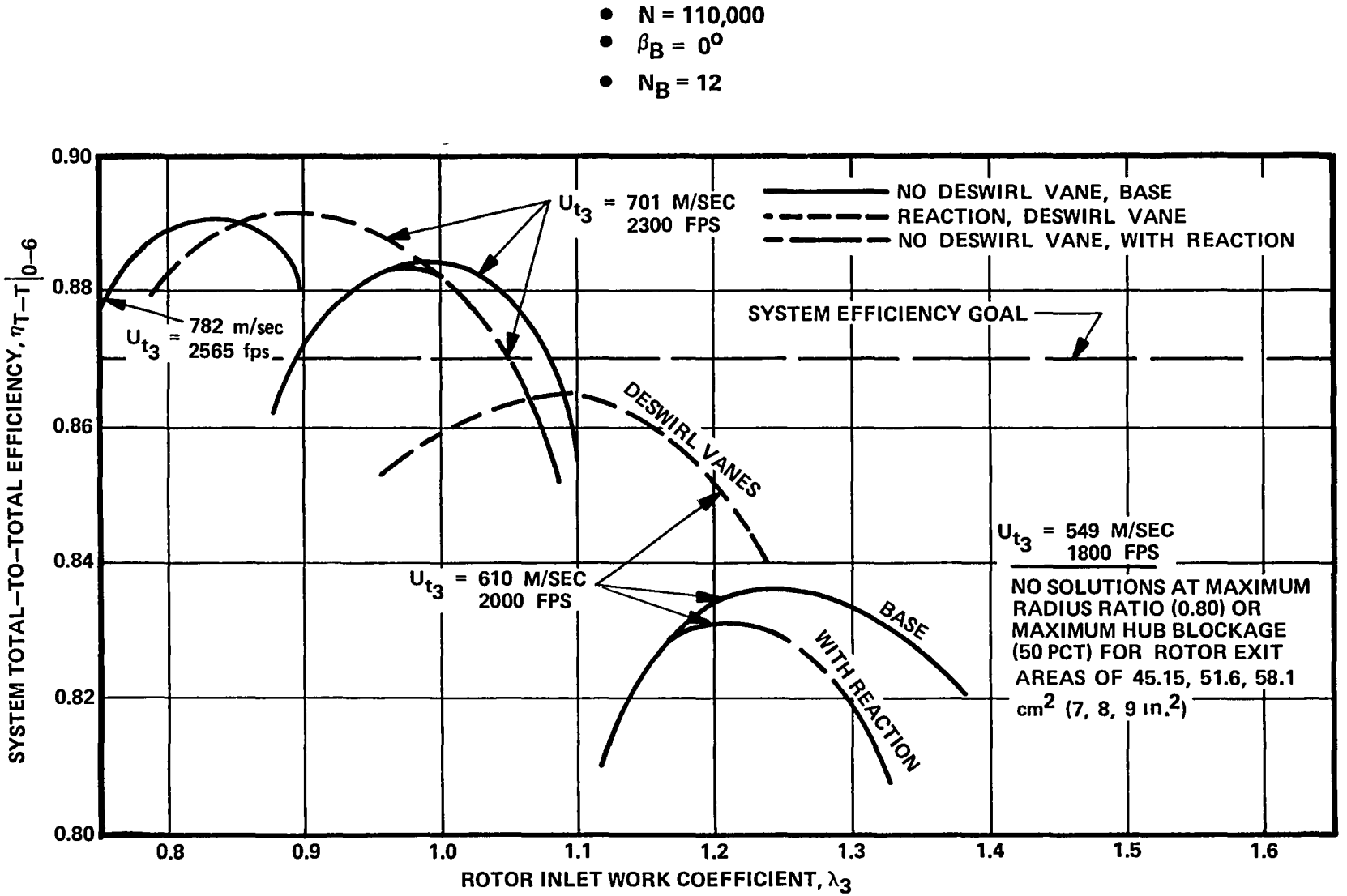

Figure 20. Turbine System Parametric Study, N = 110,000 rpm, β_B = 0°.

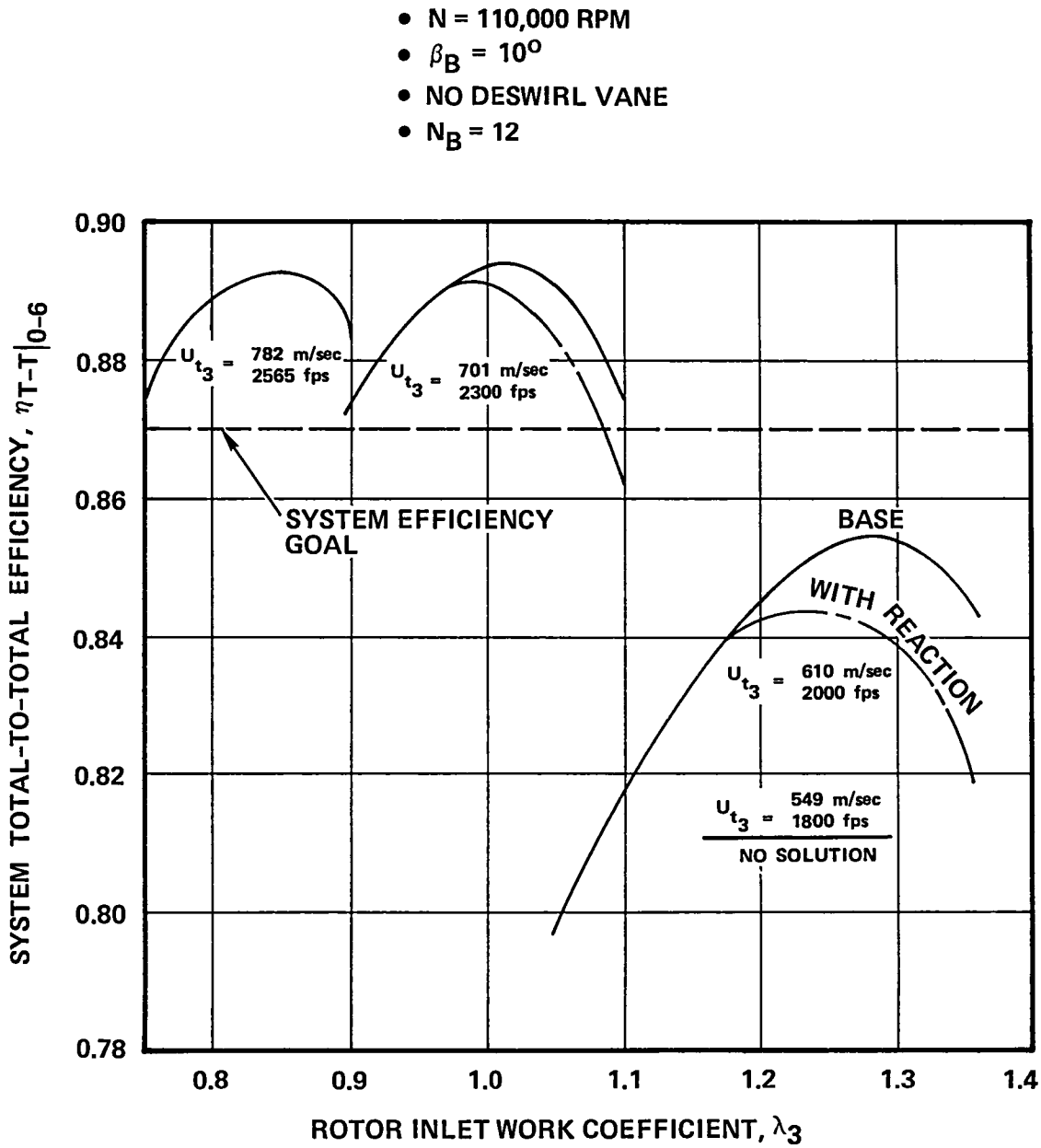

Figure 21. Turbine System Parametric Study, N = 110,000 rpm, β_B = 10°.

- N = 110,000 RPM
- $\beta_B = 20^o$
- NO DESWIRL VANES
- $N_B = 12$

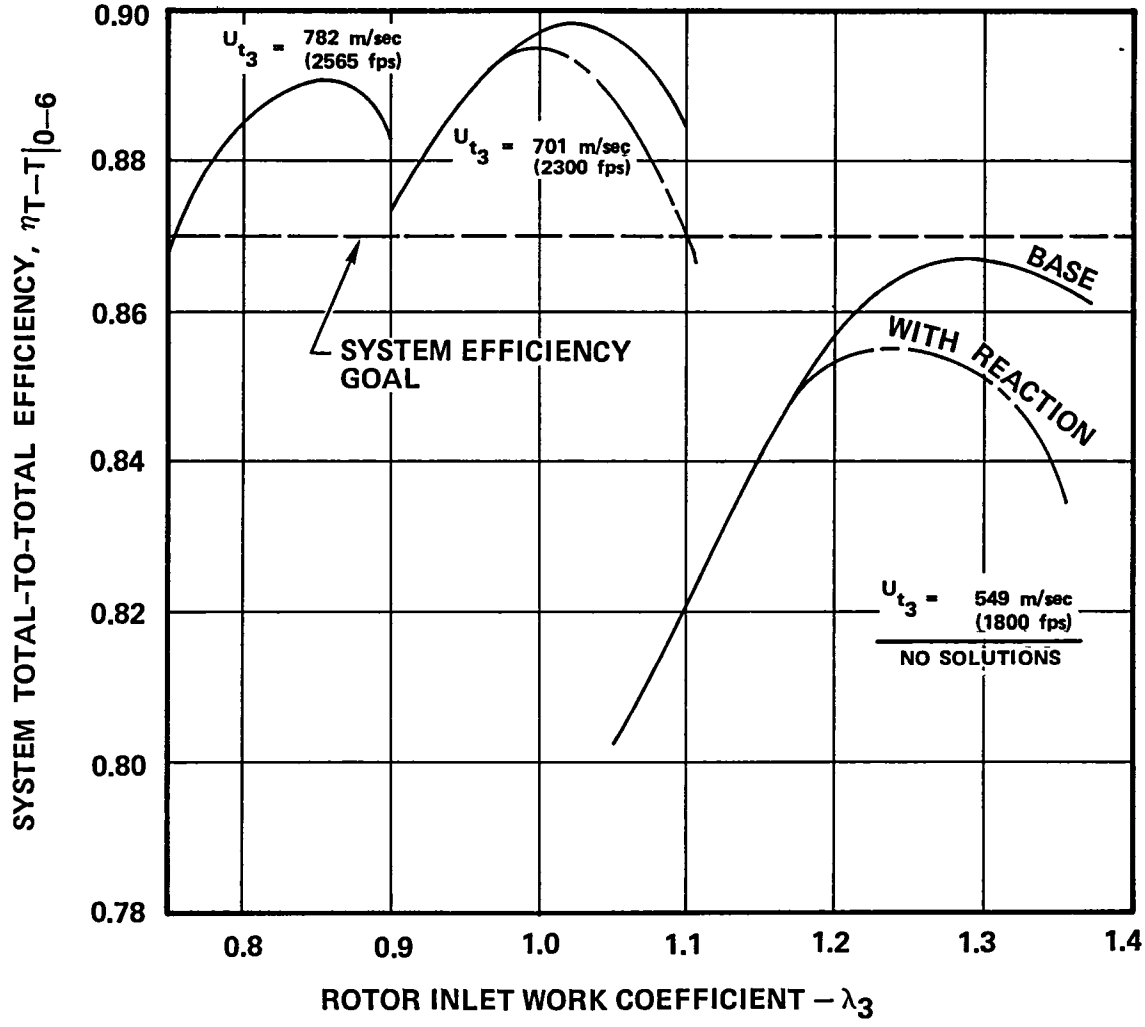

Figure 22. Turbine System Parametric Study, N = 110,000 rpm, $\beta_B = 20°$.

- At lower rotor tip speeds [549 to 610 m/sec (1800 to 2000 ft/sec)], system efficiency is increased from 2 to 6 points with the addition of deswirl vanes

In Figures 14 through 22, the peak efficiency for each value of inlet work coefficient analyzed is based on the maximum attainable efficiency for the range of rotor exit areas and radius ratios examined. Rotor exit areas of 45.2, 51.6 and 58.1 cm^2 (7, 8, and 9 $in.^2$) were specified in the parametric study and, in general, peak efficiency occurred at or near the maximum value specified. The values of rotor exit area selected were established from preliminary rotor exit (zero swirl) continuity calculations. However, as shown in Figures 20 through 22, certain combinations of rotation and tip speed will result in either negative or unacceptably low exit hub radii and no solutions will exist. Although high rotor exit area is desirable from a reduced exducer radial clearance loss standpoint, the higher exit area also requires increased hub blade thickness for a given blade number and blade stress level. The resultant increase in hub blockage could therefore negate the gains in clearance loss.

For the radius ratio, peak system efficiency occurred at 0.80 (the maximum allowable) for tip speeds up to 610 m/sec (2000 fps). However, as optimum tip speed is approached, peak system efficiency occurs at lower radius ratios (0.65). These trends are associated with the rotor exit mean work coefficient. As tip speed is reduced from the optimum value, the level of rotor exit work coefficient increases rapidly. Therefore, the rotor exit conditions and duct loss are more sensitive to changes in the rotor exit mean radius. Under these conditions, the reduction in duct loss at higher radius ratios is greater than the increase in loss due to increased exducer clearance effects. It should be noted that the optimum radius ratio of 0.80 for the lower tip speed cases also results in the highest rotor shroud curvature, and the performance effects for this parameter are currently not known. Therefore, if detailed mechanical analysis indicates this level of tip speed is required to satisfy the rotor life goals, then a rotor internal flow solution at both 0.80 and at lower values must be compared and the impact of the shroud loading evaluated. Figure 23 illustrates the effects of rotor exit area and radius ratio on peak system efficiency for 95,000 rpm and tip speeds of 610 m/sec (2000 fps) and 701 m/sec (2300 fps).

Specific vector diagrams and system parameters along the system efficiency envelope are presented in Figures 24 and 25 for 80,000 rpm and the range of tip speeds investigated. Of particular note is the magnitude of the rotor exit relative critical velocity ratio associated with the deswirl vane cases at peak system efficiency. These higher values result in increased rotor exit blockage losses. In addition, since the

RADIAL

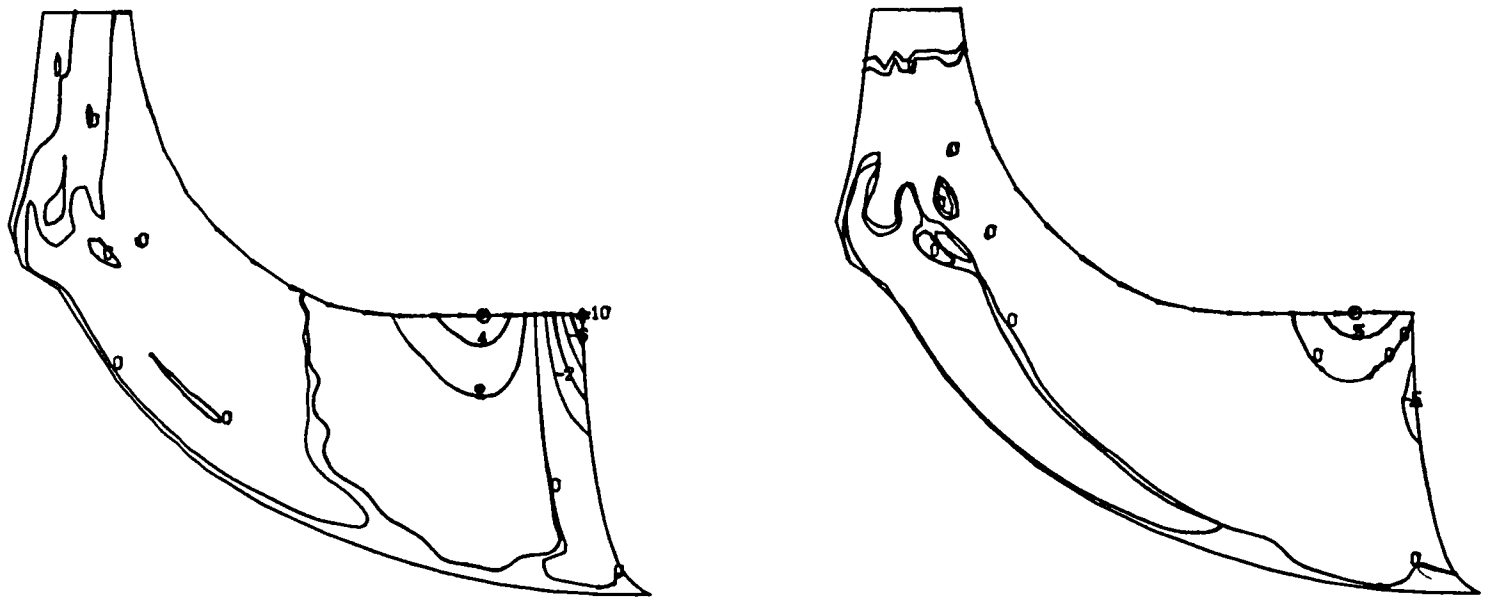

MODE 3

FREQUENCY = 24,837 Hz

MODE 4

FREQUENCY = 38,916 Hz

SCALE FACTOR = 2.00

RPM = 95,000

⊙ MAXIMUM △ MINIMUM

Figure 46. Normalized Deflections (Modes 3 and 4).

RADIAL

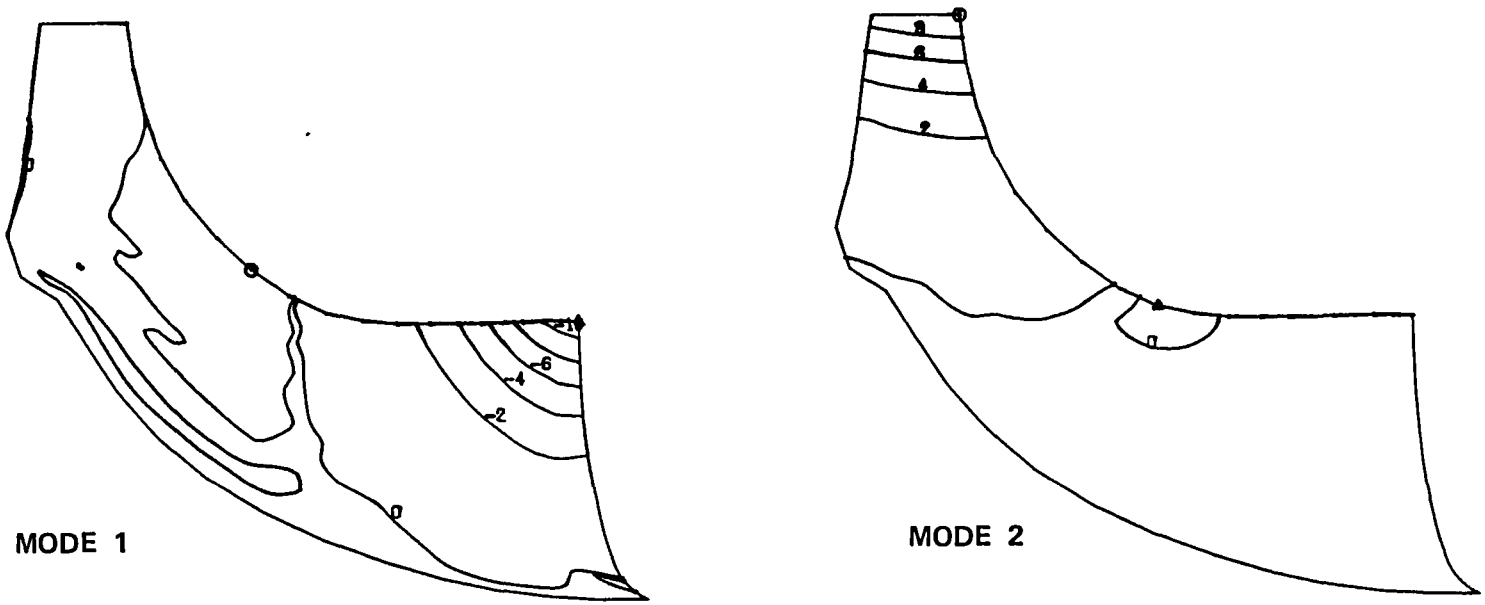

FREQUENCY = 12,295 Hz

FREQUENCY = 16,160 Hz

RPM = 95,000

SCALE FACTOR = 2.00

⏲ MAXIMUM ⚠ MINIMUM

Figure 45. Normalized Deflections (Modes 1 and 2).

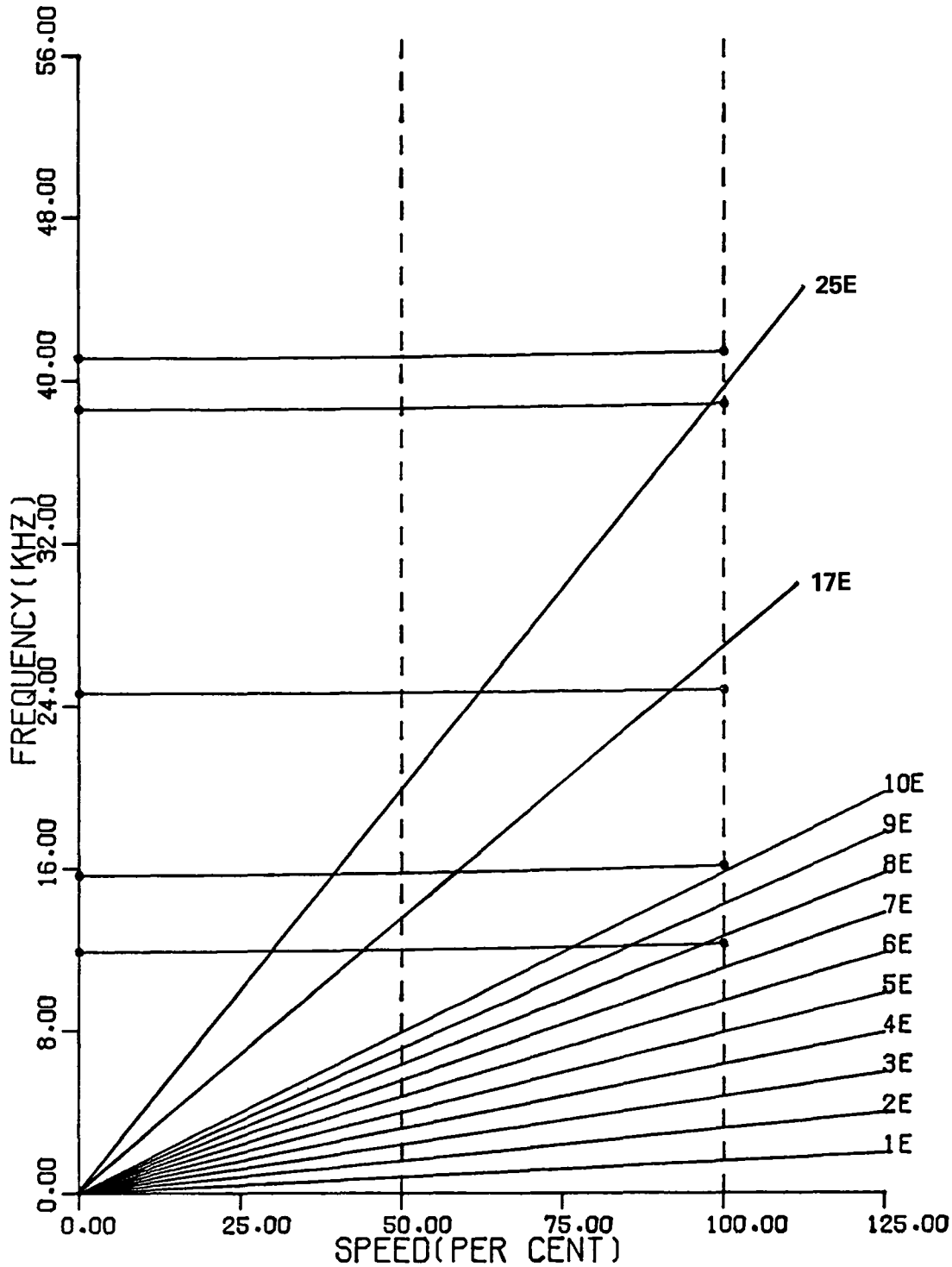

Figure 44. Campbell Diagram for 95,000-rpm Case with 45.2 cm^2 (7 $in.^2$) Exit Area.

RADIAL

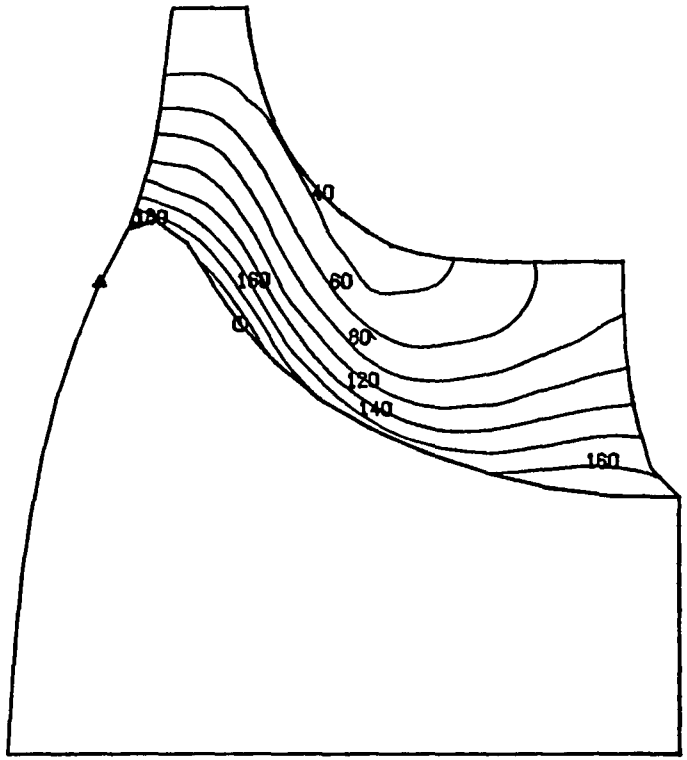

ISOPLETH INTERVAL = 0.051 cm (20 mils)

TANGENTIAL THICKNESS

SCALE FACTOR = 1.50

⏲ MAXIMUM △ MINIMUM

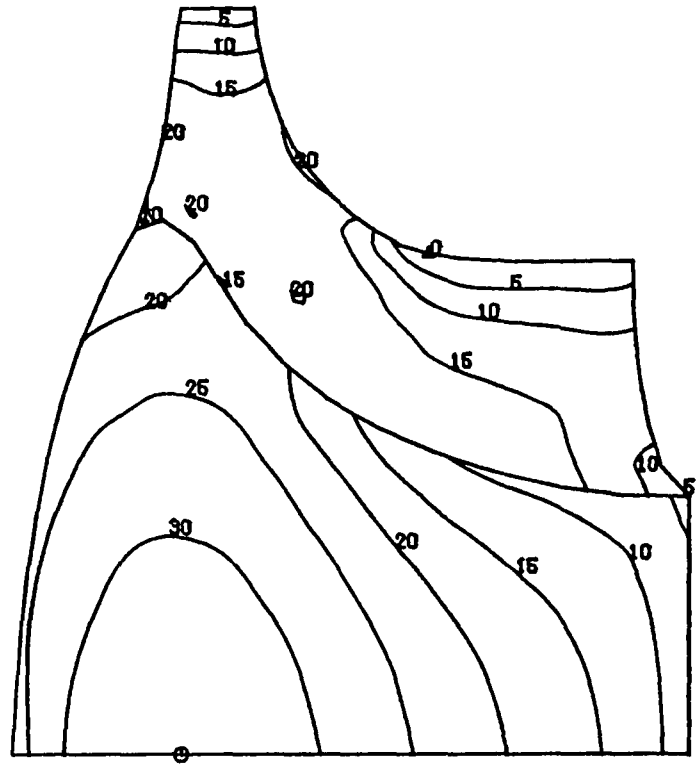

ISOPLETH INTERVAL = 3.447 kN/cm^2 (5 ksi)

RPM = 95,000

TIP SPEED = 664 m/sec (2180 fps)

N_B = 12

A_{EXIT} = 45.2 cm^2 (7 in.^{2})

Figure 43. Tangential Thicknesses and Maximum Principal Stresses.

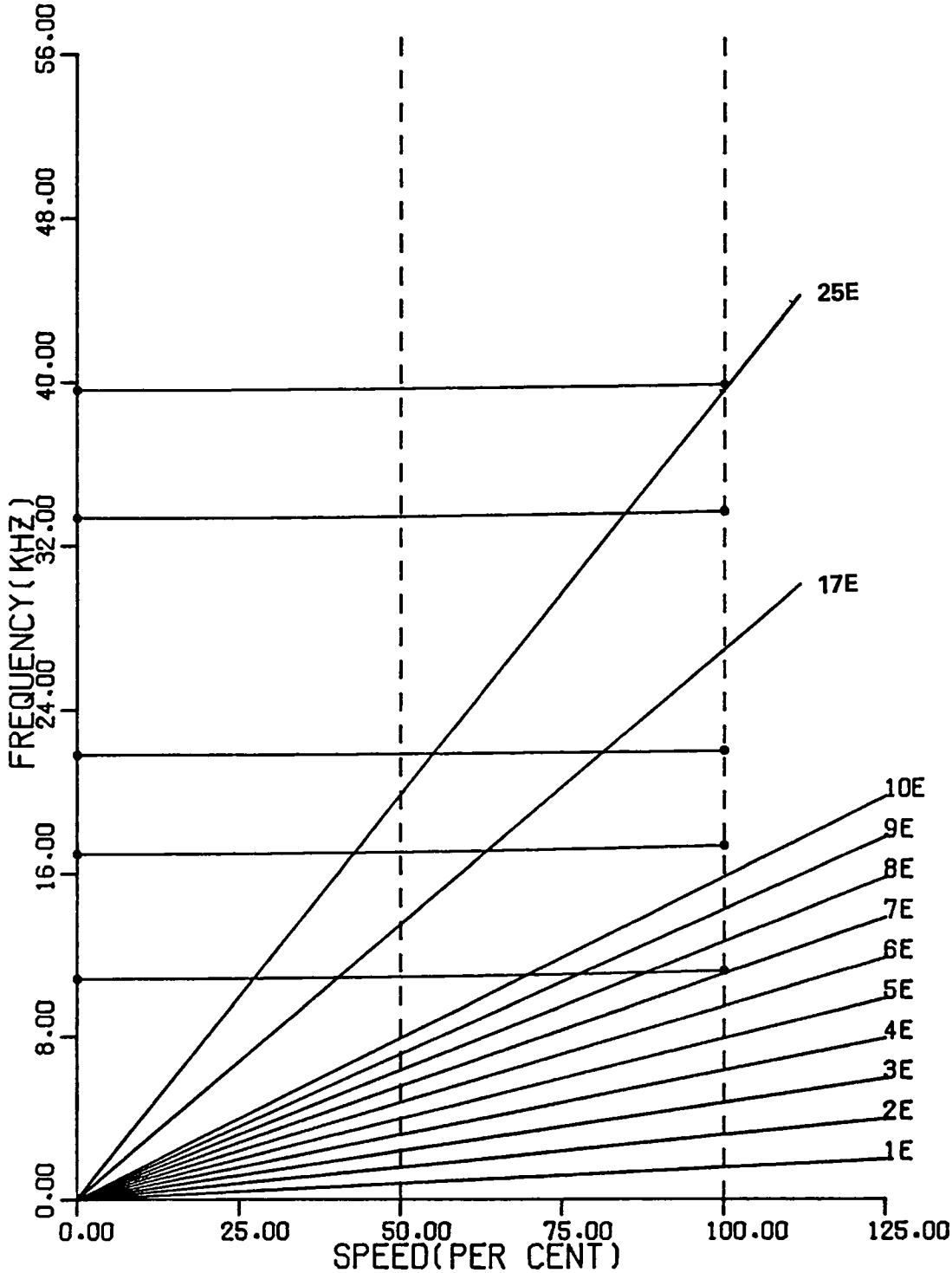

NASA ART CERAMIC TURBINE CASE NO. 2
VIBRATION FREQUENCIES 100% RPM= 95000
CAMPBELL DIAGRAM 50 % RPM= 47500

Figure 42. Campbell Diagram for 95,000-rpm Case with 58.1 cm^2 (9.0 $in.^2$) Exit Area.

RADIAL

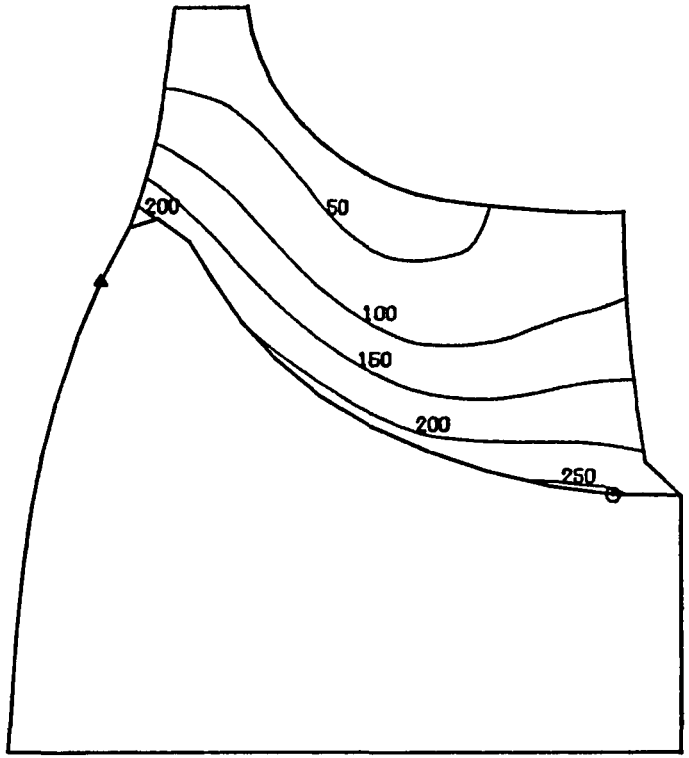

ISOPLETH INTERVAL = 0.127 cm (50 mils)

TANGENTIAL THICKNESS

SCALE FACTOR = 1.50

⏲ MAXIMUM △ MINIMUM

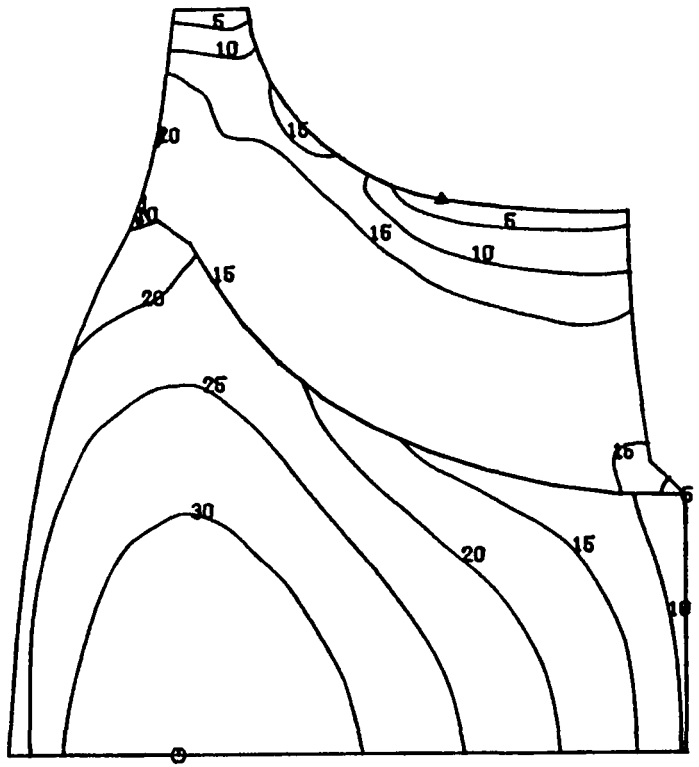

ISOPLETH INTERVAL = 3.447 kN/cm^2 (5 ksi)

RPM = 95,000
TIP SPEED = 664 m/sec (2180 fps)
N_B = 12
A_{EXIT} = 58.1 cm^2 (9 in.^{2})

Figure 41. Tangential Thicknesses and Maximum Principal Stresses.

RADIAL

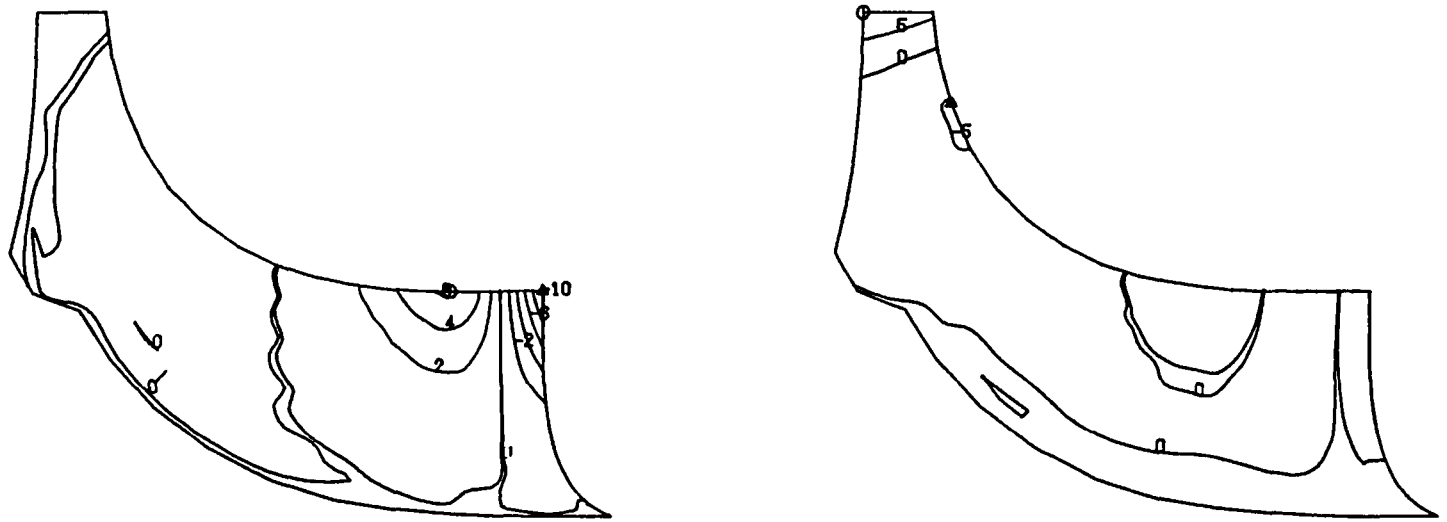

MODE 3
FREQUENCY = 26,445 Hz

MODE 4
FREQUENCY = 35,951 Hz

SCALE FACTOR = 2.00

RPM = 80,000

⏀ MAXIMUM △ MINIMUM

Figure 40. Normalized Deflections (Modes 3 and 4).

RADIAL

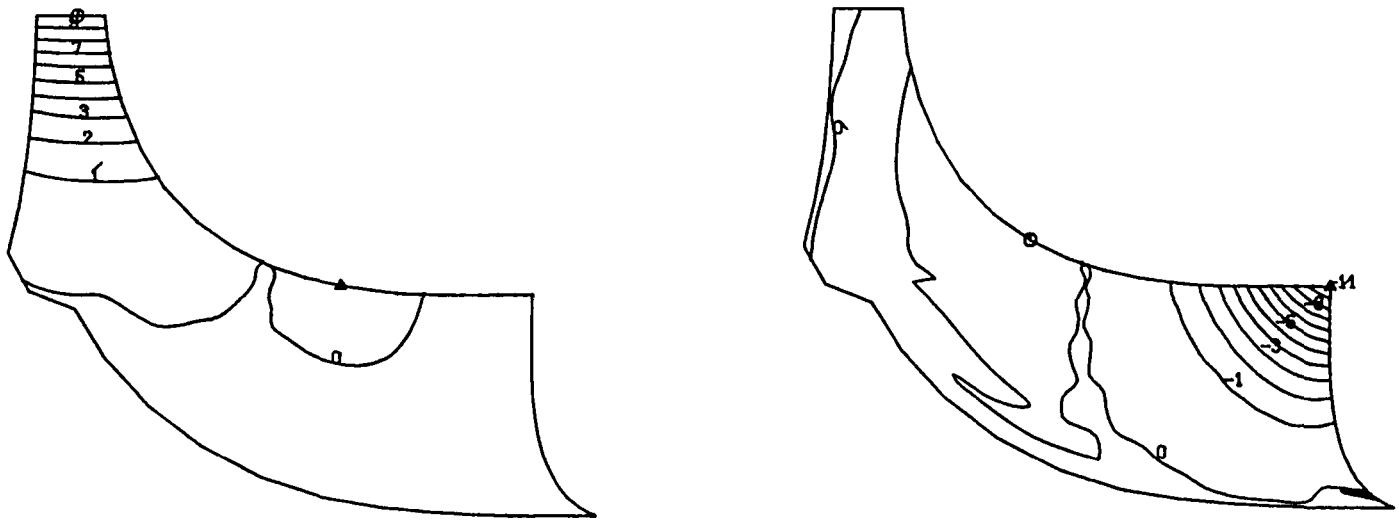

MODE 1
FREQUENCY = 12,794 Hz

MODE 2
FREQUENCY = 15,110 Hz

SCALE FACTOR = 2.00

RPM = 80,000

⊕ MAXIMUM ⊖ MINIMUM

Figure 39. Normalized Deflections (Modes 1 and 2).

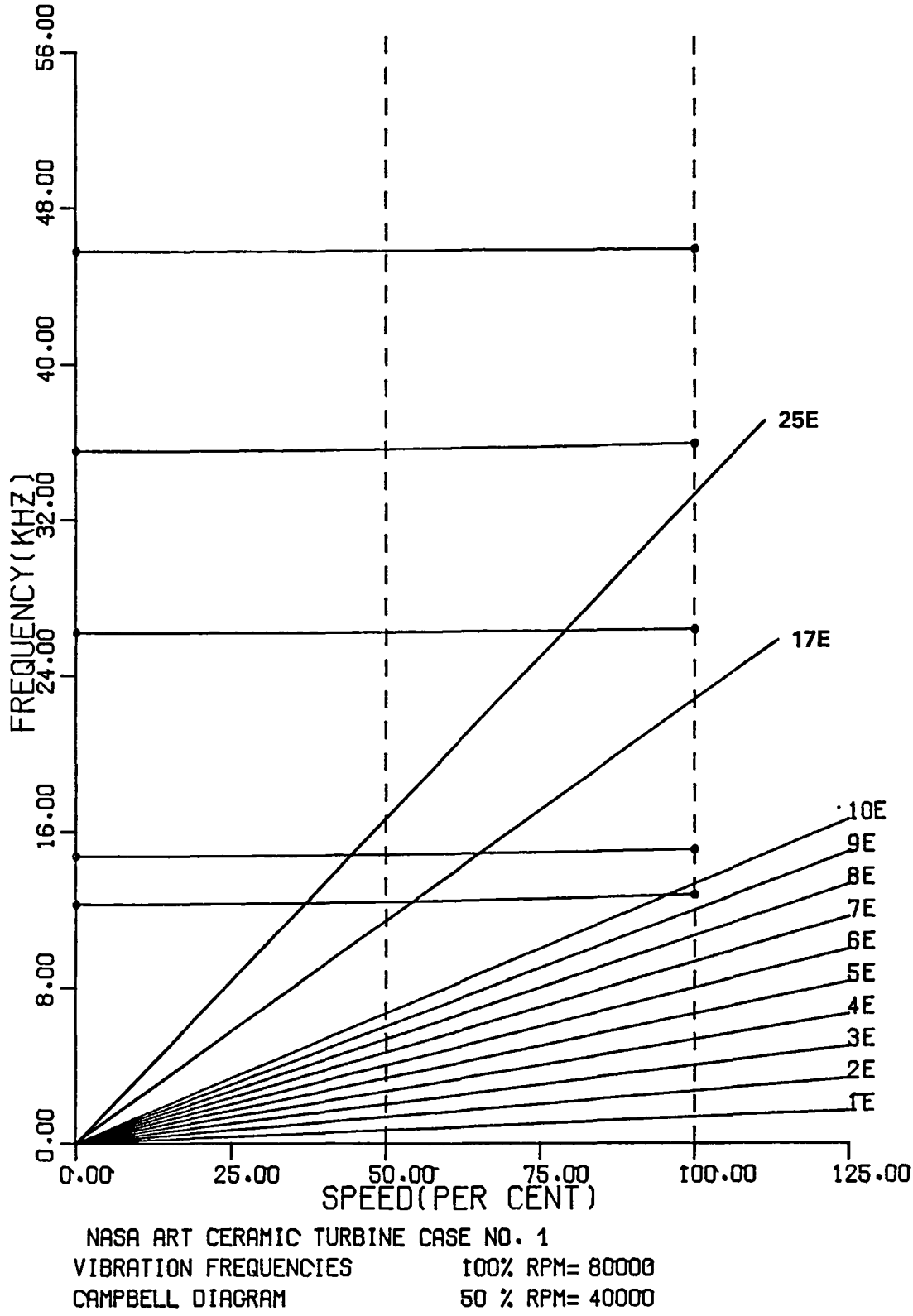

Figure 38. Campbell Diagram for 80,000-rpm Design.

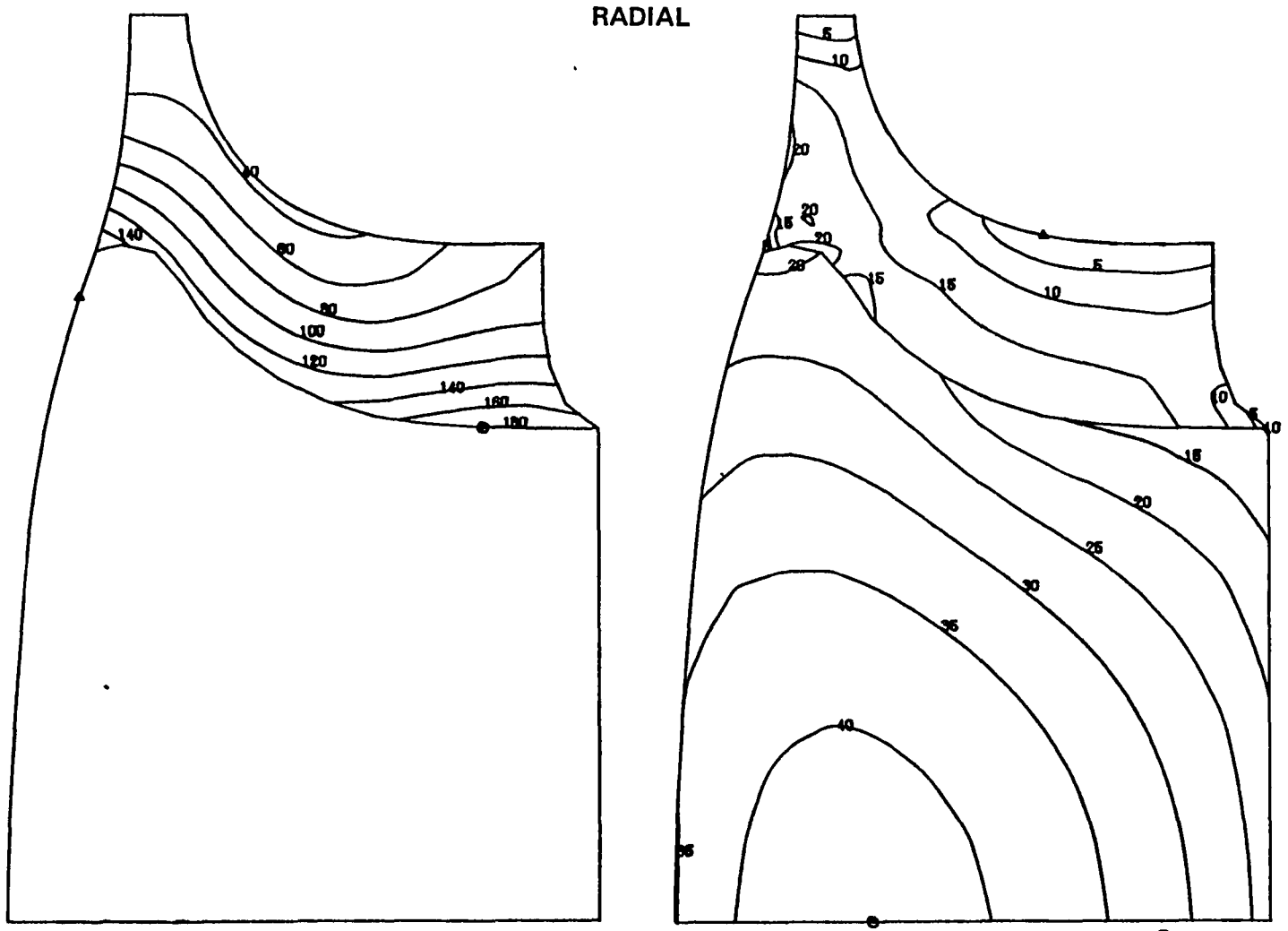

ISOPLETH INTERVAL = 0.051 CM (20 MILS)
TANGENTIAL THICKNESS
SCALE FACTOR = 1.50
⊙ MAXIMUM △ MINIMUM

ISOPLETH INTERVAL = 3.447 kN/cm^2 (5 ksi)
RPM = 80,000
TIP SPEED = 701 m/sec (2300 fps)
N_B = 12

Figure 37. Tangential Thickness and Maximum Principal Stresses.

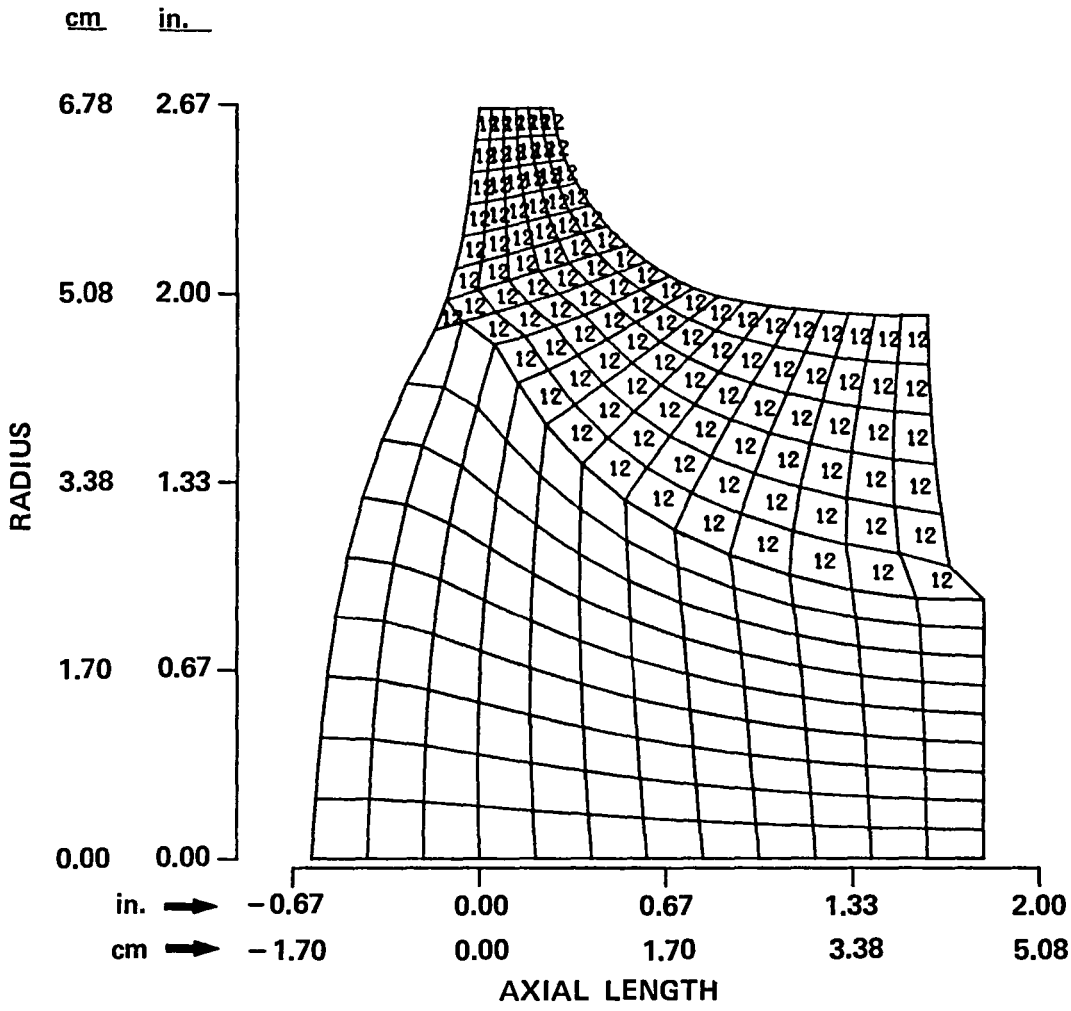

Figure 36. Two-Dimensional Finite Element Model for ISOPDQ.

The basic flow paths depicted in Figure 31 were examined for mechanical considerations using the 2-D finite element program, ISOPDQ (ref. 20), illustrated in Figure 36. Each flow path configuration was analyzed by an iteration on blade thickness and wheel/disk backface contour to achieve 2-D maximum principal blade stresses of 13.8 kN/cm^2 (20 ksi).

Figure 37 illustrates the tangential blade thicknesses and maximum principal stresses for 80,000 rpm with 12 blades. This configuration exceeds the 24.1 kN/cm^2 (35 ksi) stress limit in the disk. However, the blade vibration characteristics (Figure 38) are acceptable. The most critical blade vibration condition expected for this engine application is the stator vane passing frequency. This size engine will be designed with a range of stator counts from 17 to 25. With a stator count of 23, this design has only one blade-natural frequency in the engine operating range. This possible frequency interference is an exducer torsional third mode (Figures 39 and 40), which is not a problem with any existing radial turbines.

Figure 41 illustrates the blade tangential thicknesses and the maximum principal stresses for 95,000 rpm, with 58.1 cm^2 (9 $in.^2$) of rotor exit area and 12 blades. Both blade and disk stresses are within established limits. Based on the Campbell diagram of Figure 42, a stator count selection between 17 and 25 would not reduce the number of blade natural frequencies below two in the operating range. To alter the blade for this speed to a shape similar to the 80,000-rpm case, which exhibits better vibration characteristics, an exit area of 45.2 cm^2 (7 $in.^2$) was examined. Figure 43 illustrates the blade tangential thicknesses and maximum principal stresses for this exit area. Figure 44 shows that 23 stator vanes will reduce the number of blade-natural frequencies in the operating range to one. Figures 45 and 46 illustrate the mode shapes for this blade configuration.

Figure 47 illustrates the blade tangential stresses, and Figure 48 depicts the blade-natural frequencies for 110,000 rpm. The maximum principal stresses in the disk are somewhat lower than for 95,000 rpm, but the blade vibration characteristics appear to add considerable risk for this wheel configuration. Although maximum principal disk stresses continue to decrease as physical speed increases (Figure 49), blade vibration characteristics set a practical upward limit on physical speed to the 95,000- to 100,000-rpm range.

After the physical speed range was established, other mechanical parameters were examined. The first of these variables was the number of blades. When the blade count was varied from 10 to 16, very little change was observed in maximum stress at the center of the wheel (Figure 50). These slight changes in bore stress with changes in blade count indicate that bore stress is more dependent on disk size than blade configuration.

with an axial blade length of 4.1 cm (1.6 in.). However, the final axial length and blade number was established during the detail rotor design.

3.9 Parametric Study for Two-Dimensional Mechanical Analysis

The mechanical analysis was initiated with the characteristic flow path configurations that resulted from the parametric study for 80,000, 95,000, and 110,000 rpm.

The life objective of the program was to achieve a fast fracture modulus of rupture (MOR) probability of success of 0.9999, using a selected ceramic material with a characteristic strength of 62.1 kN/cm^2 (90 ksi) and a Weibull modulus of 15. These material property values are projections of selected ceramic material capability for the 1983 time period and were derived from a review of current ceramic matrials and associated processing capabilities. The following projected 1983 properties for near-theoretical density Si_3N_4 and SiC were used as a basis for this design study:

Material	Projected Strength (KSI)		Weibull m	
	RT	1100°C	RT	1100°C (2012°F)
Si_3N_4	100	90	15	15
SiC	90	90	15	15

To provide meaningful probability of success calculations, stresses must be integrated over both the surface area and volume. Three-dimensional stress analysis is required to make the integrations. Initially, however, to examine a large number of configurations in the parametric study, a 2-D stress analysis at room temperature was used.

Based on previous experience with ceramic radial turbines (utilizing similar material properties), stress limits of 13.8 kN/cm^2 (20 ksi) in the blades and 24.1 kN/cm^2 (35 ksi) in the disk were established. The blade limit for the 2-D analysis [13.8 kN/cm^2 (20 ksi)] was fixed at a level providing adequate stress margin to accommodate stress concentrations in the complex geometry of the blade/disk interface region. The 2-D finite element program does not compute concentrations in this transition region.

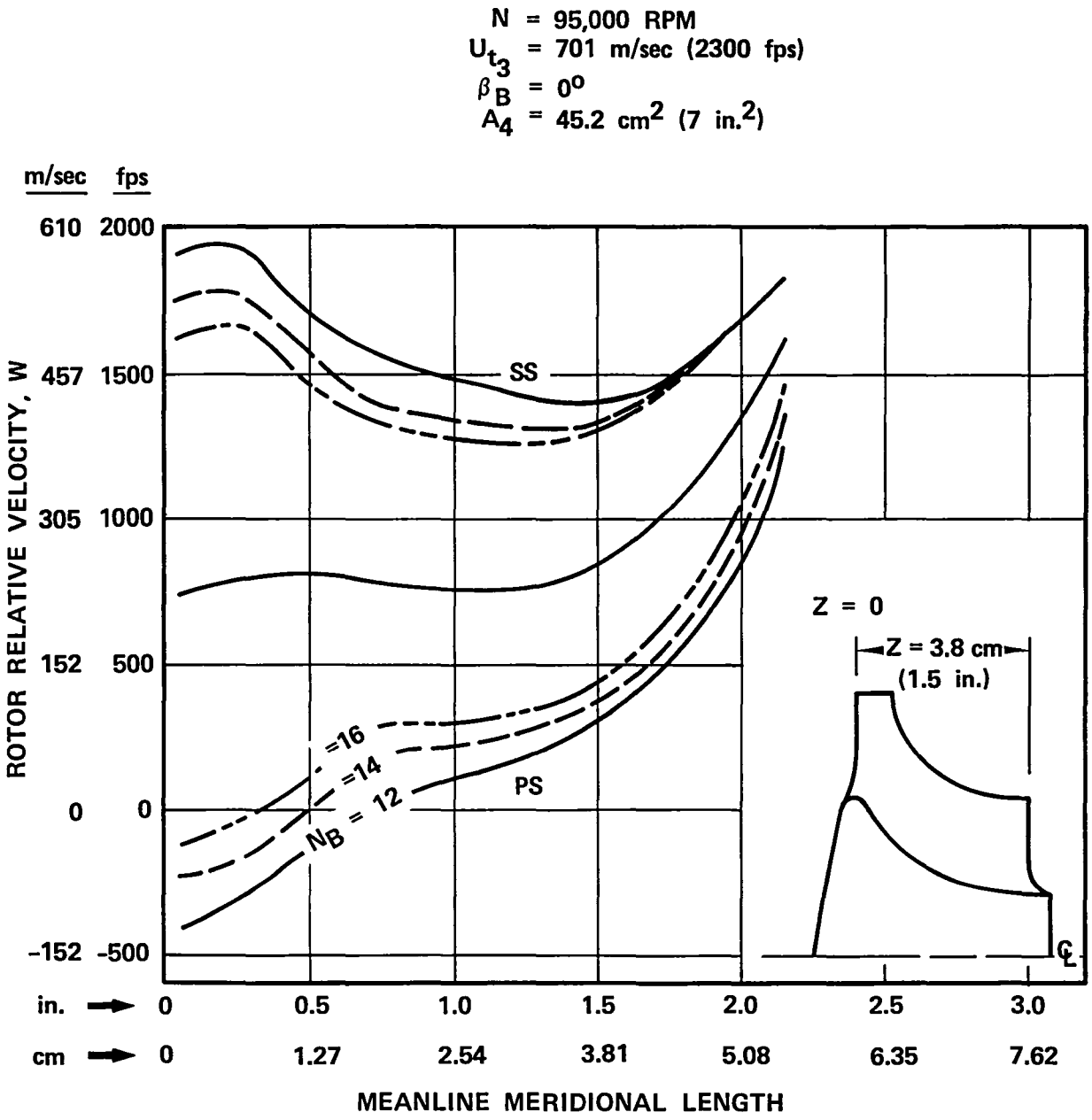

Figure 35. Rotor Solidity Study, Axial Length = 3.8 cm (1.5 in.).

N = 95,000 RPM
U_{t_3} = 701 m/sec (2300 in.)
β_B = 0°
A_4 = 45.2 cm^2 (7 $in.^2$)

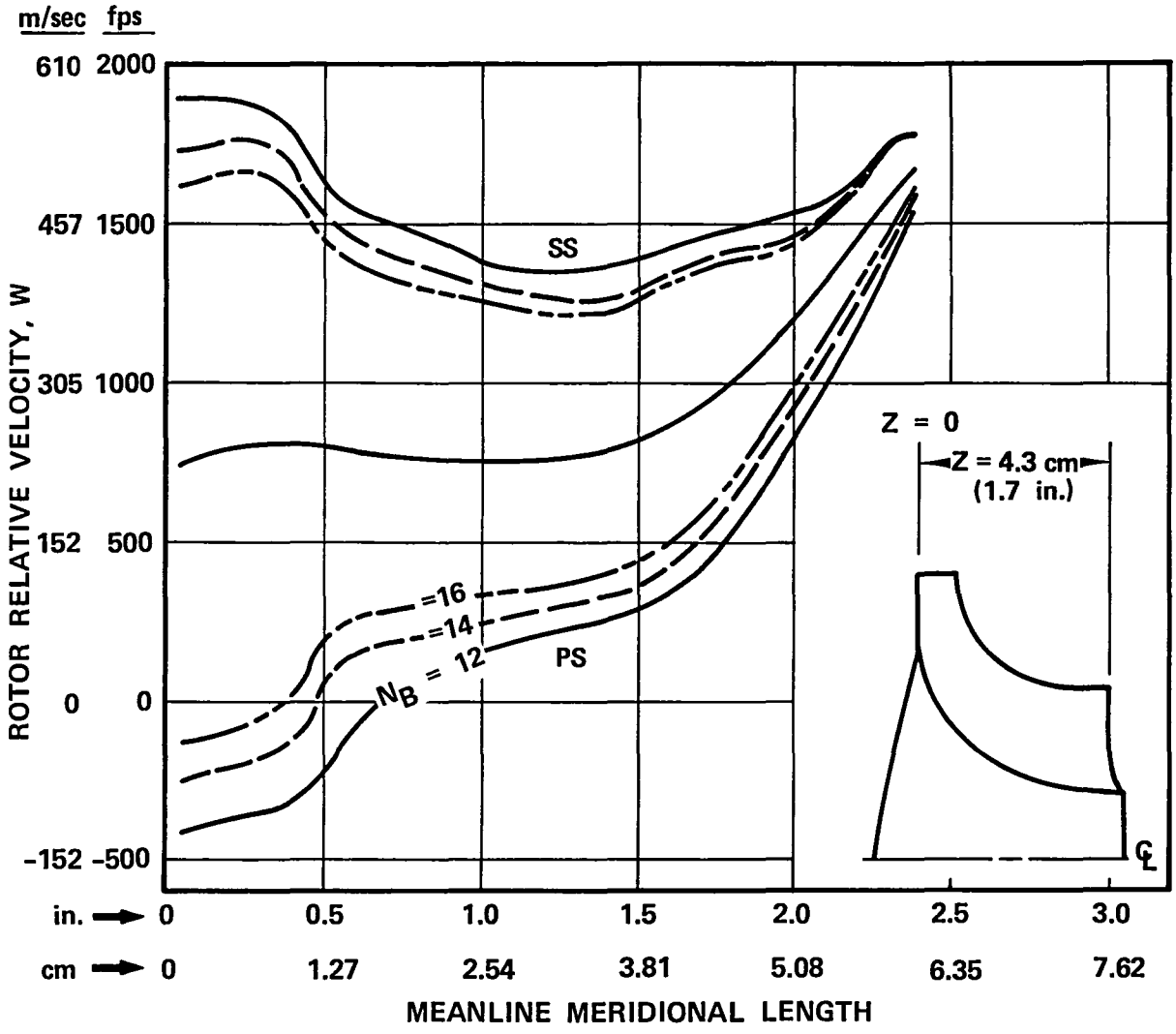

Figure 34. Rotor Solidity Study, Axial Length = 4.3 cm (1.7 in.).

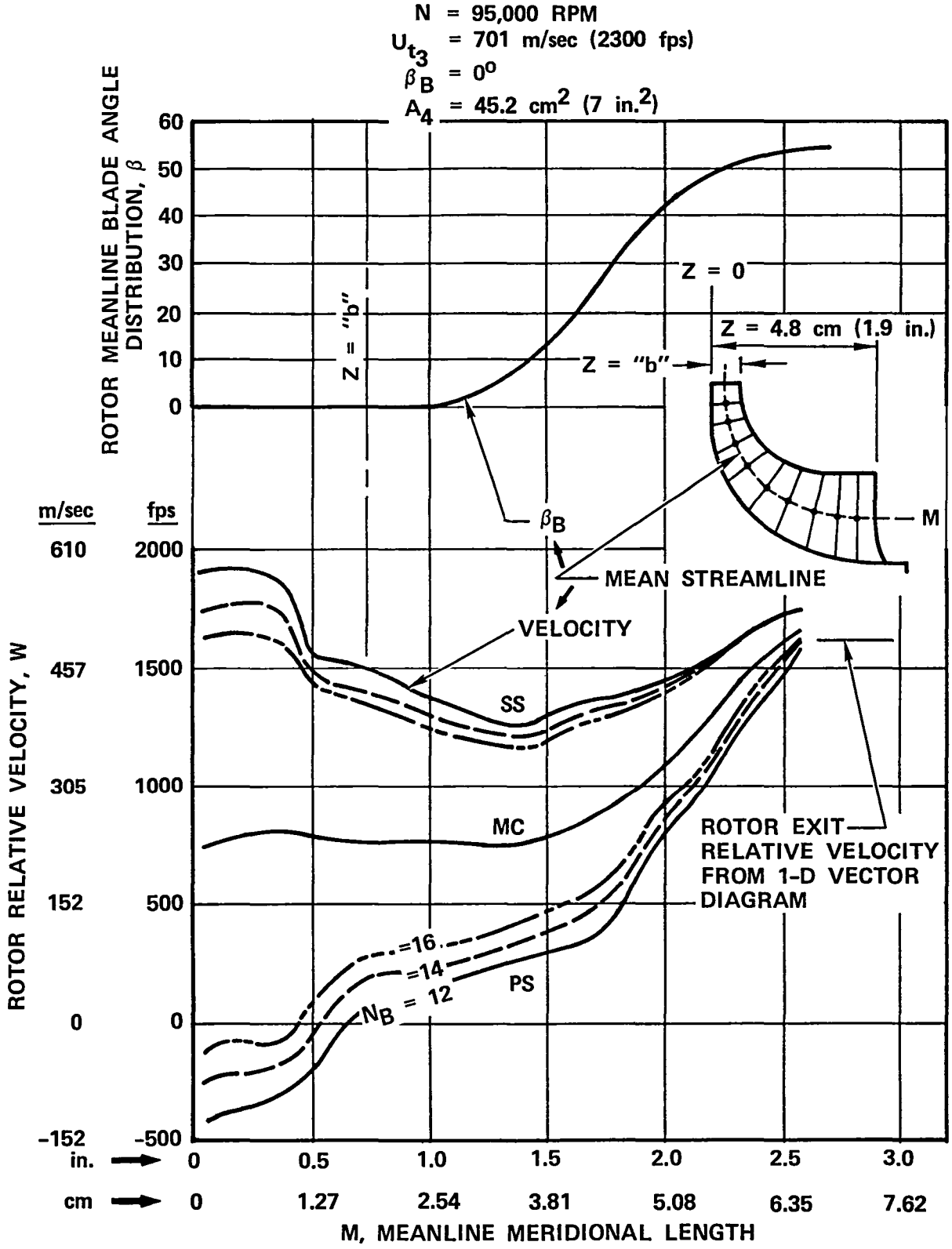

Figure 33. Rotor Solidity Study, Axial Length = 4.8 cm (1.9 in.).

N = 95,000 rpm
U_{t_3} = 701 m/sec(2300 fps)
β_B = 0°

λ_3 = 1.0
A_4 = 58.1 cm^2 (9 in.^{2})

NO DESWIRL VANES
R_{t_4}/R_{t_3} = 0.650

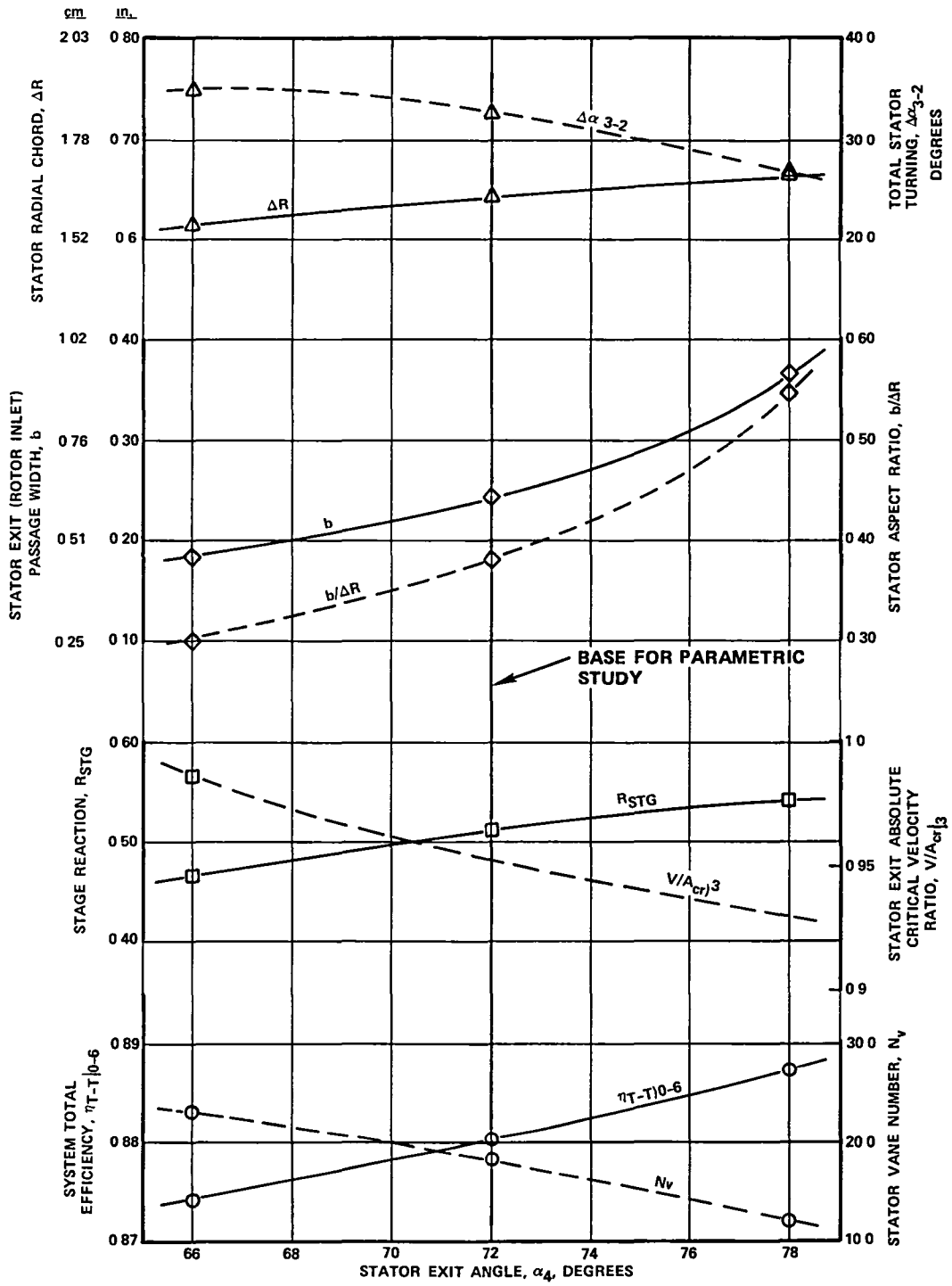

Figure 32. Stator Solidity Study, N = 95,000 rpm, β_B = 0°.

3.8 Stator and Rotor Solidity Studies

Since rotor inlet incidence loss is a function of the inlet stage work coefficient, the effect of stator exit flow angle can be examined independently at a constant work coefficient. The parametric study was based on a constant exit angle of 72 degrees, which has proven to be a reasonable compromise between the sensitivity of manufacturing tolerances and rotor shroud and backface clearance effects. The effect of varying the stator exit angle is illustrated in Figure 32. For the study, stator trailing edge thickness and blockage were held at 0.030 in. and 10 percent, respectively. The following characteristics are observed:

- From continuity, increasing the stator exit angle increases the stator exit "b" width (also the rotor inlet "b" width)
- For a constant stator loading, exit blockage, and trailing edge thickness, increasing stator exit angle increases the stator aspect ratio ($b/\Delta R$)
- Increasing the stator exit angle reduces the rotor inlet relative velocity and increases rotor reaction
- For an increase in stator exit angle from 66 to 78 degrees, system efficiency increases by 1.3 points due to reduced shroud and backface clearance effects and increased reaction effects

The rotor axial chord was evaluated on the basis of a mean line loading. The loading was established by treating the entire flow path as a stream tube and by solving the equations of continuity and energy from inlet to exit with the estimated flow path and rotor blade angle distribution. The condition of zero absolute vorticity was used to establish the blade suction and pressure surface velocities.

The results of this analysis for the 701-m/sec (2300-fps), 95,000-rpm configuration are presented in Figures 33 to 35 for axial lengths of 4.8, 4.3, and 3.8 cm (1.9, 1.7, and 1.5 in.), respectively. For each axial length examined, a range of rotor blade numbers from 12 to 16 was evaluated. The results show that inducer loading was not affected by axial length, since the blade angle distribution in this region was fixed with radial blades. However, in the exducer and trailing edge region, the blade loading was significantly affected by axial length due to the rate of change in rotor blade angle. Conversely, the rotor blade number resulted in a change in rotor blade loading throughout the entire flow path, as expected. On the basis of this study, an axial length between 4.1 and 4.3 cm (1.6 and 1.7 in.) resulted in satisfactory rotor blade velocity distributions. The majority of the mechanical analysis was performed

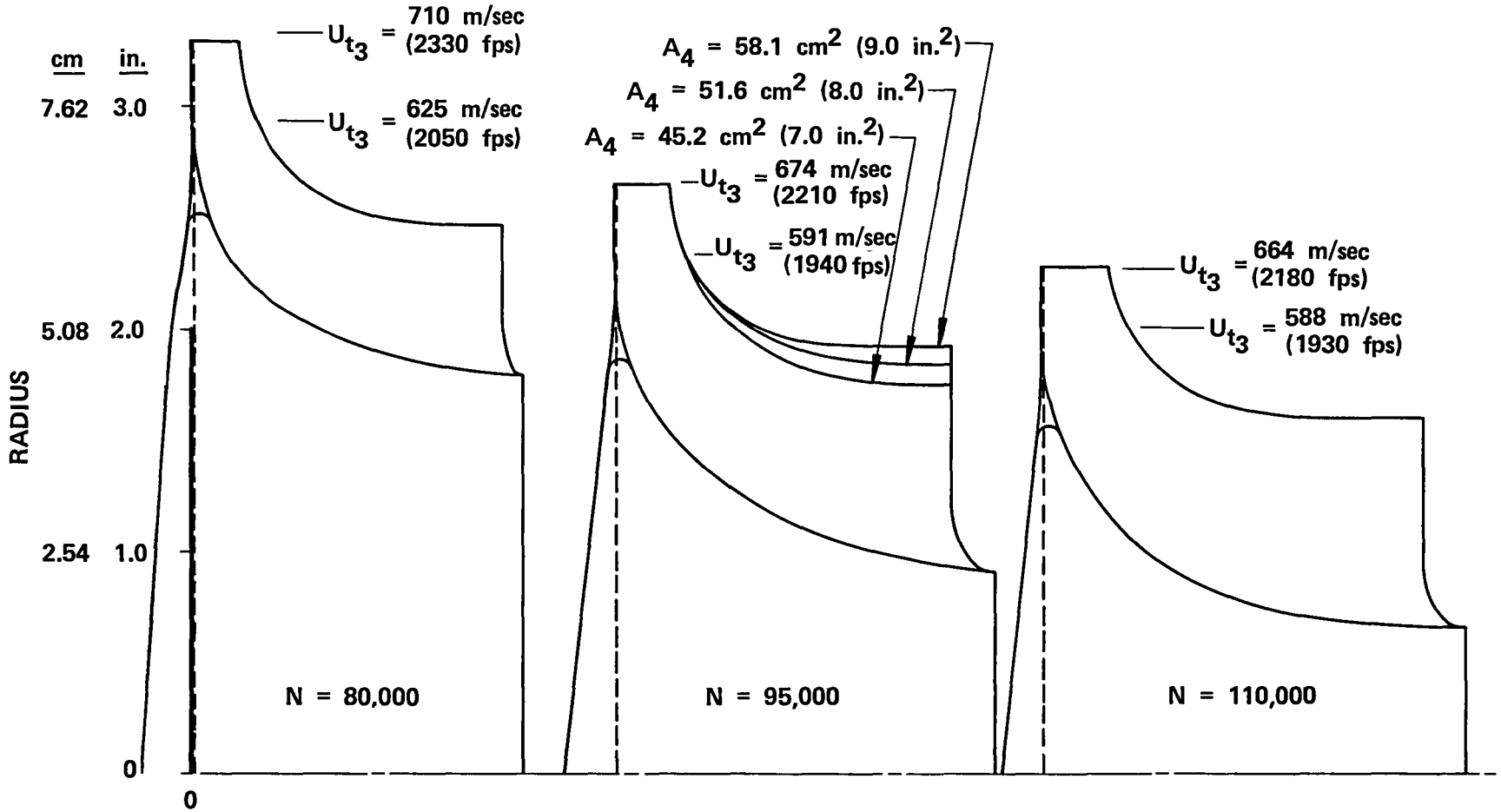

Figure 31. Characteristic Rotor Flow Path Configurations for Selected Parametric Study Rotational Speeds.

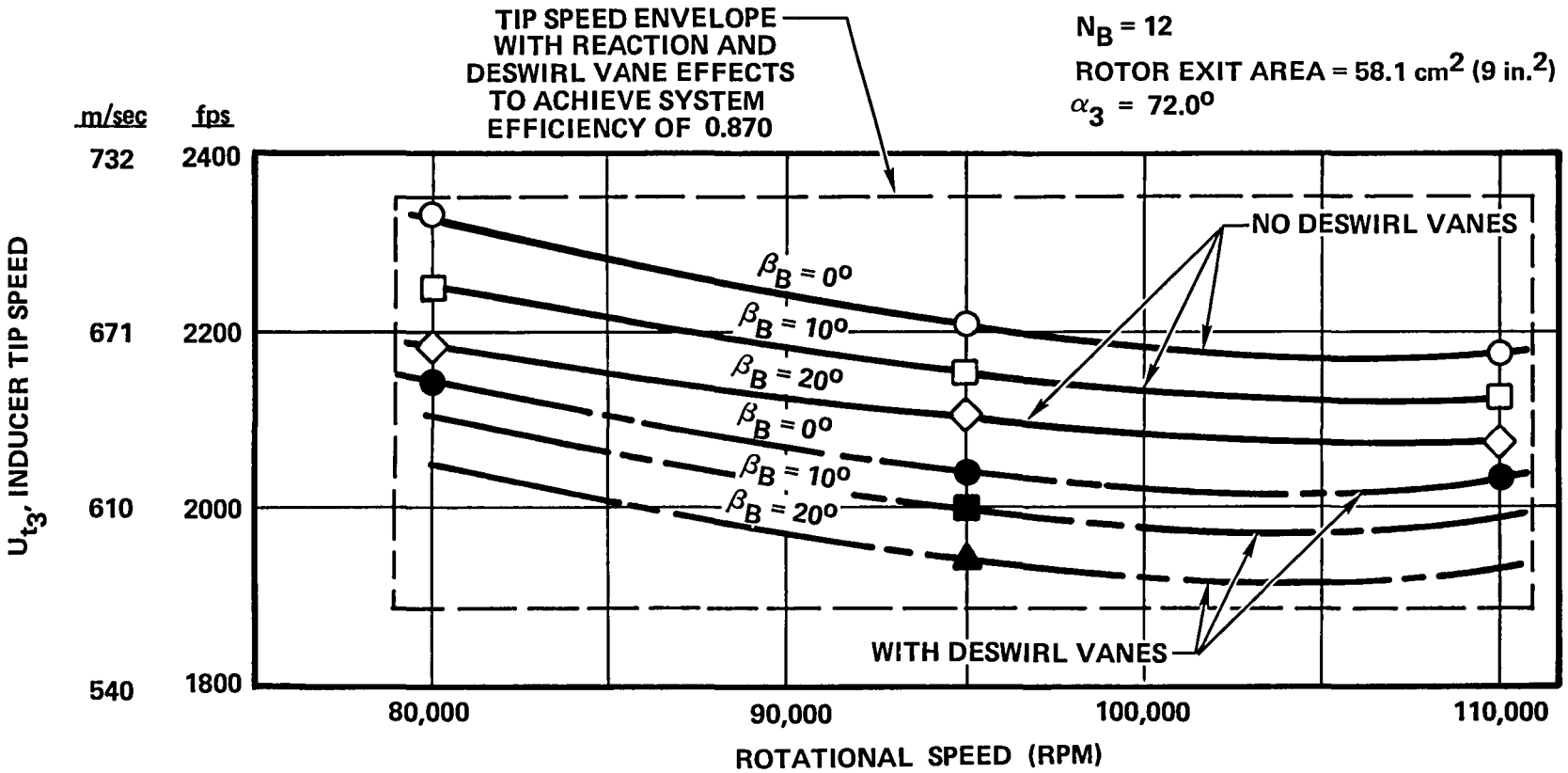

Figure 30. Tip Speed Envelope with Reaction and Deswirl Vane Effects, but No Rotor Exit Blockage Effects.

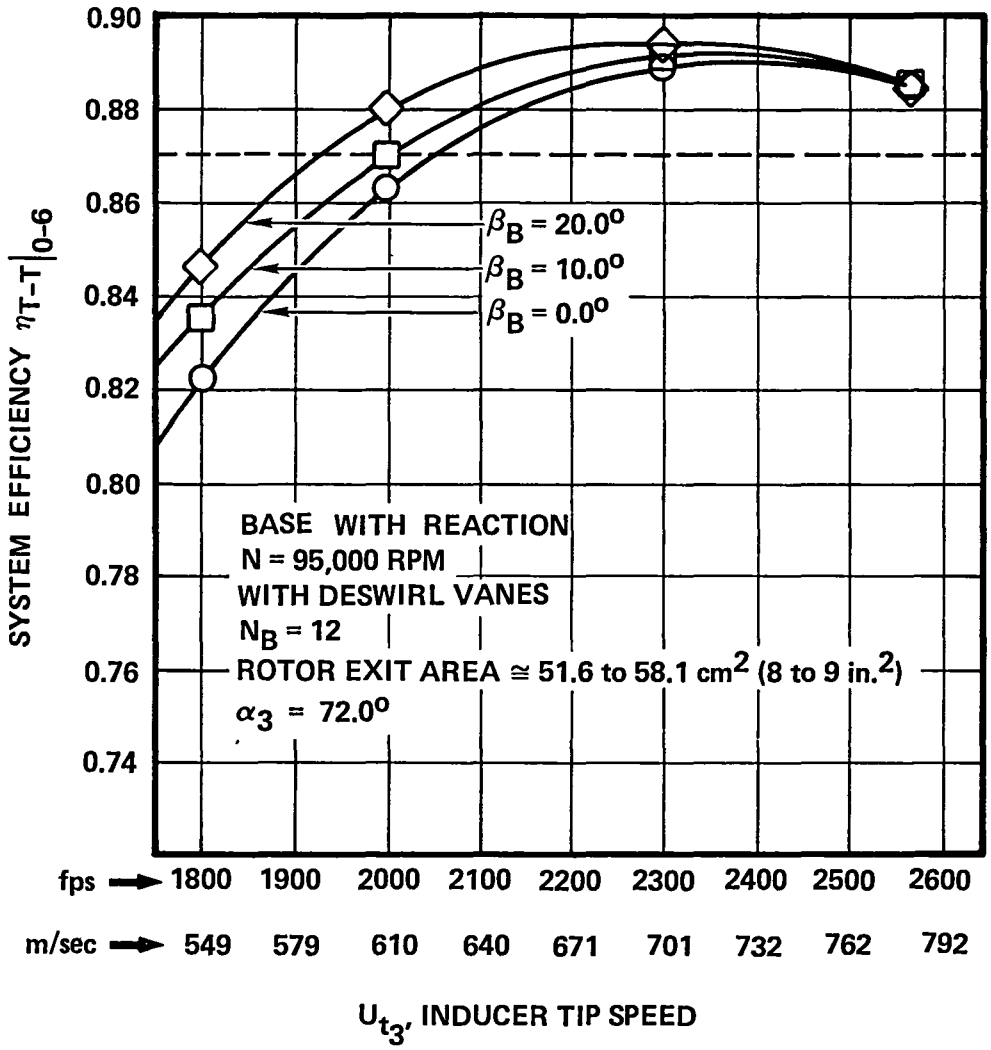

Figure 29. Peak System Efficiency for 95,000 rpm with Deswirl Vanes.

- N = 110,000
- N_B = 12
- REACTION EFFECTS
- NO DESWIRL VANES
- ROTOR EXIT AREA ≅ 58.1 cm^2 (9 $in.^2$)
- α_3 = 72.0°

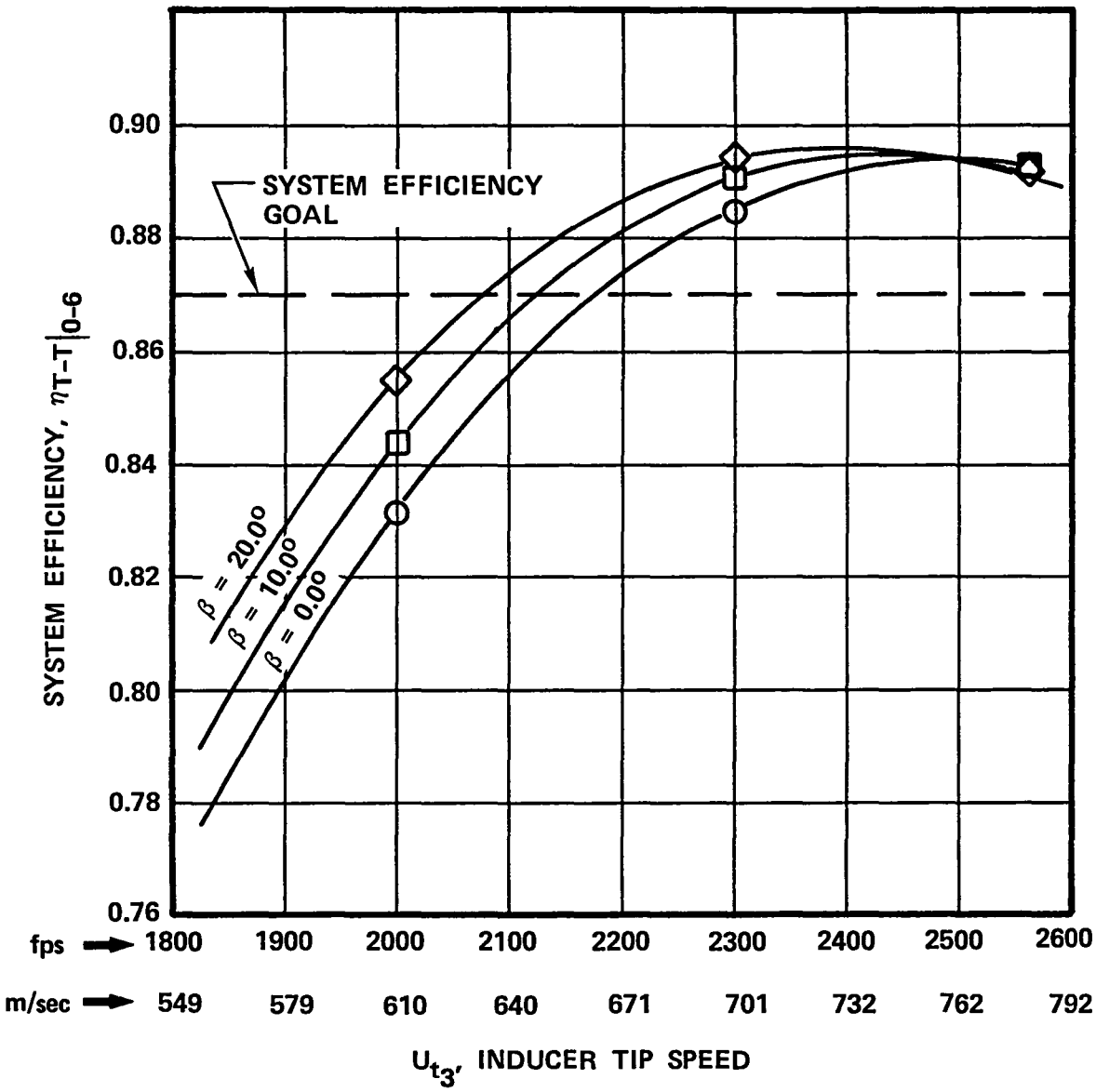

Figure 28. Peak System Efficiency for N = 110,000 rpm.

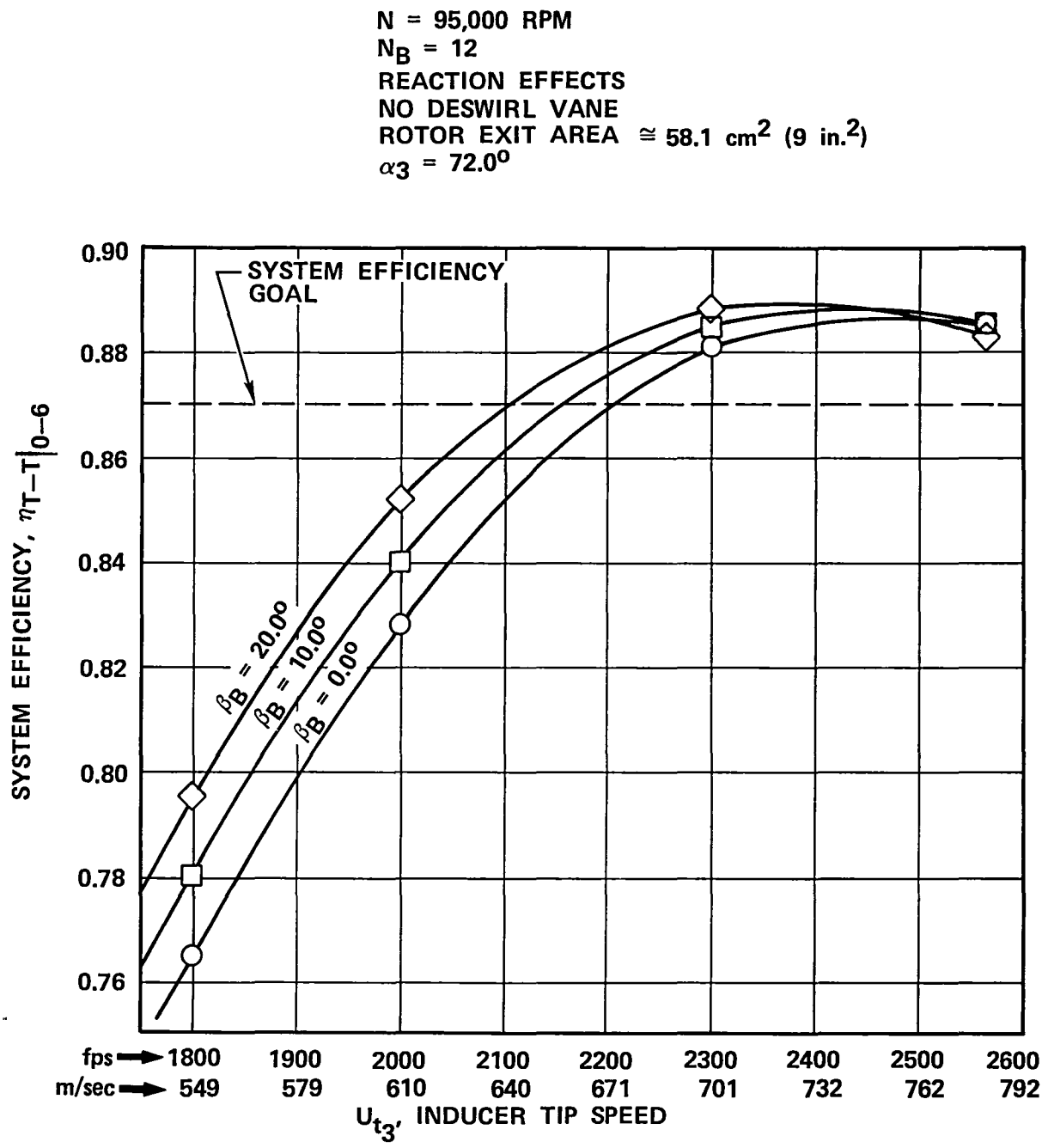

Figure 27. Peak System Efficiency for N = 95,000 rpm.

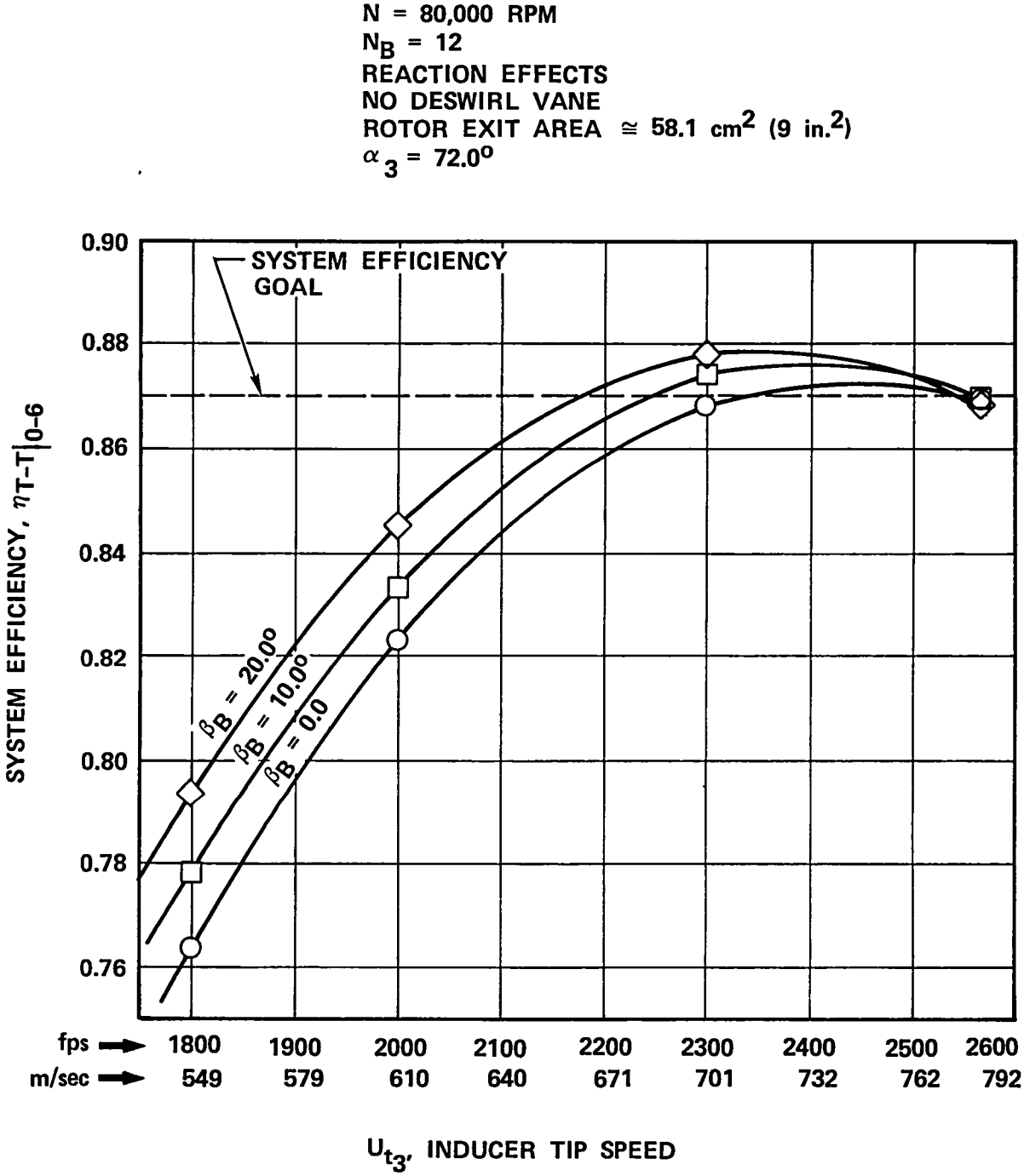

Figure 26. Peak System Efficiency for N = 80,000 rpm.

characteristic shown is at the rotor exit mean-line, significantly higher relative critical velocity ratios would occur in the rotor exit tip region and shock losses should be evaluated.

To define a tip speed envelope that will achieve the cycle performance goals, the peak system performance from Figures 14 through 22 was first plotted as a function of tip speed and range of inducer blade angles, as shown in Figures 26 through 29. The results showed the magnitude of tip speed required for each rotational speed and also the effect of rotor inlet blade angle on required tip speed. Figure 29 shows these characteristics with deswirl vanes for 95,000 rpm. These results were cross-plotted in Figure 30 in terms of tip speed versus shaft speed, and a tip speed envelope was obtained. The envelope shows that without rotor exit blockage effects, tip speed requirements range between 579 and 716 m/sec (1900 and 2350 fps) depending on inlet blade angle, shaft speed and deswirl vane specification.

Characteristic rotor flow paths for the three shaft speeds are presented in Figure 31. At 80,000 rpm, the basic flow path resulted in a relatively small blade, large disk configuration. Conversely, at 110,000 rpm the flow path resulted in a relatively large blade, small disk configuration. Although the radius ratio at 80,000 rpm could be decreased to match the exit hub radius at 110,000 rpm, this was not shown for two reasons. First, the parametric study showed increasing performance as radius ratio increased. Second, the inducer blade height increased by a factor of approximately 2.0, requiring a significant increase in blade thickness to maintain equivalent inducer blade stress levels. In addition, the increased blade height was expected to result in undesirable blade vibration characteristics.

Additional observations from Figure 31 are:

- In addition to the smaller blade height dimensions associated with 80,000 rpm, the large disk also would increase rotor weight and inertia, which penalizes vehicle response time; therefore, driveability may suffer. However, rotor exit hub blockage would be minimized, and the number of blades could be increased.

- At 110,000 rpm, rotor weight and inertia would be minimized, and rotor blade height would be maximized, but the reduced rotor exit hub radius would significantly increase exit blockage or severely limit the number of blades. Mechanically, the relatively tall exducer blades could result in unacceptable blade vibration characteristics.

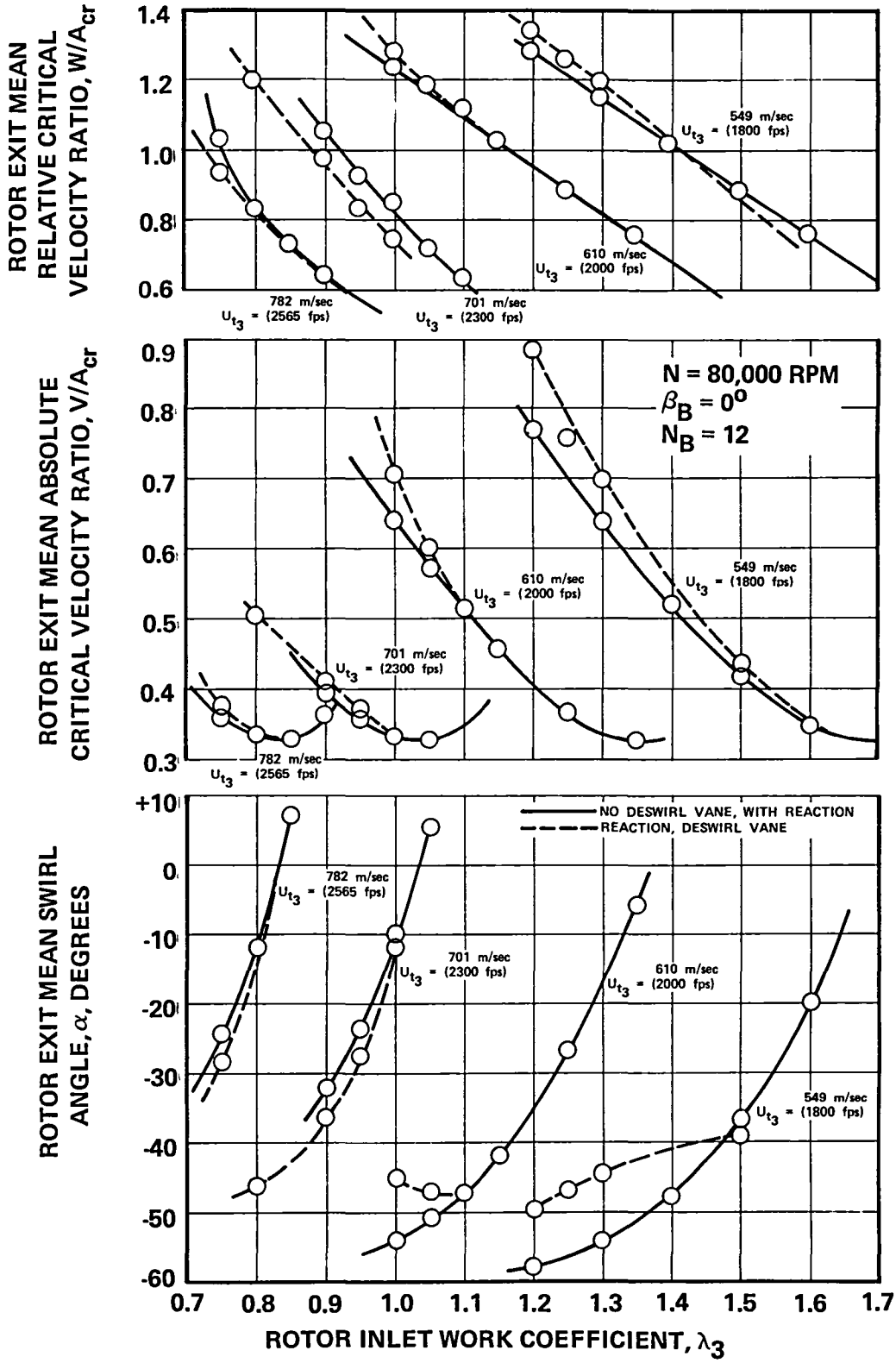

Figure 25. Turbine Vector Diagram and System Parameters Along Individual Tip Speed Envelopes, N = 80,000 rpm, β_B = 0° (Cont).

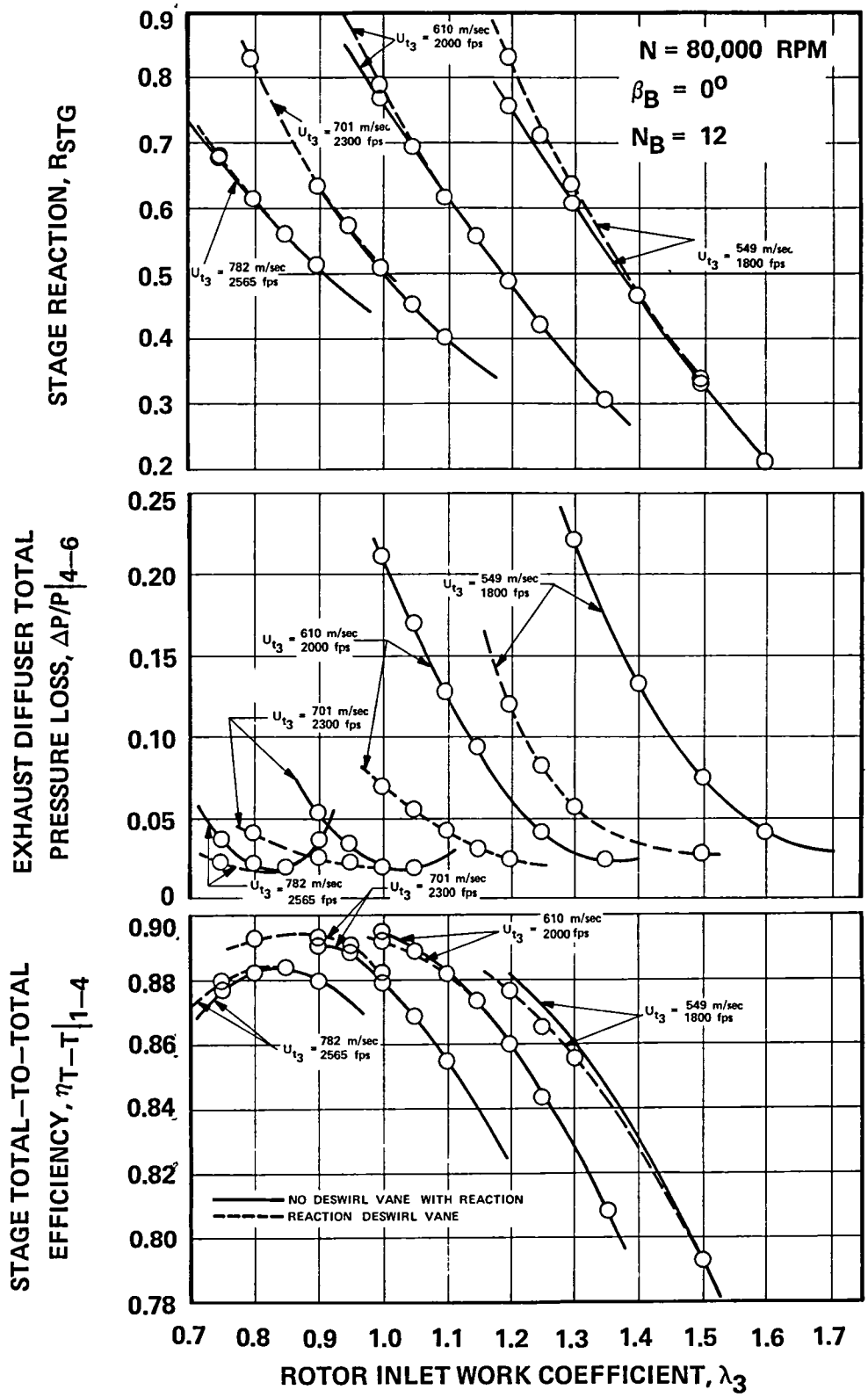

Figure 24. Turbine Vector Diagram and System Parameters Along Individual Tip Speed Envelopes, N = 80,000 rpm, β_B = 0°.

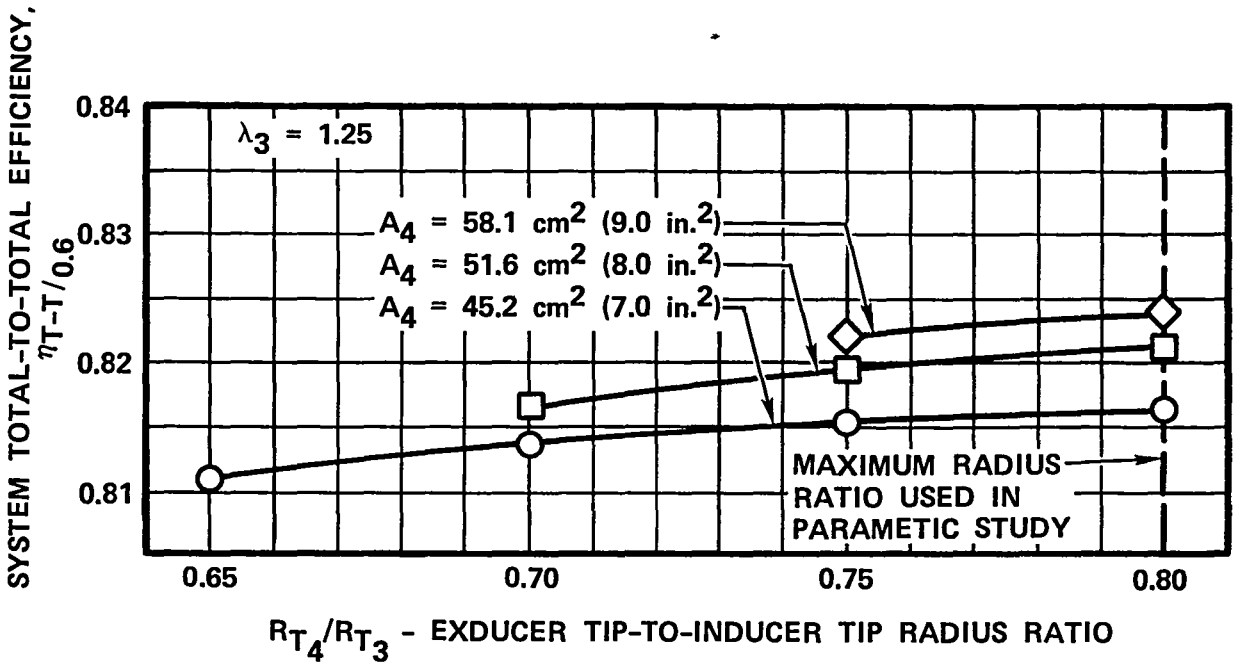

(A) U_{t_3} = 610 m/sec (2000 fps)

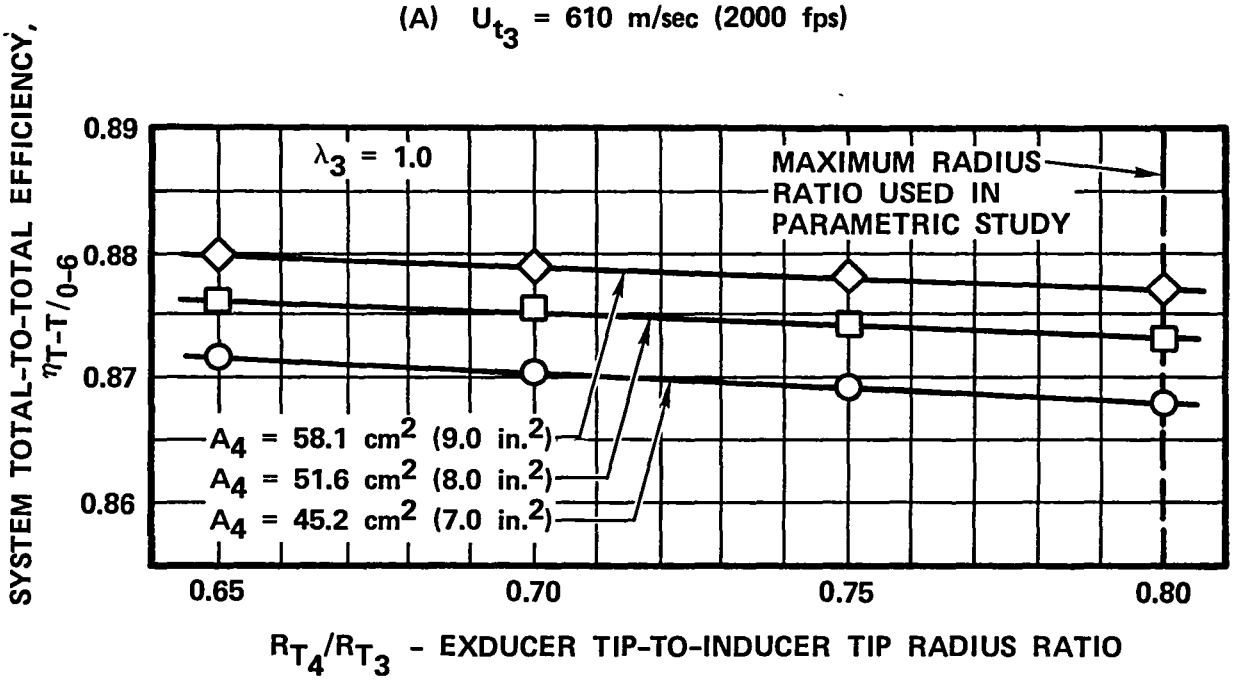

(B) U_{t_3} = 701 m/sec (2300 fps)

Figure 23. Effects of Rotor Exit Area and Radius Ratio on Turbine System Efficiency, N = 95,000 rpm, β_B = 0°, No Deswirl Vanes.

RADIAL

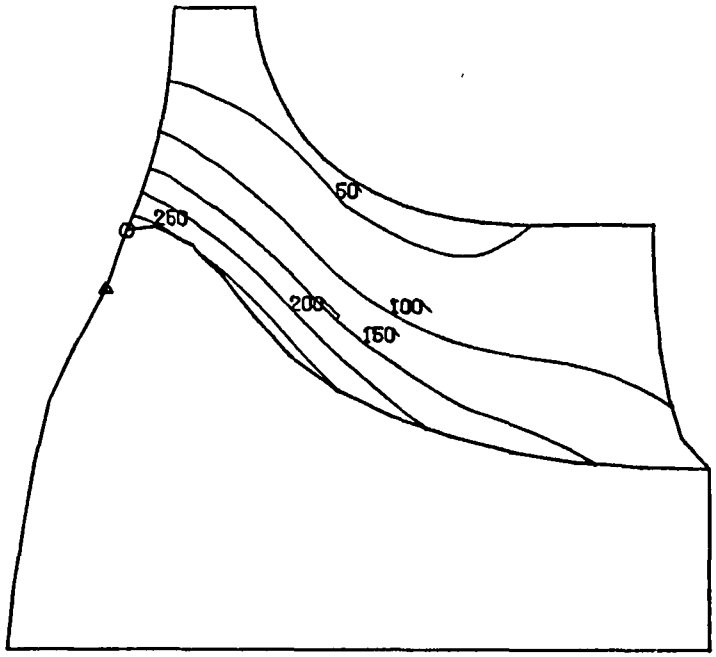

ISOPLETH INTERVAL = 0.127 cm (50 mils)

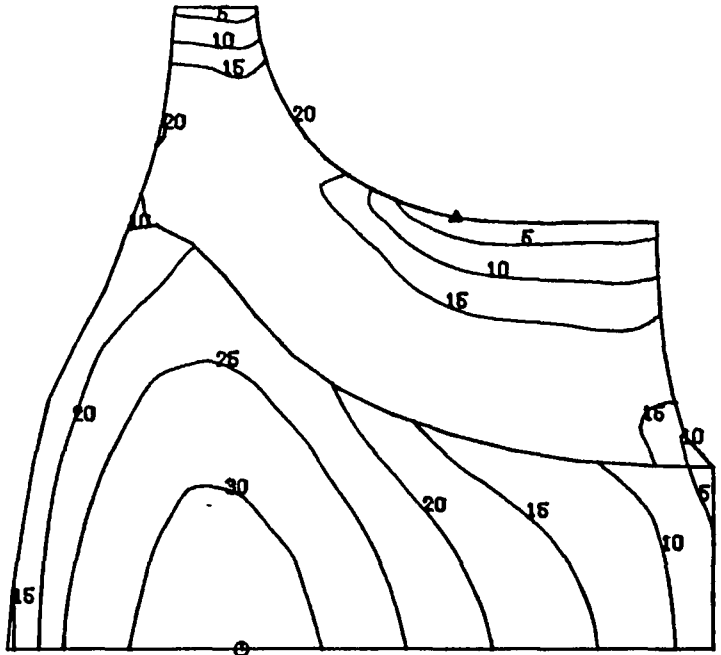

ISOPLETH INTERVAL = 3.447 kN/cm^2 (5 ksi)

TANGENTIAL THICKNESS

SCALE FACTOR = 1.50

⊙ MAXIMUM △ MINIMUM

RPM = 110,000
TIP SPEED = 658 m/sec (2160 fps)
N_B = 12

Figure 47. Tangential Thicknesses and Maximum Principal Stresses.

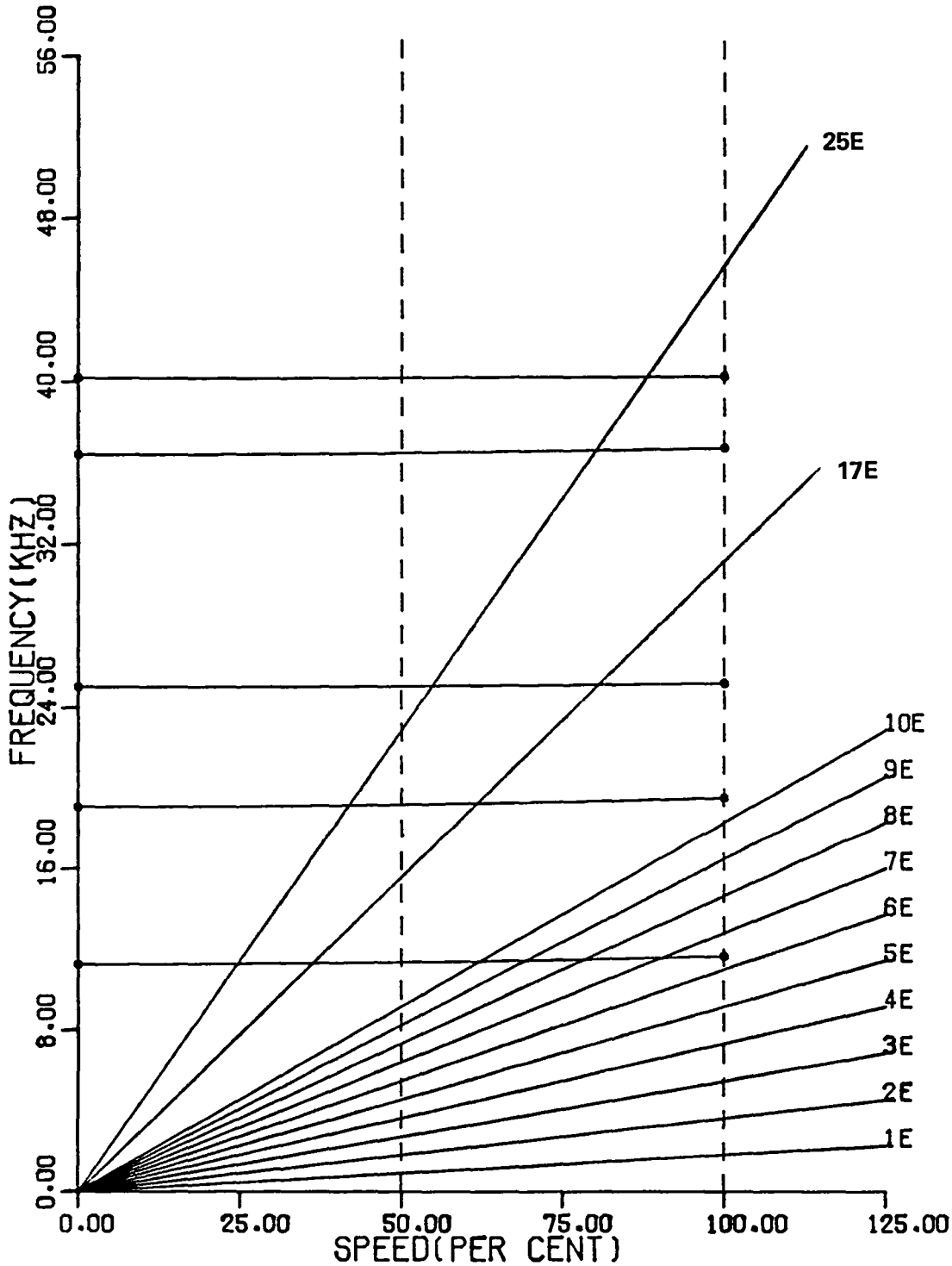

Figure 48. Campbell Diagram for 110,000-rpm Case.

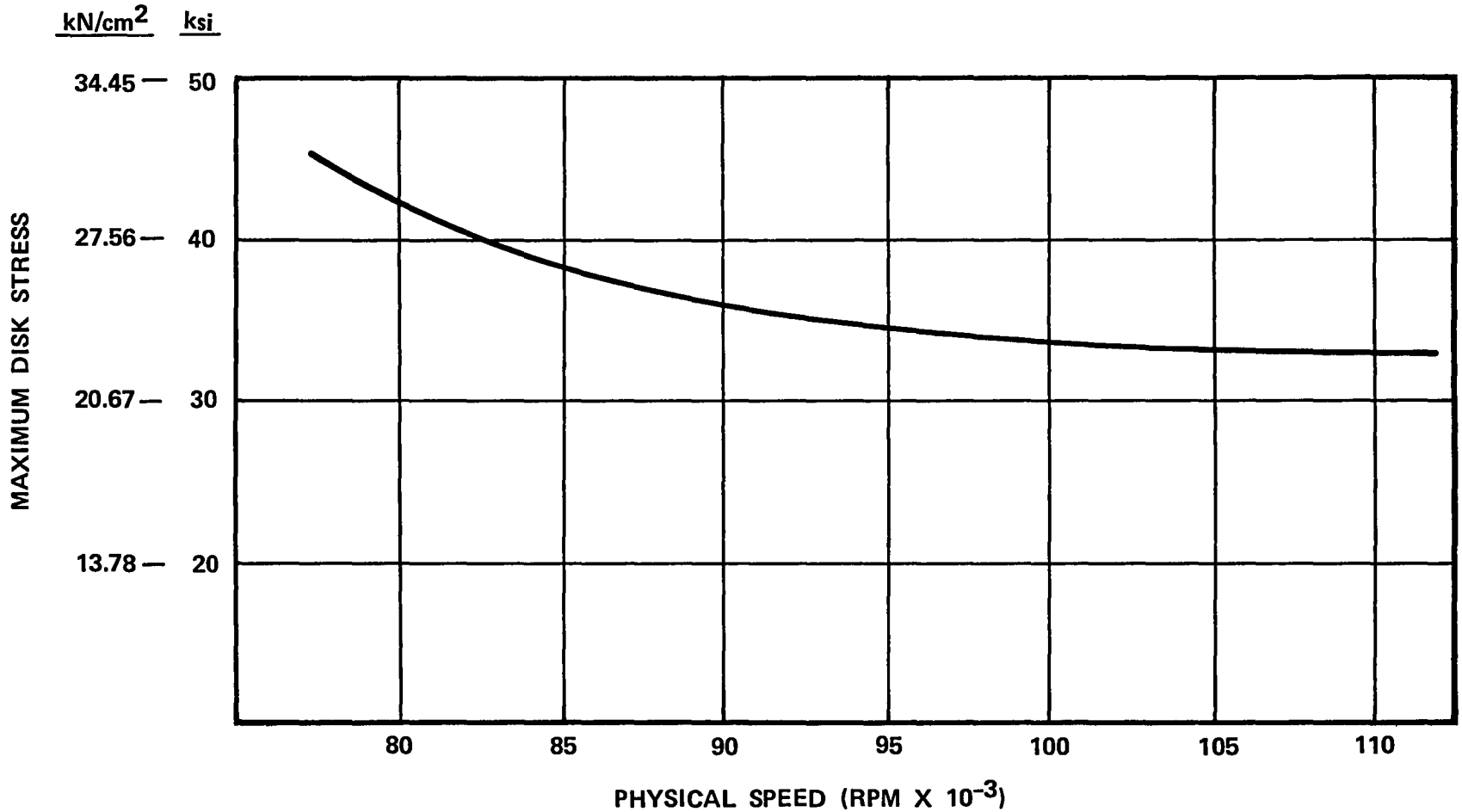

Figure 49. Effect of Speed on Maximum Principal Disk Stress.

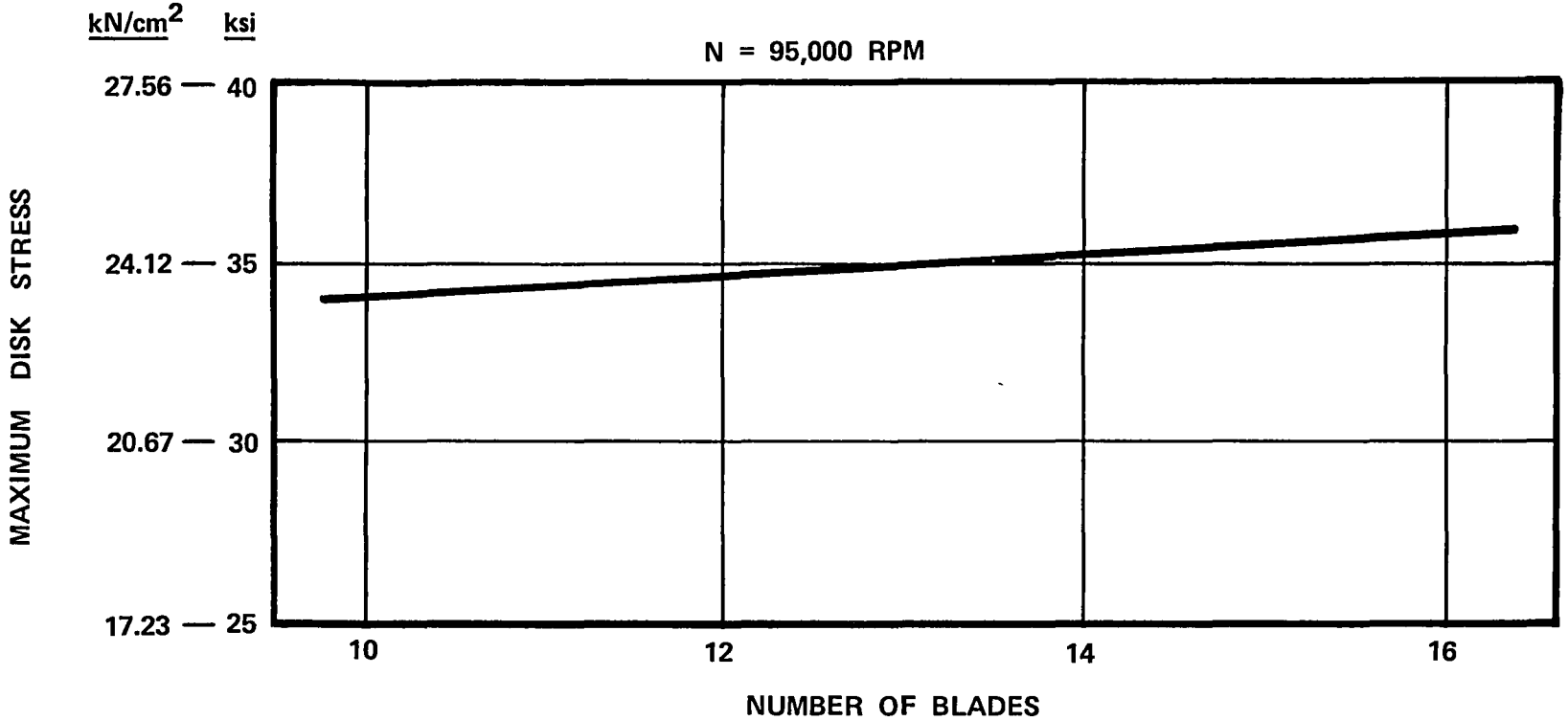

Figure 50. Maximum Disk Stress Versus Number of Blades.

Another parameter to be varied was tip speed. This variation was accomplished by keeping the flowpath constant for 95,000 rpm, with an exit area of 45.2 cm^2 (7 in^2.) and varying the inducer tip radius. Figures 51 and 52 show the tangential thicknesses and maximum principal stresses for tip speeds of 634 m/sec (2080 fps), and 70 m/sec (2300 fps), respectively. The maximum disk stresses for the 701 m/sec (2300 fps) are somewhat higher than for the 634 m/sec (2080 fps) but are within the 24.132 kN/cm^2 (35 ksi) stress limit. Figure 53 summarizes the maximum disk stresses as tip speed is varied.

3.10 Parametric Study of Detail Aerodynamic Analysis

Since mechanical analysis indicated that disk stress and blade thickness would increase with the higher rotor exit area, and the rotor blade vibration characteristics were more favorable at the lower 45.2 cm^2 (7 $in.^2$) rotor exit area, typical vector diagrams with and without deswirl vanes were selected for 45.2 cm^2 (7 $in.^2$) cases. Two-dimensional vector diagrams were calculated as a function of rotor exit blockage.

For the case without deswirl vanes, the rotor exit average relative critical Mach number (W/A_{Cr}) varies between 0.70 and 0.80, and with a deswirl vane, the critical Mach number varies between 1.0 and 1.1. The general results in terms of a rotor relative total pressure loss ratio and hub blockage are presented in Figure 54. When the effects of rotor blockage and blade number are combined, a minimum loss with and without deswirl vanes is defined as in Figure 55. The high penalty associated with the deswirl vane case is attributed to the higher rotor exit Mach number and exit angle due to the increased rotor exit swirl.

To illustrate the combined effects of stage reaction and rotor exit blockage on system efficiency, the 95,000 rpm base solutions from Figure 17 were utilized. The results are presented in Figure 56. Since the parametric study indicated system efficiency increased with increasing rotor exit area, the overall effect of exit area, with reaction and blockage also was included. The radius ratio was fixed at 0.80. The characteristics derived from the basic parametric study are shown at the bottom of Figure 56 as a function of inducer tip speed and exit area. The change in efficiency as a function of stage reaction alone is next shown (derived from Figure 13). As indicated, the benefits of higher exit area are already partially offset due to lower reaction. In addition, the higher incidence loss associated with low tip speeds is further compounded by relatively high losses due to reduced reaction.

The rotor exducer blade thickness and blockage correlation derived from the 2-D mechanical analyses, together with the calculated 2-D rotor exit vector diagrams then were used to obtain a efficiency penalty for rotor exit blockage. Since the rotor

RADIAL

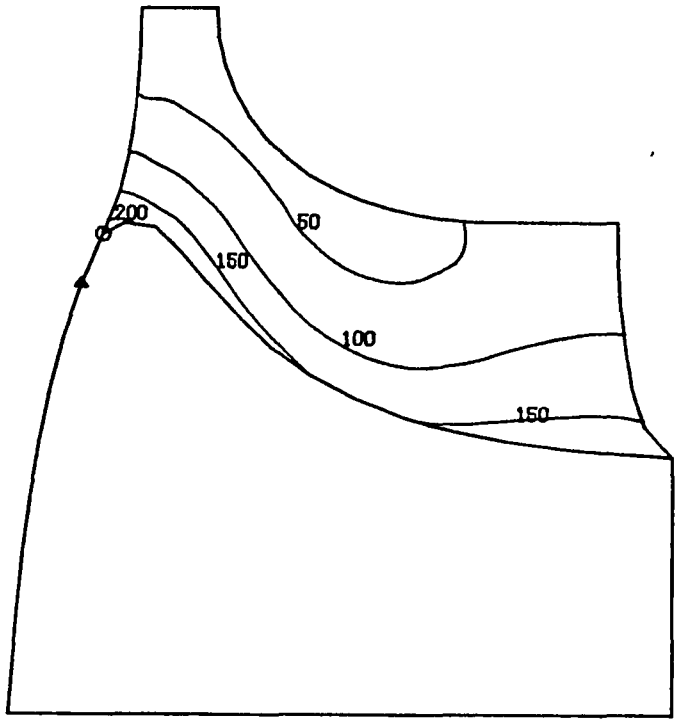

ISOPLETH INTERVAL = 0.127 cm (50 mils)

TANGENTIAL THICKNESS

SCALE FACTOR = 1.50

⏲ MAXIMUM ⏃ MINIMUM

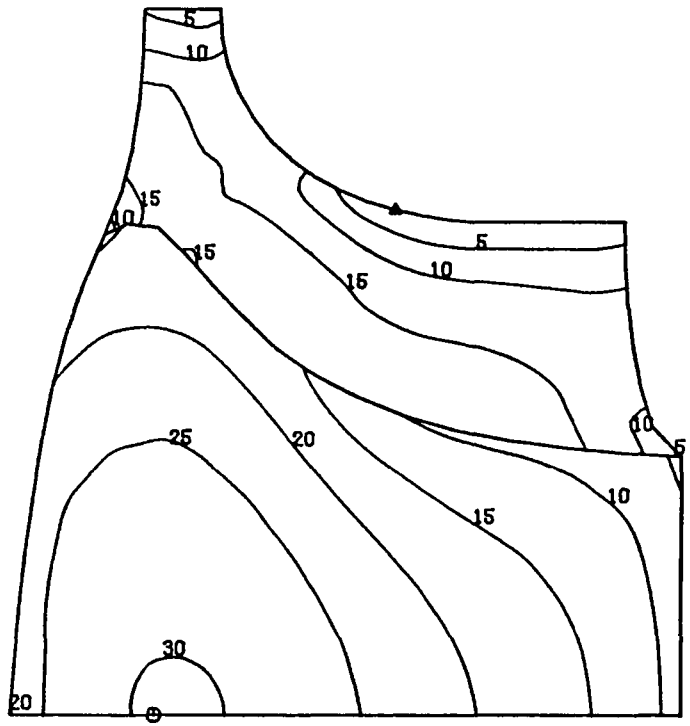

ISOPLETH INTERVAL = 3.447 kN/cm^2 (5 ksi)

RPM = 95,000
TIP SPEED = 634 m/sec (2080 fps)
N_B = 12

Figure 51. Tangential Thicknesses and Maximum Principal Stresses.

RADIAL

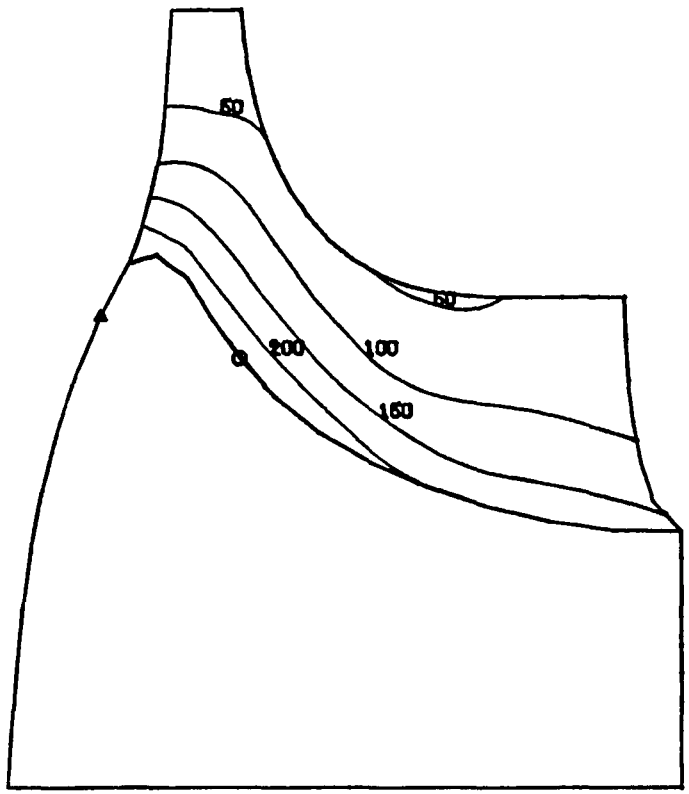

ISOPLETH INTERVAL = 0.127 cm (50 mils)

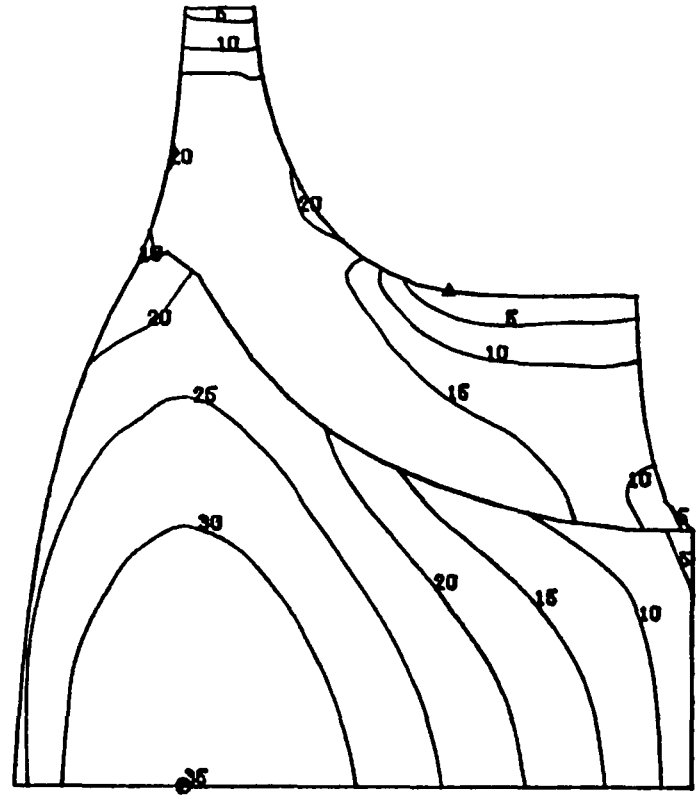

ISOPLETH INTERVAL = 3.447 kN/cm^2 (5 ksi)

TANGENTIAL THICKNESS

SCALE FACTOR = 1.50

⏲ MAXIMUM △ MINIMUM

RPM = 95,000

TIP SPEED = 701 m/sec (2300 fps)

Figure 52. Tangential Thicknesses and Maximum Principal Stresses.

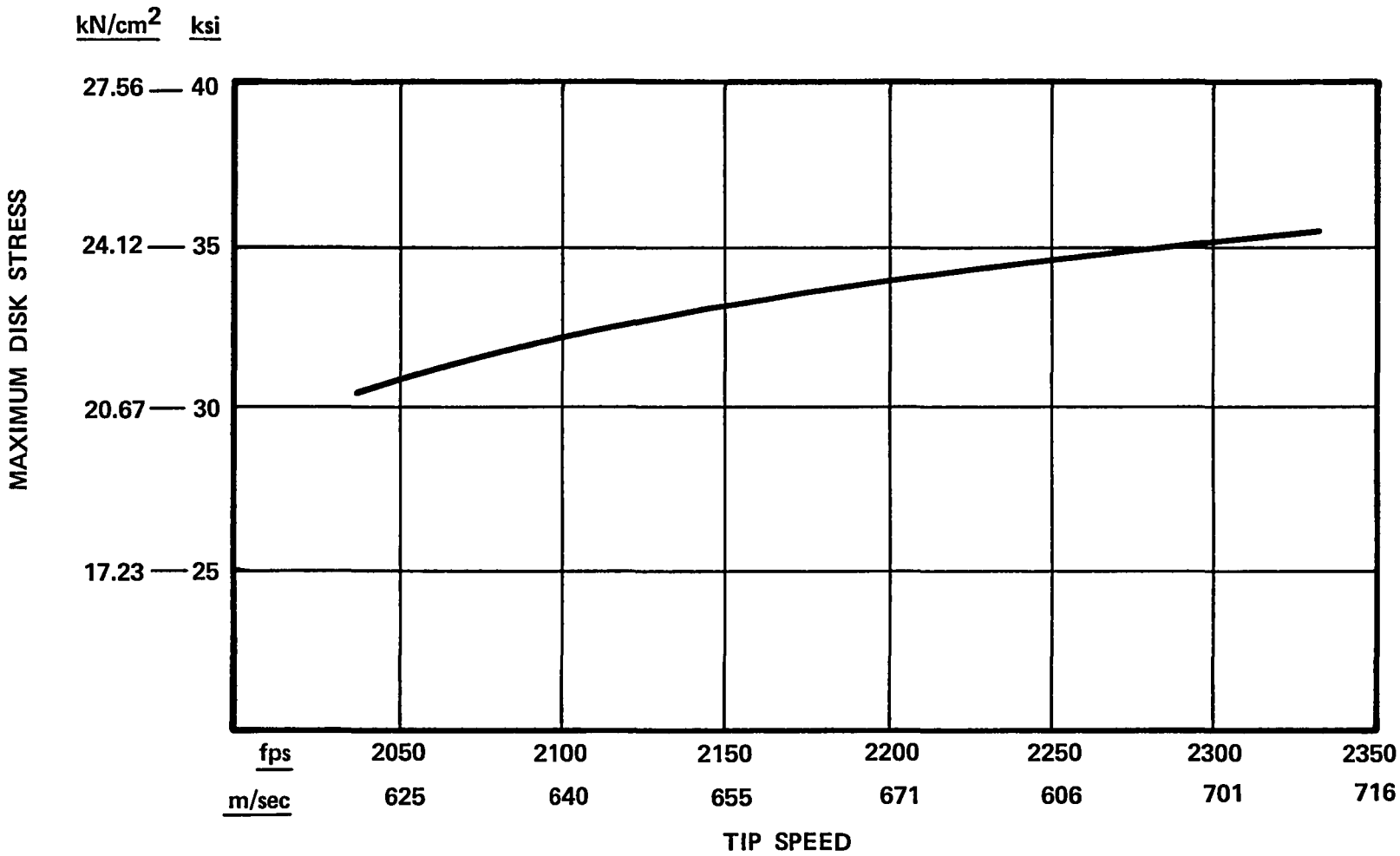

Figure 53. Maximum Disk Stress Versus Tip Speed, A_4 = 45.2 cm^2 (7 $in.^2$), N = 95,000 rpm, N_B = 12.

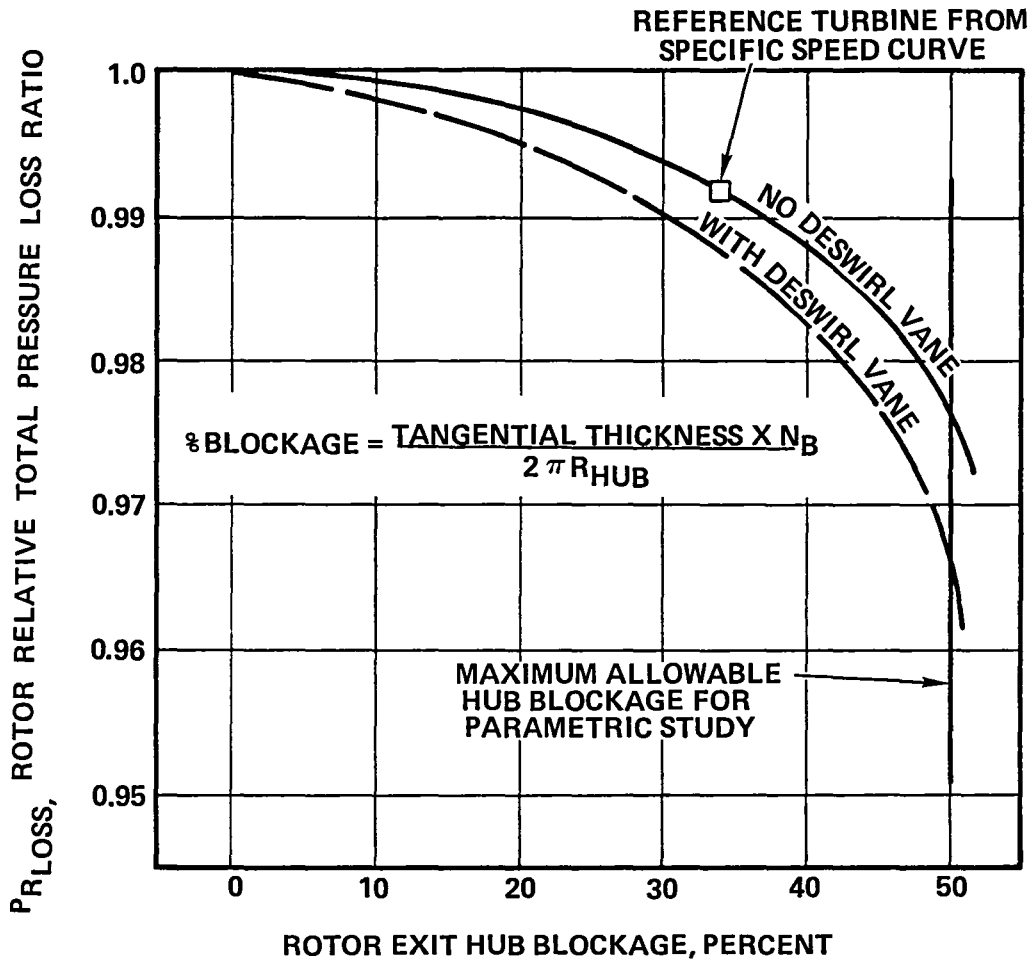

Figure 54. Effect of Rotor Exit Hub Blockage on Rotor Loss.

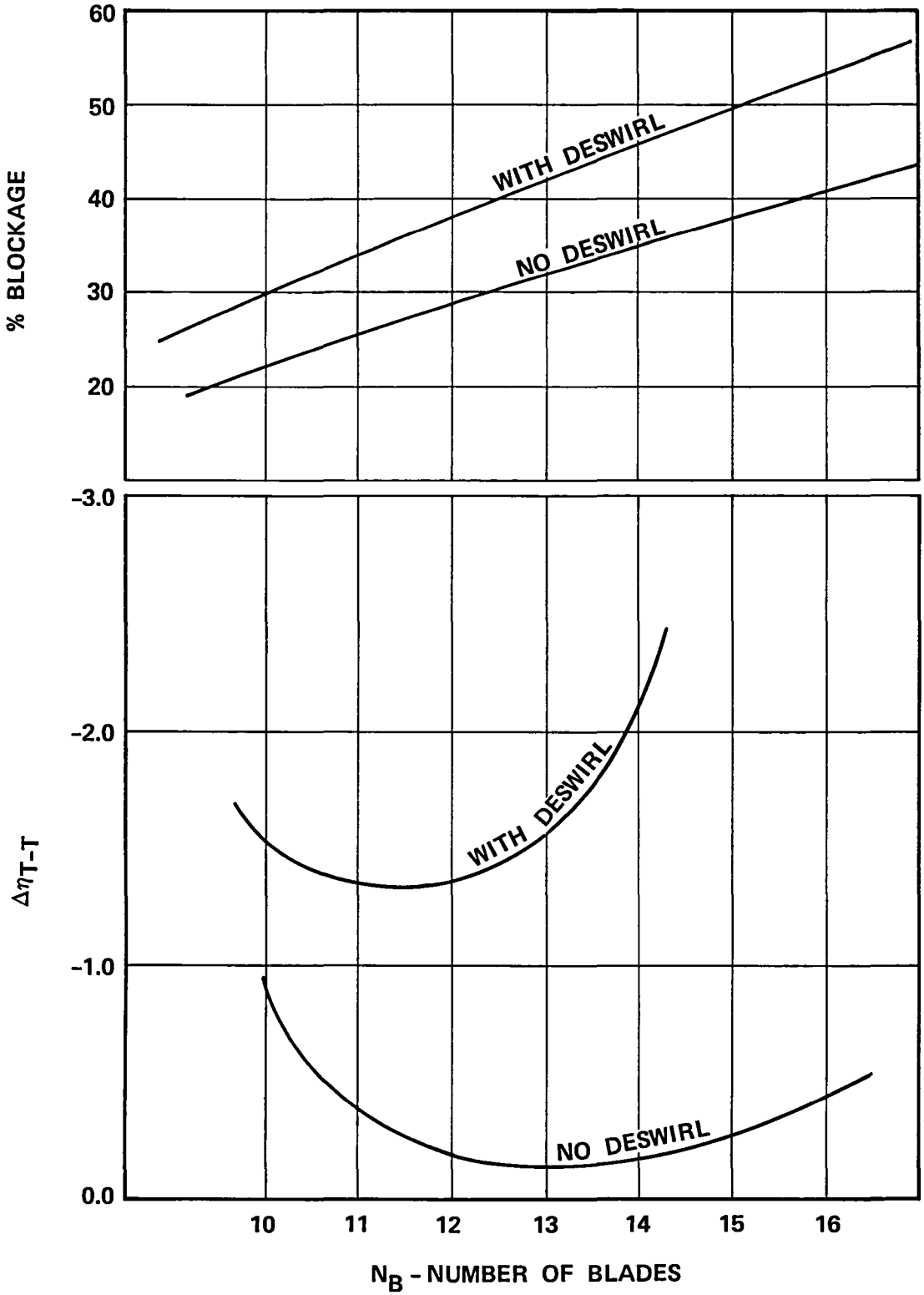

Figure 55. Effect of Rotor Exit Hub Blockage and Blade Number on System Efficiency.

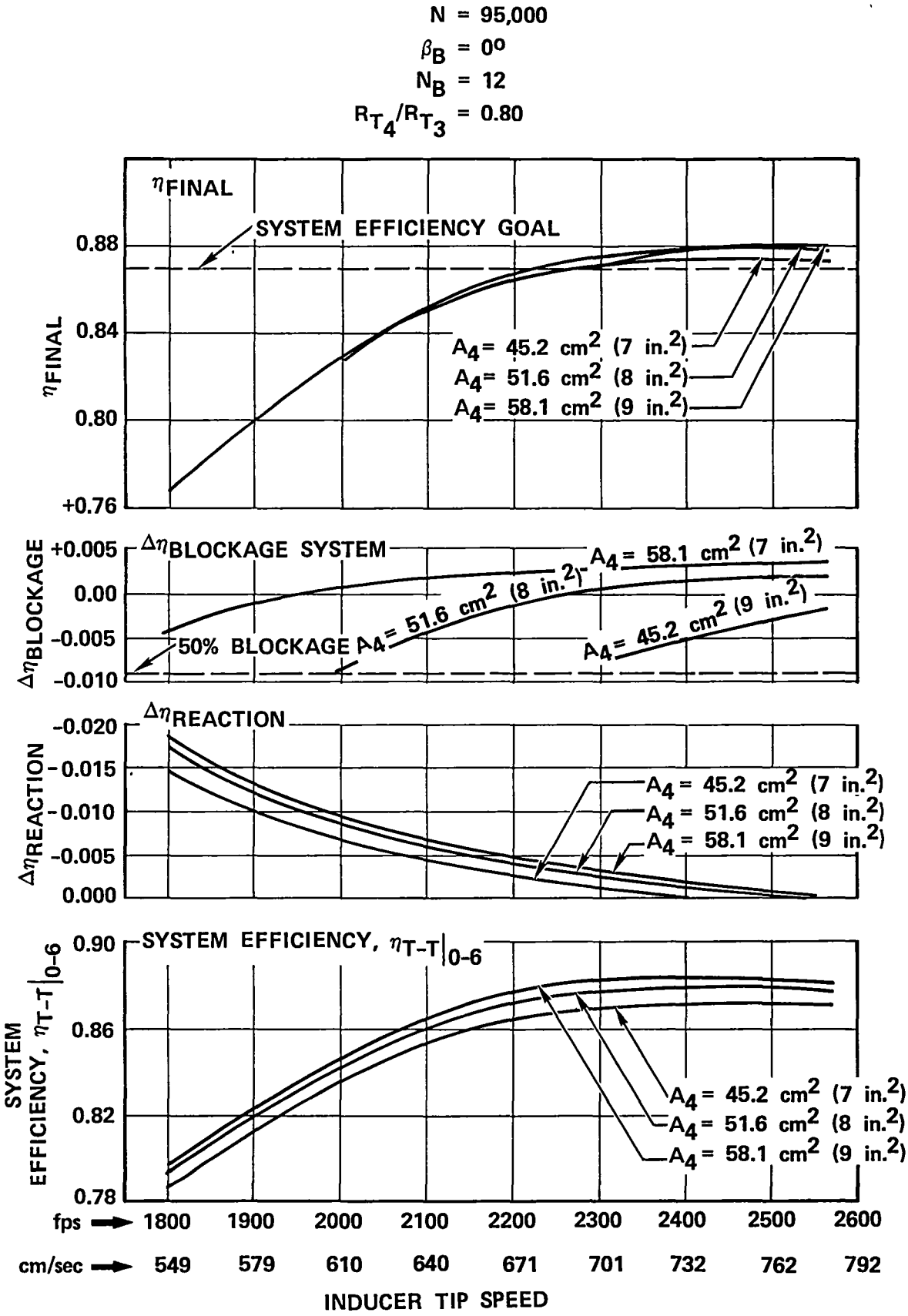

Figure 56. Effects of Reaction, Rotor Exit Area, and Blockage on System Efficiency.

radius ratio was set at 0.80, the higher tip speeds result in a blockage penalty that is less than the reference turbine (i.e., positive $\Delta\eta$ blockage). The combined effects of reaction and blockage are indicated by η final. The advantages of the higher rotor exit area designs are reduced significantly and are limited to higher tip speeds due to the maximum allowable blockage of 50 percent.

Up to this point, the aerodynamic and mechanical analyses indicate the following trends:

- The effects of reaction, exit area and blockage increased the required tip speed of all solutions by 37 to 76 m/sec (120 to 250 fps)

- The effect of rotor exit hub blockage increased the tip speed level of the 95,000-rpm solutions to the level required at 80,000 rpm. Since the disk stress, weight, and inertia are higher at 80,000 rpm, these solutions were eliminated

- Comparison between the solutions at 95,000 and 110,000 rpm show that disk stress is slightly lower at 110,000 rpm, but the rotor exit hub blockage is significantly higher. To reduce the thickness requirement would require a reduction in rotor exit annular area to approximately 36.1 cm^2 (5.6 $in.^2$), which decreases stage efficiency and increases the required tip speed. For this reason, the optimum solutions would be between 90,000 and 100,000 rpm.

The tip speed characteristics for 95,000 rpm are presented in Figure 57 as a function of imposed effects of reaction, blockage, and exit annular area. The relative merit between radial and nonradial blading was examined next with a three-dimensional stress analysis. The rotor blade angle distributions for a 10- and 20-degree inlet angle were estimated from previous nonradial rotor optimization.

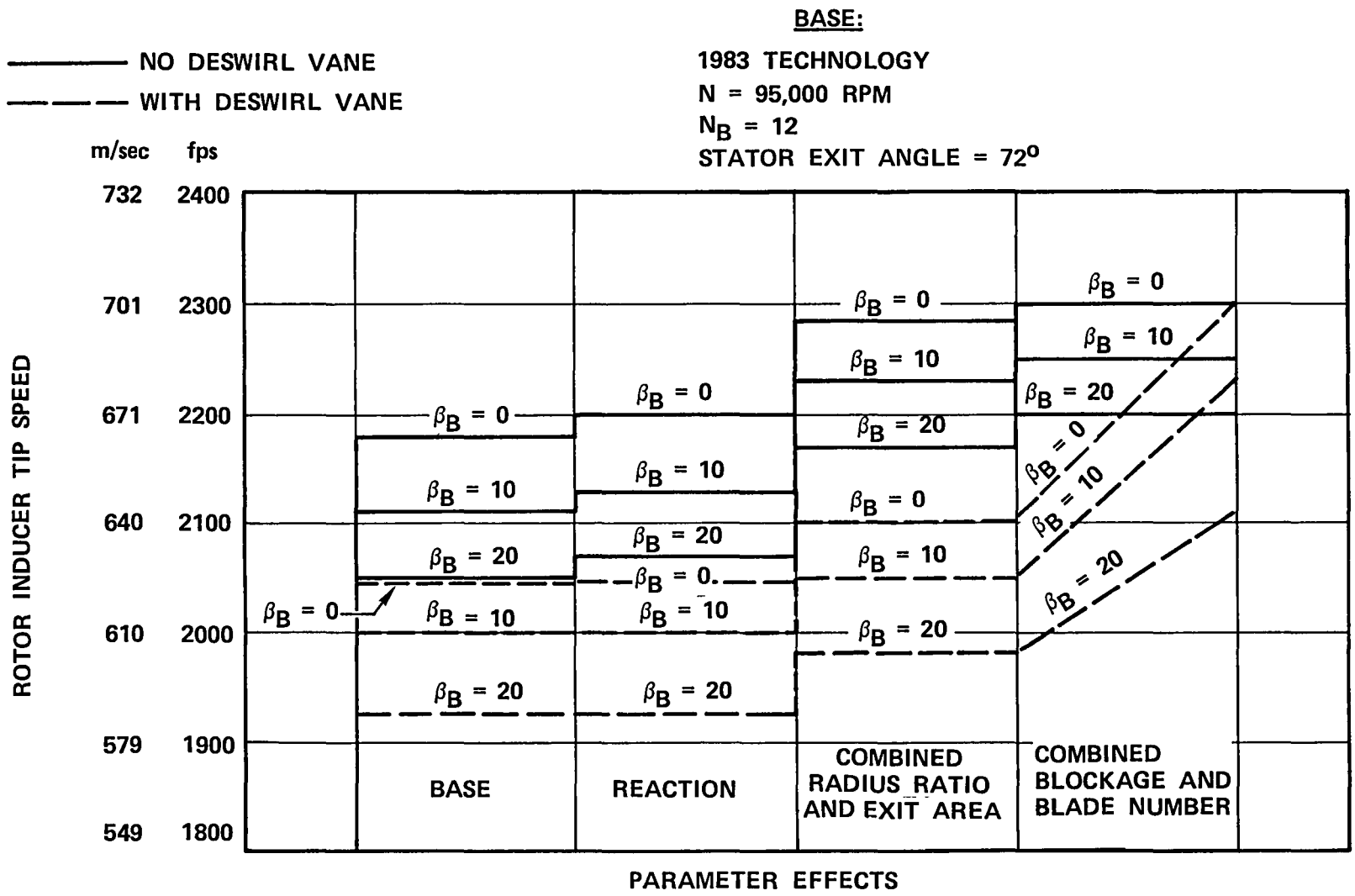

Figure 57. Effect of Reaction, Blockage, and Exit Annular Area on Tip Speed Characteristics for Design System Efficiency of 0.87.

4.0 DETAIL ROTOR AERODYNAMIC AND MECHANICAL DESIGN

The three rotor configurations (without deswirl vanes) corresponding to inlet blade angles of 0, 10, and 20 degrees were selected for detail aerodynamic and mechanical analysis. The tip speeds for these designs were based on the data presented in Figure 57 and represent the predicted values required to achieve the cycle system efficiency goal of 0.87 with all known losses and mechanical considerations accounted for. The design parameters for the detail design configurations are presented in Table IV. Rotor flow path and blade geometries are presented in Appendix C.

4.1 Aerodynamic Detail Design

The rotor inlet and exit flow path dimensions (derived from Figure 57) were established from the optimized one-dimensional vector diagrams. The rotor solidity study, described in Section 3.8, indicated that an axial length of 4.06 cm (1.60 in.) should result in satisfactory rotor blade loadings for the radial blade case. For the nonradial rotors, previous designs have demonstrated that additional axial length is required, due to the increased rotor turning.

The detail rotor design was initiated with preliminary estimates of hub and shroud contours, blade thicknesses, and angle distributions. These quantities were input to a radial turbine geometry program along specified station lines (quasi-orthogonals) for the internal flow solution. The resultant data matrix was curve-fit to define the total blade geometry. The computer program is a modification of the current centrifugal impeller geometry program that allowed an arbitrary blade to be defined.

To perform the internal flow analysis, the level and distribution of losses in the rotor must be specified in addition to the rotor blade geometry and thermodynamic conditions. The magnitude of the total stage loss is determined from the efficiency analysis described in paragraph 3.4. The stator loss is estimated from stator reaction rig tests performed at AiResearch; the remaining loss is assigned to the rotor.

The computer program for the rotor internal flow analysis solves the radial-equilibrium equation by satisfying the continuity, momentum, and energy equations in the meridional plane in a manner similar to references 21 and 22. Blade surface velocities are computed from the local rate of change in moment of momentum, the condition of zero absolute vorticity, and linear velocities between suction and pressure surfaces. Stanitz (ref. 23) has shown that this method produces satisfactory results compared with relaxation solutions of the potential flow equation. Numerous iterations between the geometry program and internal flow analysis program are required to achieve satisfactory blade loading for each thickness distribution examined.

TABLE IV. SELECTED CONFIGURATIONS FOR DETAIL AERODYNAMIC AND MECHANICAL DESIGN

Design Parameters	Units	Configurations		
		$\beta_B = 0°$	$\beta_B = 10°$	$\beta_B = 20°$
Rotational Speed N,	rpm	95,000	95,000	95,000
Inducer Tip Speed, U_{t_3},	cm/sec (fps)	701 (2300)	686 (2250)	671 (2200)
Stage Work Coefficient, λ_{STG}		1.033	1.091	1.142
Rotor Inlet Work Coefficient, λ_3		1.000	1.030	1.085
Specific Speed, N_s	rpm $(ft^{3/4}/sec^{1/2})$	0.537 (69.20)	0.537 (69.20)	0.537 (69.20)
Stage Reaction, R_{STG}		0.541	0.545	0.511
Reynold's Number, Re X 10^{-5}		1.028	1.050	1.074
Exducer Tip-to-Inducer Tip Radius Ratio, R_{t_5}/T_{t_4}		0.632	0.646	0.661
Rotor Exit Annular Area, A_4	cm^2 $(in.^2)$	45.2 (7)	45.2 (7)	45.2 (7)
Rotor Exit Absolute, Swirl, α_4	degrees	-0.76	-13.40	-11.50
Number of Rotor Blades, N_B		12.0	12.0	12.0
Turbine Inlet Scroll Loss, $\Delta P/P$		0.0057	0.0056	0.0056
Rotor Exit Diffuser Loss, $\Delta P/P$		0.0303	0.0322	0.0311
Stage Total-to-Total Efficiency, $\eta_{T-T\ 1-4}$		0.889	0.892	0.893
System Total-to-Total Efficiency, $\eta_{T-T\ 0-6}$		0.870	0.872	0.873

The criteria for satisfactory blade loadings are monotonically increasing velocities and minimum blade surface diffusions. For highly loaded rotors (that normally imply increased loading in the rotor inducer region), these criteria are not satisfied. In addition, inlet flow deviations based on Stanitz's criteria are not expected to apply; therefore, the loadings in the inducer region become ill-defined. Under these conditions, more rigorous stream-function methods for evaluating the blade surface velocities are not warranted. The rotor internal flow analysis is further compounded by rotor exit flow deviations. Deviations are expected even with isentropic flows due to the rotor relative vorticity. Approximate methods for predicting these deviations were proposed by Mizumachi (ref. 24) in 1971, then Khalil (ref. 25) derived a rigorous method in 1977. However, these deviations have been modified significantly by the transport of secondary flows from the inducer to the exducer tip region.

The final rotor flow path configurations are presented in Figure 58. As indicated, the hub and shroud contours were maintained for all three rotor inlet blade angle solutions. A constant flow path configuration allowed a more meaningful mechanical comparison, and previous nonradial rotor designs have presented no particular advantage from modifying the rotor meridional flow path under these conditions. Conversely, rotor axial length was fairly sensitive (to achieve satisfactory loading) when a rotor inlet blade angle was introduced.

The change shown in Figure 58 is based on iterating axial length until approximately equal rotor inducer loadings for all three blade angles were achieved. An alternate approach would be to evaluate a rotor loading parameter along the hub, mean on shroud lines and iterate axial length until equal loading parameters were achieved. The final rotor blade angle distributions for inlet blade angles of 0, 10, and 20 degrees are presented in Figure 59 as a function of percent meridional distance. Also shown are the locations at inlet and exit where flow deviations from the blade were assumed.

The rotor inlet deviations are apparently due to rotor relative vorticity effects, and the location where the flow starts to follow the blade was based on Stanitz (ref. 1) correlation and was applied to radial turbines by Katsanis (ref. 22). The deviations at the rotor exit are even more complex, since the rotor relative vorticity effects are compounded by large secondary flow migration to the rotor exit tip region. The approach currently utilized at AiResearch is to assume the rotor exit flow is turned to the rotor mid-throat angle, and the additional uncovered downstream turning is the total deviation at each radial location. The net effect with this procedure is to assume deviation increases from approximately zero at the hub to

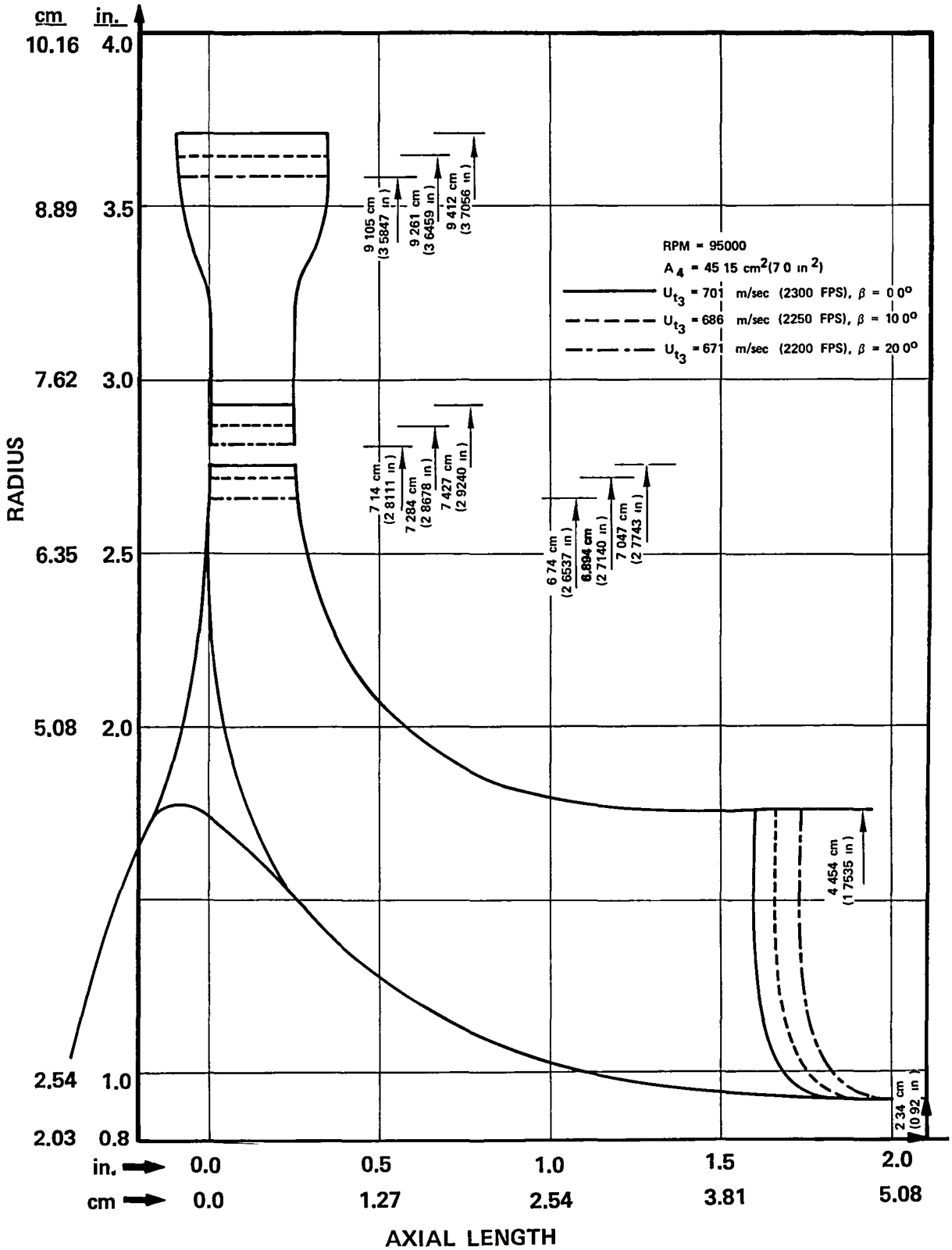

Figure 58. Final Rotor Flow Path Configurations.

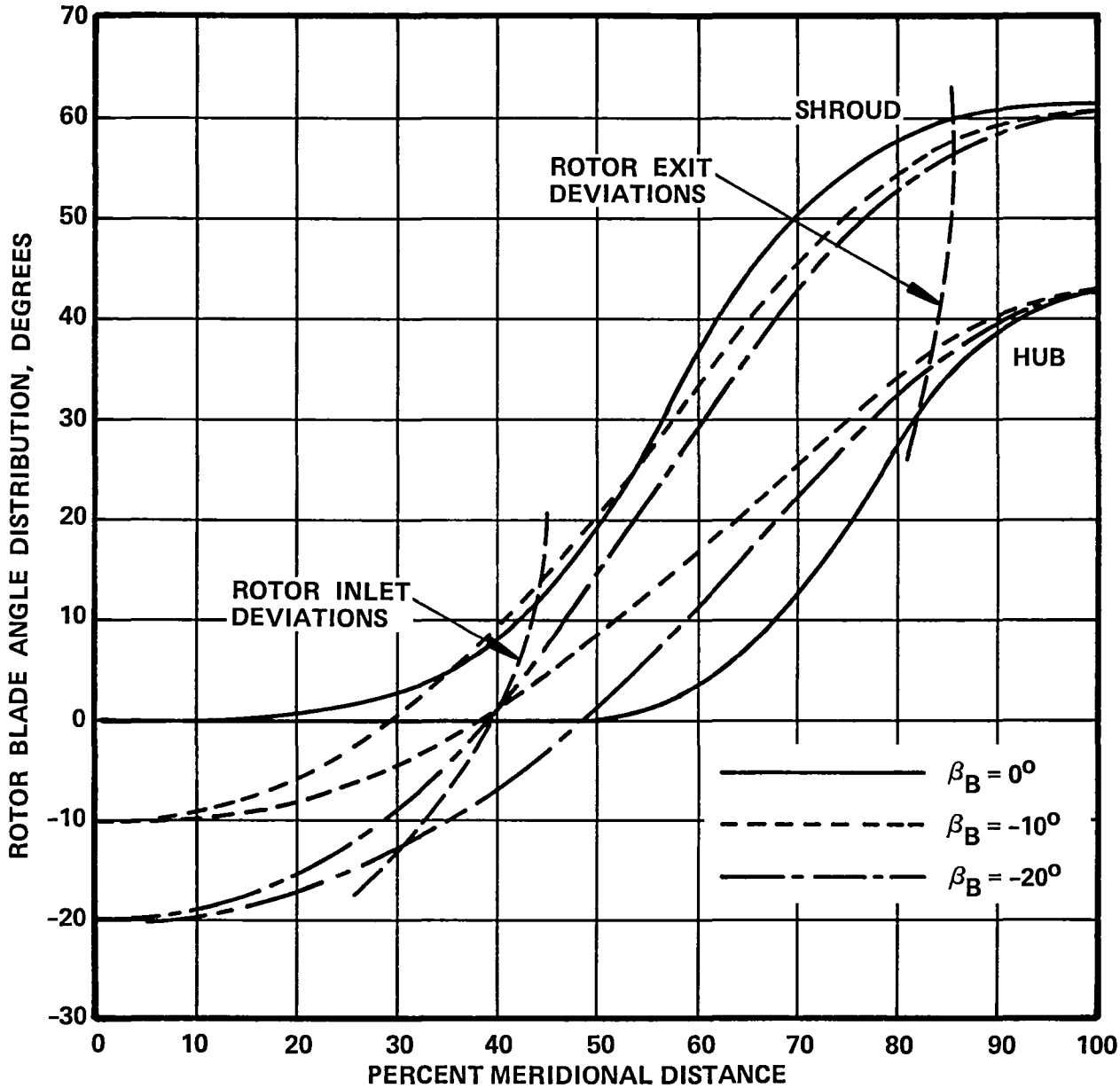

Figure 59. Rotor Blade Angle Distribution Versus Percent Meridional Distance.

a relatively high value at the tip and accounts for the deviations expected in the tip region from the secondary flows. However, the parametric study results are based on precise inducer-to-exducer work splits. Achieving the exact vector diagrams desired would require either a significant increase in rotor internal flow knowledge or experimental iterations of rotor exit blade angles.

The rotor suction and pressure surface velocity distributions for the three inlet blade angle cases are presented in Figure 60 as a function of meridional distance. With 12 rotor blades and the adjustments in axial length, the loading throughout the blades is similar and is expected to achieve equal performance levels.

4.2 Detailed Mechanical Design

Ceramic materials possess large variations in strength properties, due to brittle characteristics. Consequently, probabilistic techniques must be utilized to accurately evaluate ceramic components.

The probabilistic component evaluation technique employed by AiResearch is based on the Weibull statistical strength model (ref. 26). The working relationships permit the calculation to be made from a combination of local stress, component size, and Weibull parameters for both area- and volume-controlled fracture.

$$CPF = 1 - e^{-R}$$

where R is defined as:

$$R = \frac{1}{V_t}\int\left(\frac{\sigma_V - \theta_{ov}}{\theta_{uv}}\right)^{Bv} dv + \frac{1}{A_t}\int\left(\frac{\sigma_A - \theta_{oa}}{\theta_{ua}}\right)^{Ba} da$$

and

A_t = Test-bar surface area

V_t = Test-bar volume

σ_V = Elemental volumetric stress

σ_A = Elemental surface stress

θ_{ov} = Volumetric zero failure stress

θ_{oa} = Surface zero failure stress

θ_{uv} = Volumetric characteristic stress

θ_{ua} = Surface characteristic stress

Ba = Surface Weibull slope

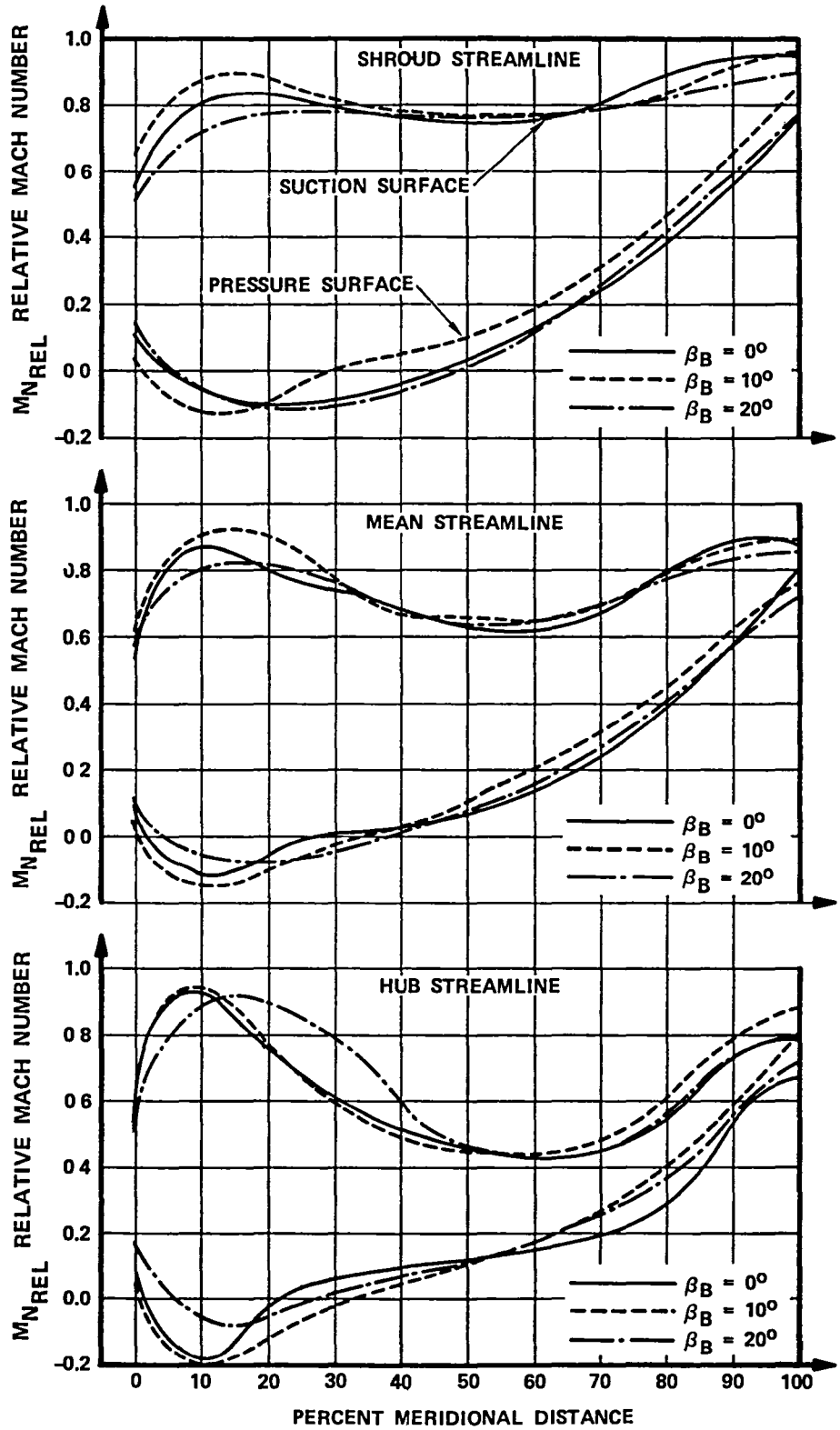

Figure 60. Velocity Distributions.

Bv = Volumetric Weibull slope

da = Differential surface area

dv = Differential volume

This probabilistic computer code distinguishes between surface and volume strength relationships and permits assessment of overall component risk in a method compatible with finite element techniques. All three principal stresses are considered and the codes can assess effect of multiaxial stress states and change in reliability due to proof testing (ref. 27).

As previously mentioned, cumulative probabilities of success computations require 3-D finite element stress results. The 3-D model for the optimized radial-blade configuration is shown in Figure 61. Detailed stress analyses for a similar radial inflow turbine rotor configuration in the AFT101 program, under DOE/NASA contract DEN3-167, have shown that stresses and cumulative probabilities of success are quite similar for both room-temperature and maximum power steady-state operating conditions. This AGT study also showed that minimum cumulative probabilities of success are computed during transient operation. Unfortunately, transient thermal studies could not be completed for the radial and non-radial blade configurations of this study because of financial restrictions. Consequently, all comparative stress analyses were carried out for room-temperature operation. However, probabilities of success were computed using anticipated 1983 material properties at elevated temperature (characteristic strength of 62.053 KN/cm^2 (90.0 KSI) and a Weibull modulus of 15.0). The parametric study indicated that the 95,000-rpm wheel, with an inlet tip speed of 701 m/sec (2300 fps), was the preferred radial-blade configuration and is summarized on Table V. When this configuration was first examined mechanically (Figure 52), disk stresses were marginally high. To reduce disk stresses, the saddle height of the wheel was reduced by removing disk material above the self-sustaining radius of the disk. The resulting wheel stress field at room temperature is illustrated in Figure 62. The peak bore stress was reduced from 24.132 kN/cm^2 (35.0 ksi) to 22.339 kN/cm^2 (32.4 ksi). The resulting probability of survival for the radial wheel using anticipated 1983 ceramic material properties [characteristic strength of 62.053 kN/cm^2 (90.0 ksi) and Weibull modulus of 15.0] is 0.9999. This cumulative probability of survival (CPS) meets the objective of the program.

Once the baseline radial blade design was analyzed, the nonradial inlet design feature was studied using the 3-D stress and probabilistic evaluation computer code. Initially, an inlet angle of 10 degrees was examined with the blade thickness distribution for the radial blade configuration. To achieve the same efficiency as the radial blade design, the required tip speed for this nonradial configuration was reduced to 686 m/sec

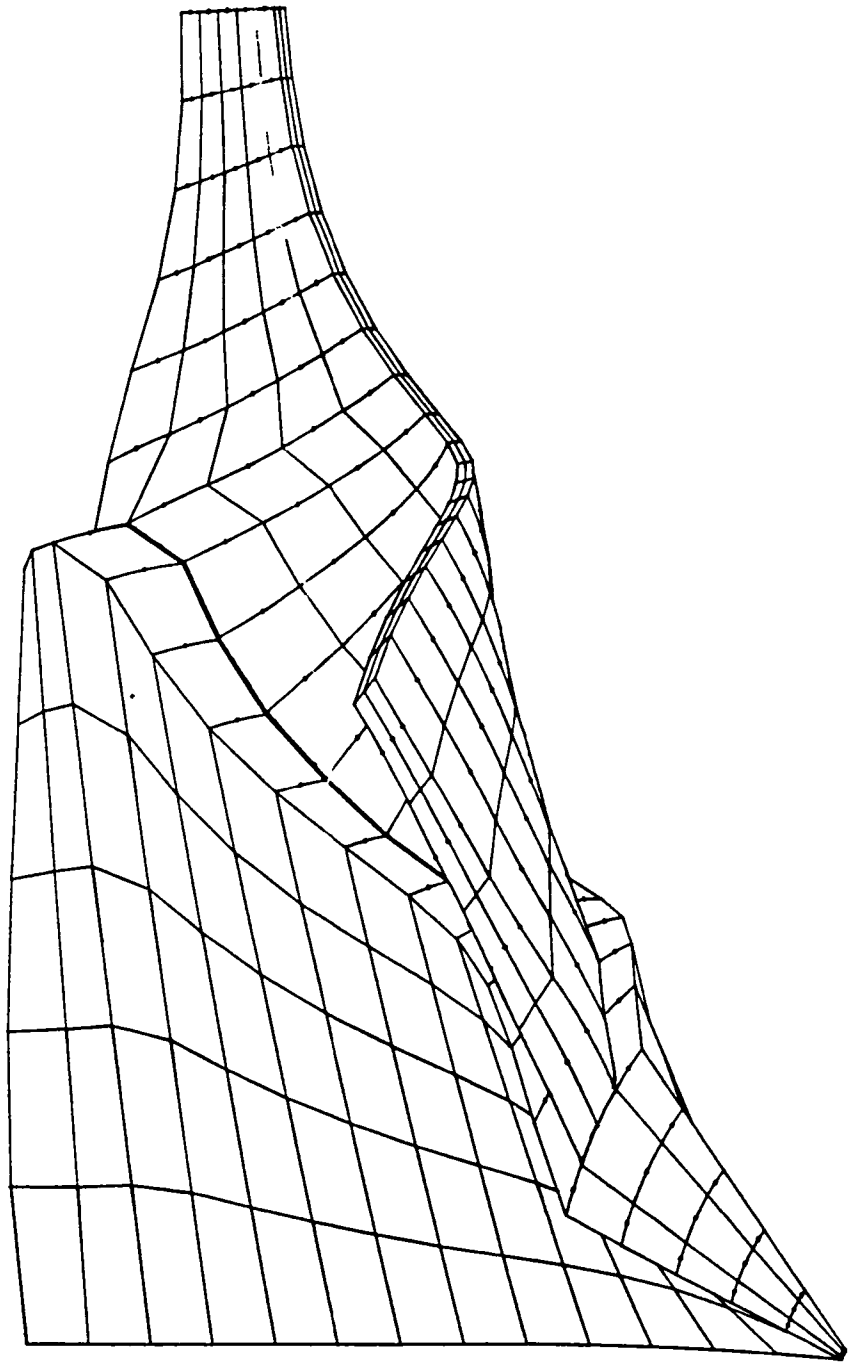

Figure 61. Typical Three-Dimensional Finite Element Model.

TABLE V. OPTIMUM CONFIGURATION DERIVED FROM PARAMETRIC STUDY AND 3-D MECHANICAL ANALYSIS

Parameter	Optimum
Shaft speed	95,000
Inducer tip speed	701 cm/sec (2300 fps)
Rotor inlet blade angle	0 degrees
Rotor blade number	12 to 14
Rotor exit swirl	-10 degrees
Rotor exit critical velocity ratio	0.449
Rotor inducer-to-exducer tip radius ratio	0.632

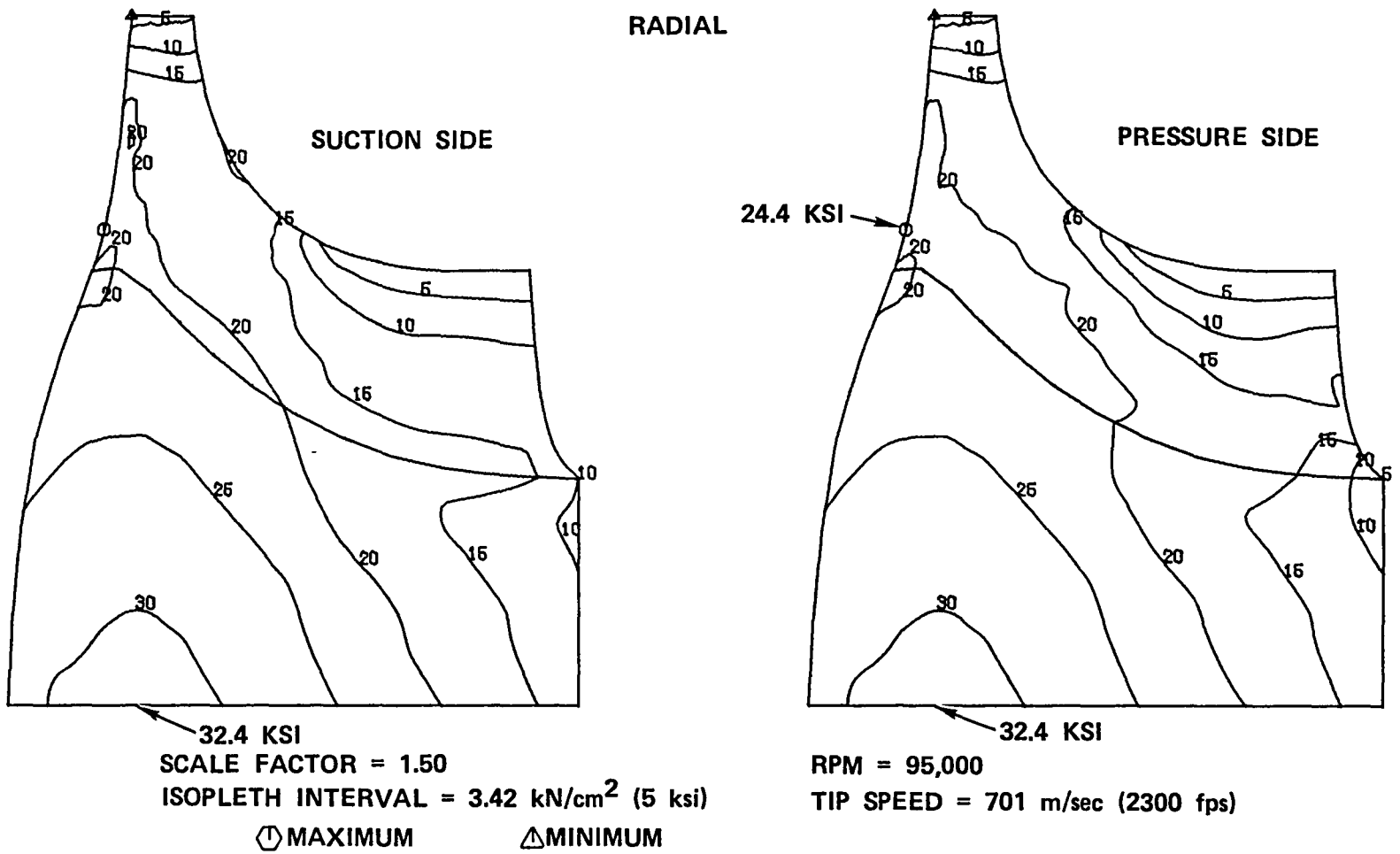

Figure 62. Maximum Principal Stresses.

(2250 fps). Principal stress results for this configuration (Figure 63) indicate high bending stresses in the wheel inlet. These produce a low probability of survival of 0.9394. Experience with nonradial blades from other research programs indicated that these bending stresses could be reduced by incorporating rake to the blade design. Figures 64 and 65 illustrate configurations without and with rake (-30 degrees), respectively. The principal stresses for the rake case (Figure 66) improve the cumulative probability of success to 0.9986. Although this CPS value is significantly better than the no-rake design, the goal of 0.9999 was not reached.

Blade thickness distribution was the next parameter to be studied. Increased blade thickness was incorporated in the inducer portion of the -30 degree rake case (Figure 67). The resulting principal stresses, illustrated in Figure 68, produce a cumulative probability of survival of 0.9993.

Based on the improvements in blade stresses and CPS with the modified blade thickness distribution, a new distribution was generated that increased the blade thickness in both the inducer and exducer. The resulting principal stresses (Figure 69) created a cumulative survival probability of 0.9998. The disk stresses were increased slightly due to thicker blades.

The thickness distribution was modified once again by thickening the blades in the high stress regions. The resulting blade stresses were significantly reduced (Figure 70). Disk stresses were again increased slightly. The survival rate for this configuration, 0.9997, was lower than the previous blade thickness design because of the higher disk stresses.

The 20-degree inlet configuration was analyzed with two different blade thicknesses: the radial blade and the thickest distribution for the 10-degree inlet. To achieve an efficiency equivalent to the radial design, tip speed was reduced to 671 m/sec (2200 fps). As expected, the radial blade thickness distribution produced extremely high blade stresses (Figure 71) and an unacceptable cumulative probability of survival of 0.0001. With the thick-blade distribution, the blade stresses were considerably reduced (Figure 72), and resulting cumulative probability of success was 0.4865. The blade stresses could be reduced by a further increase in blade thickness, but these increases would increase disk stresses. Increased thickness would prevent the 20-degree inlet case from ever achieving a survival rate as high as the radial blade design.

The peak blade and disk stresses and cumulative probabilities of survival for the different wheel geometries are tabulated on Table VI. In summary, the radial blade is the only wheel design that meets the 0.9999 CPS program goal; nonradial configurations do not possess survival rates as high. Blade thicknesses had to be increased significantly to keep the blade

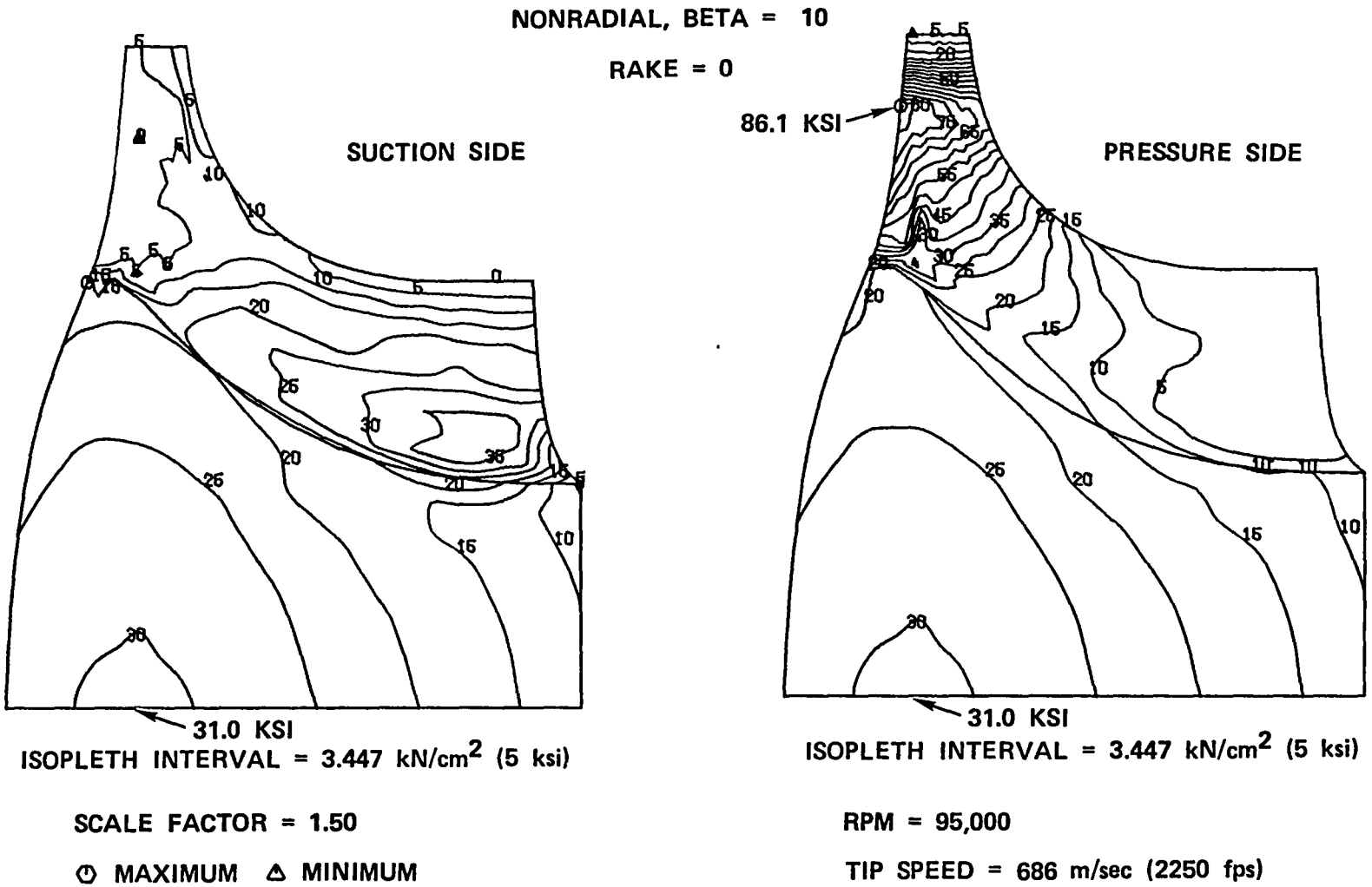

Figure 63. Maximum Principal Stresses.

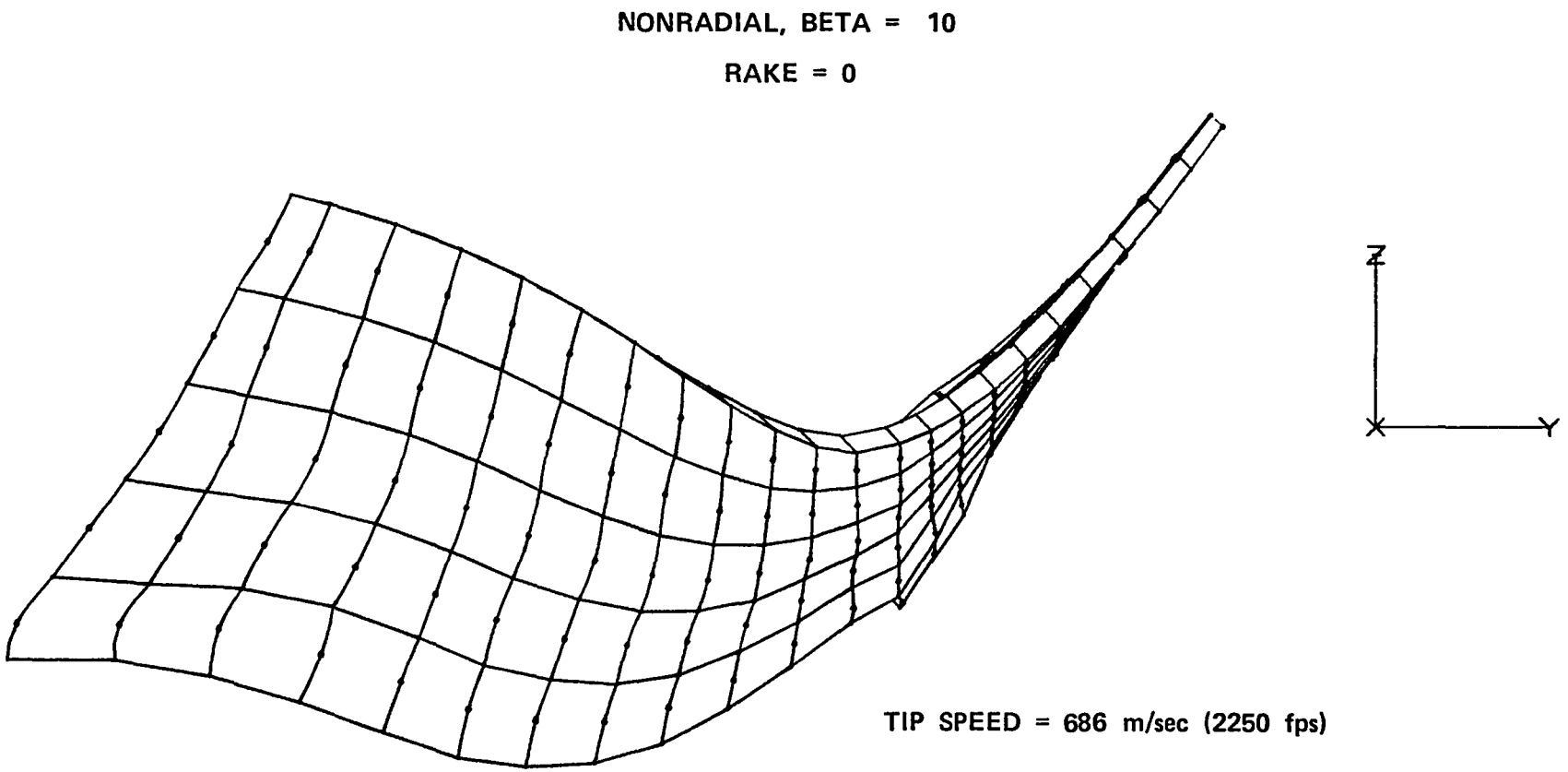

Figure 64. Blade Shape, Original Thickness (Rake = 0).

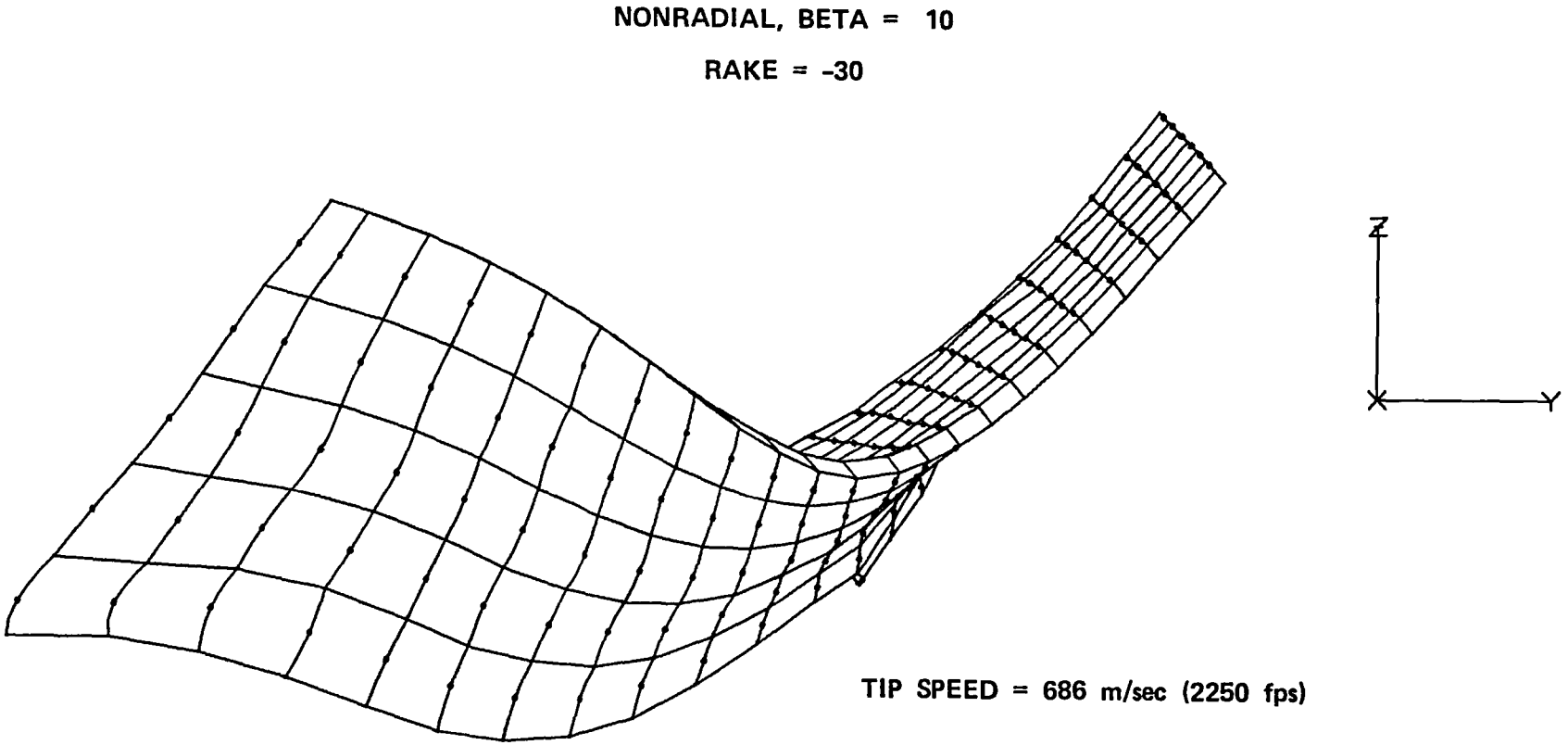

Figure 65. Blade Shape, Original Thickness (Rake = -30).

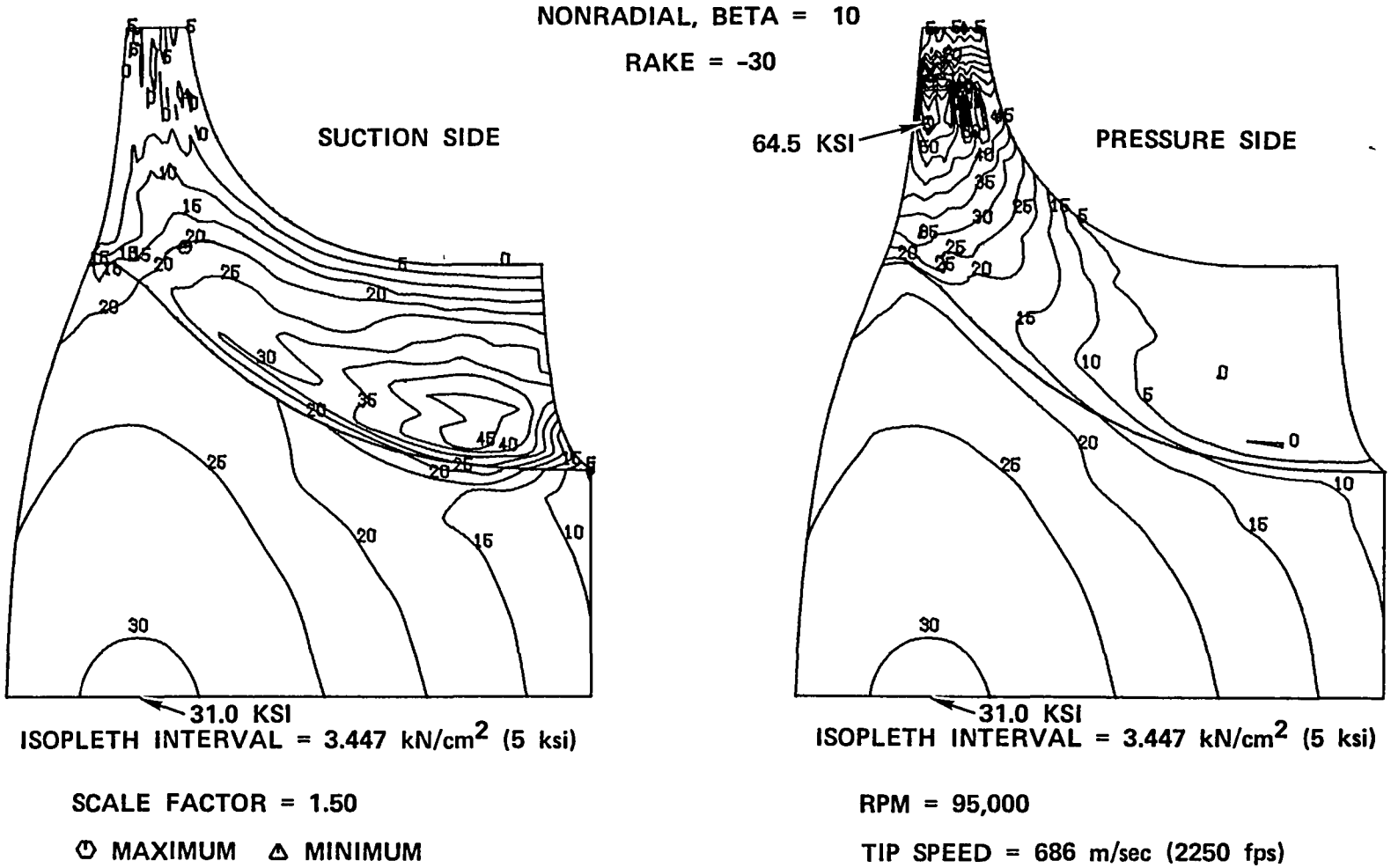

Figure 66. Maximum Principal Stresses, Original Thickness.

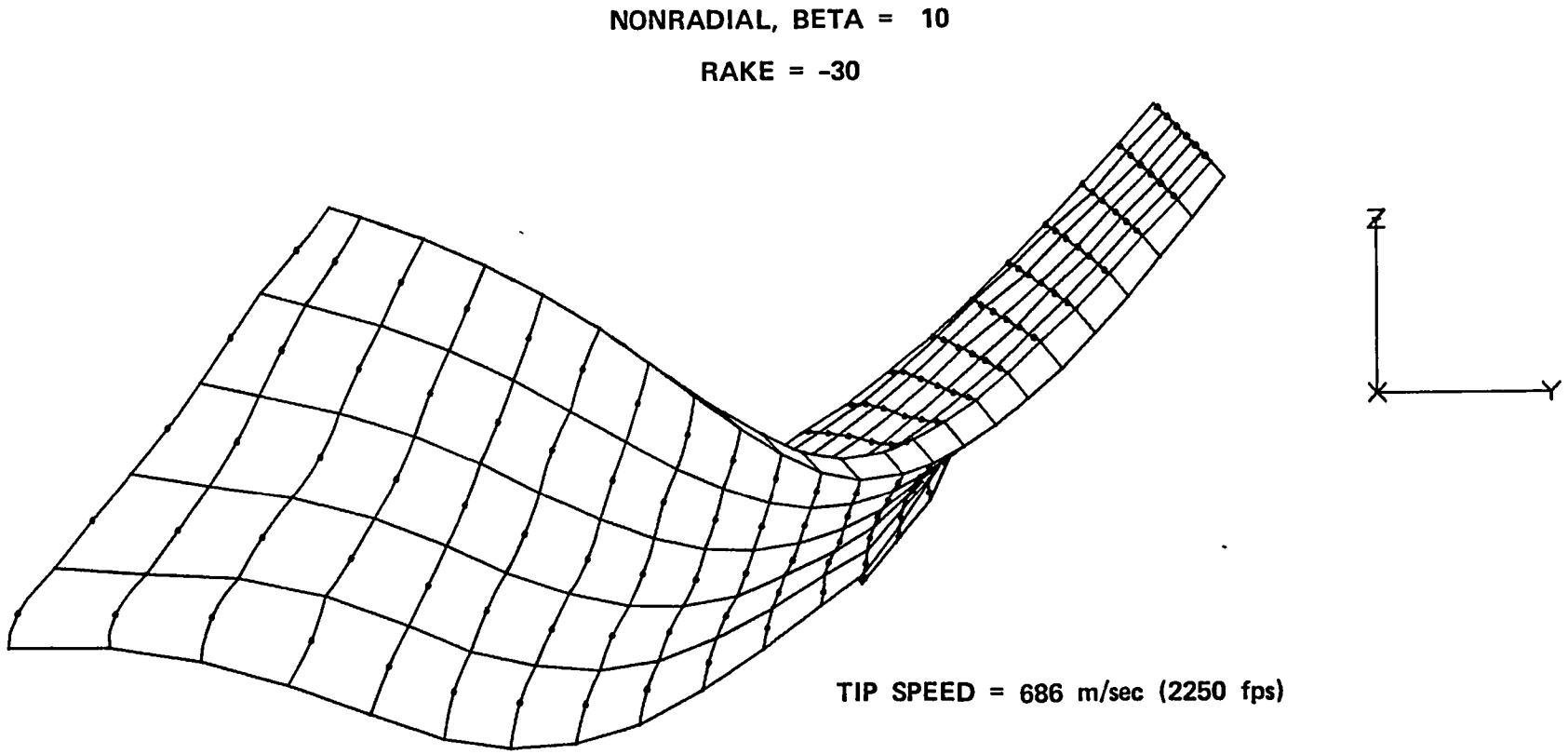

Figure 67. Blade Shape, Modified Thickness.

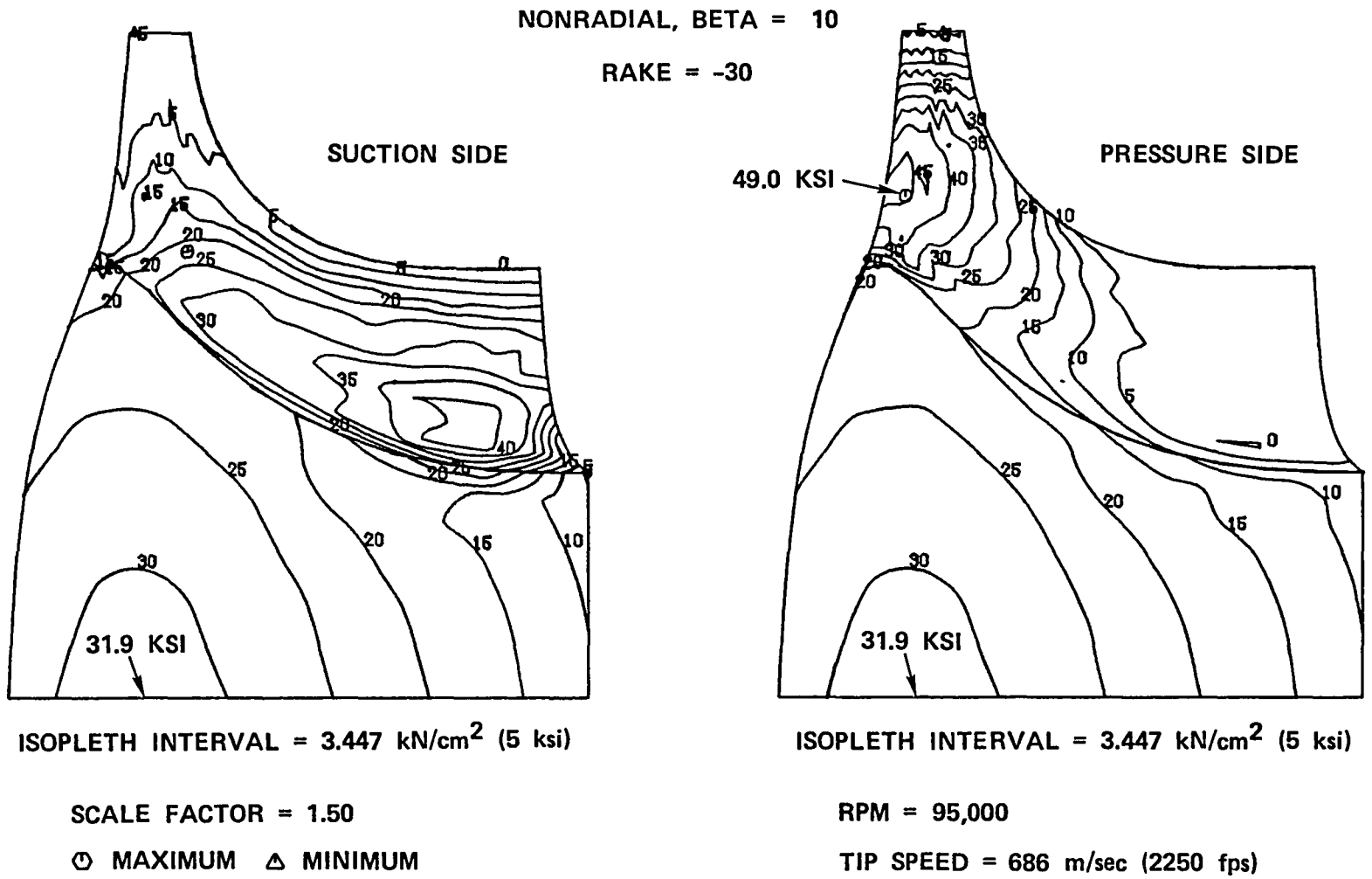

Figure 68. Maximum Principal Stresses, Modified Thickness(1).

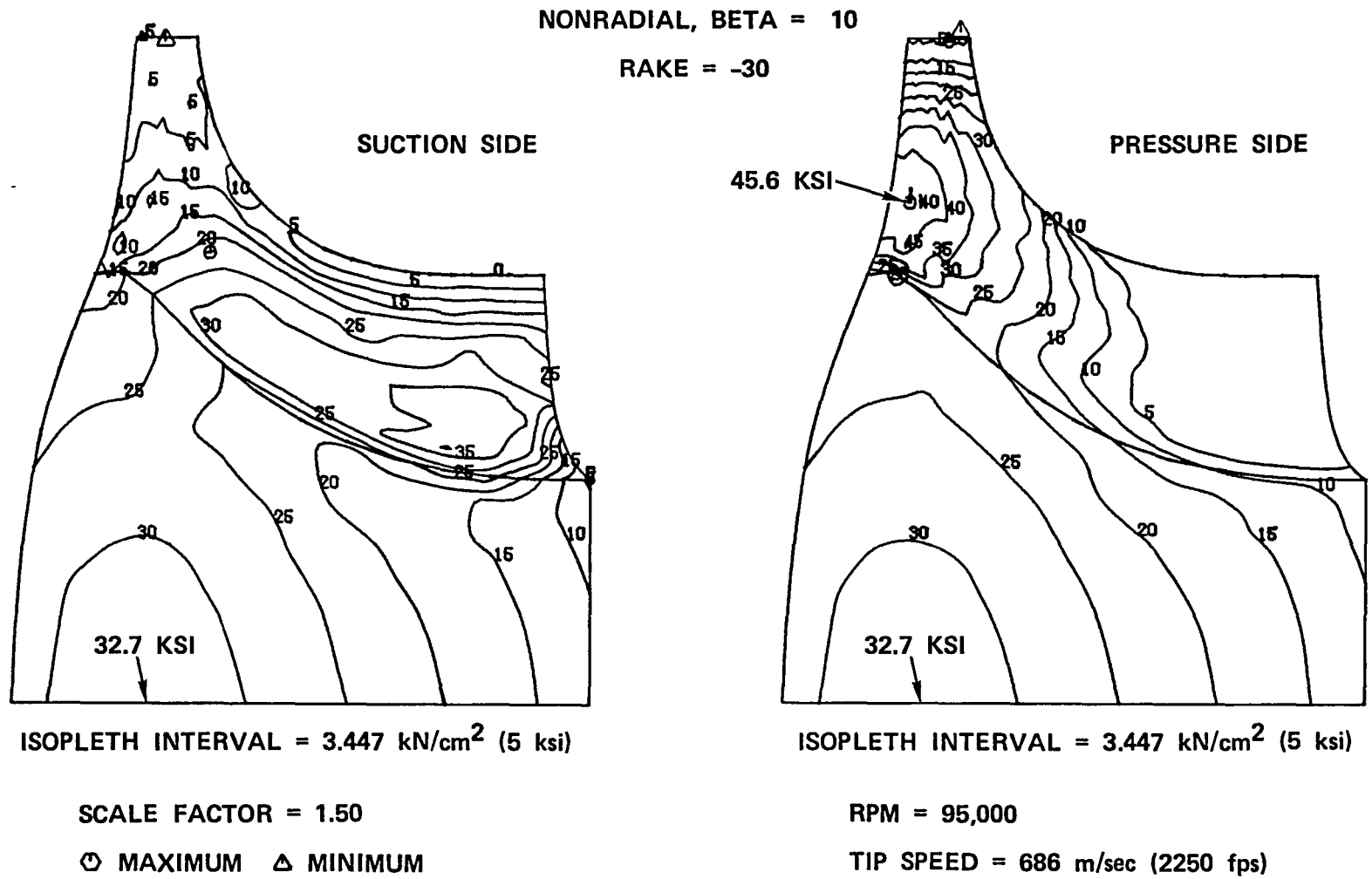

Figure 69. Maximum Principal Stresses, Modified Thickness (2).

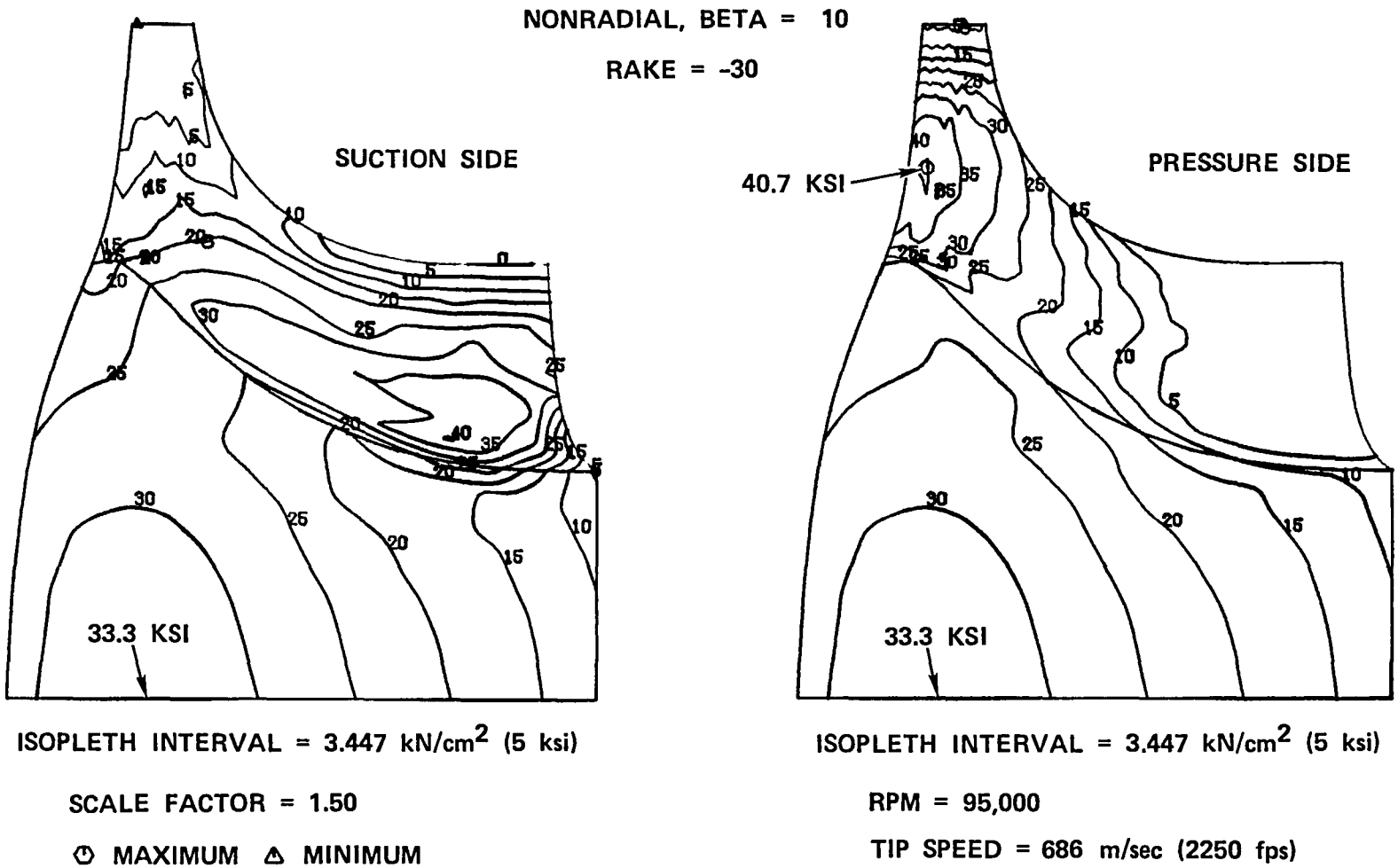

Figure 70. Maximum Principal Stresses, Modified Thickness (3).

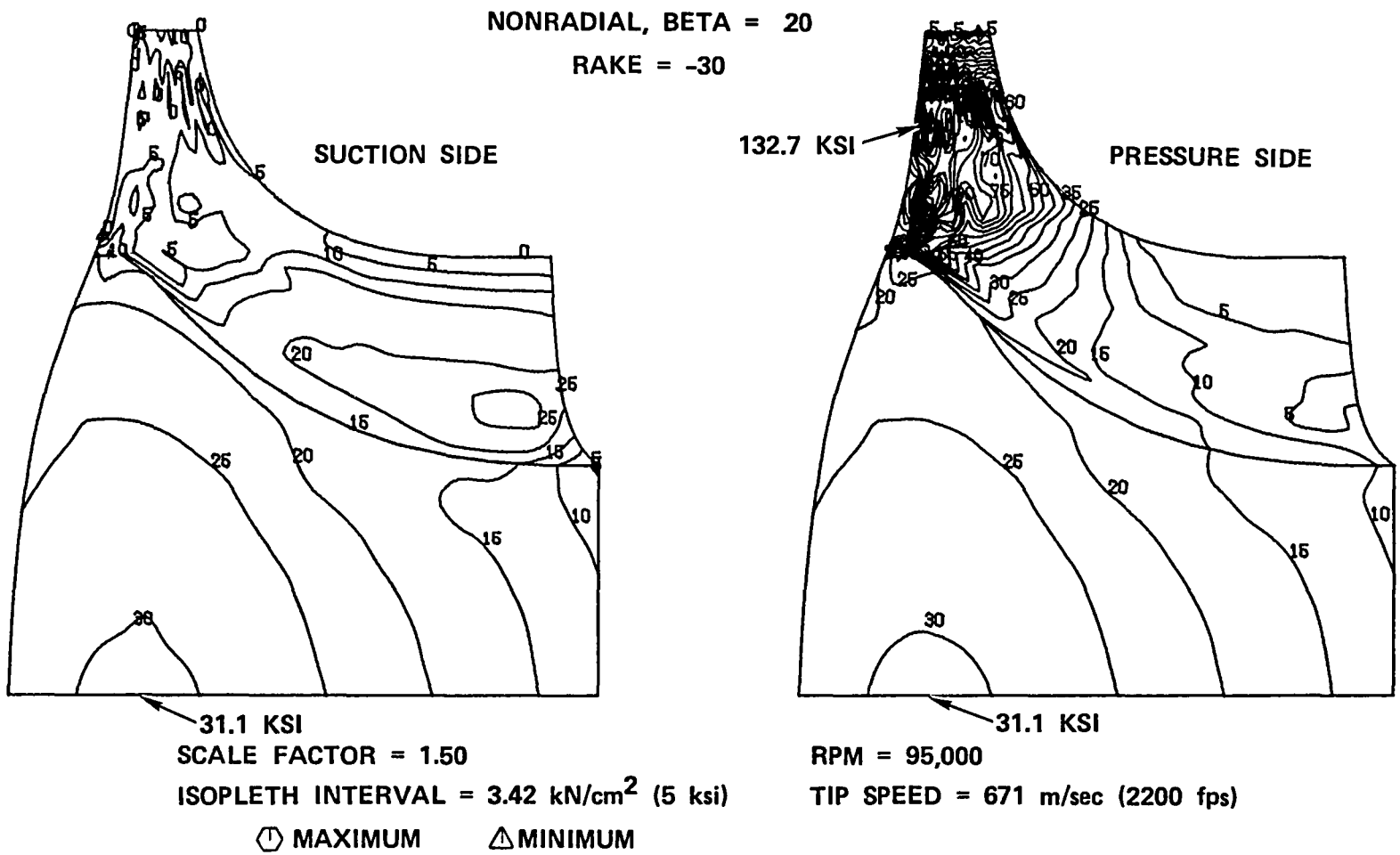

Figure 71. Maximum Principal Stresses, Original Thickness.

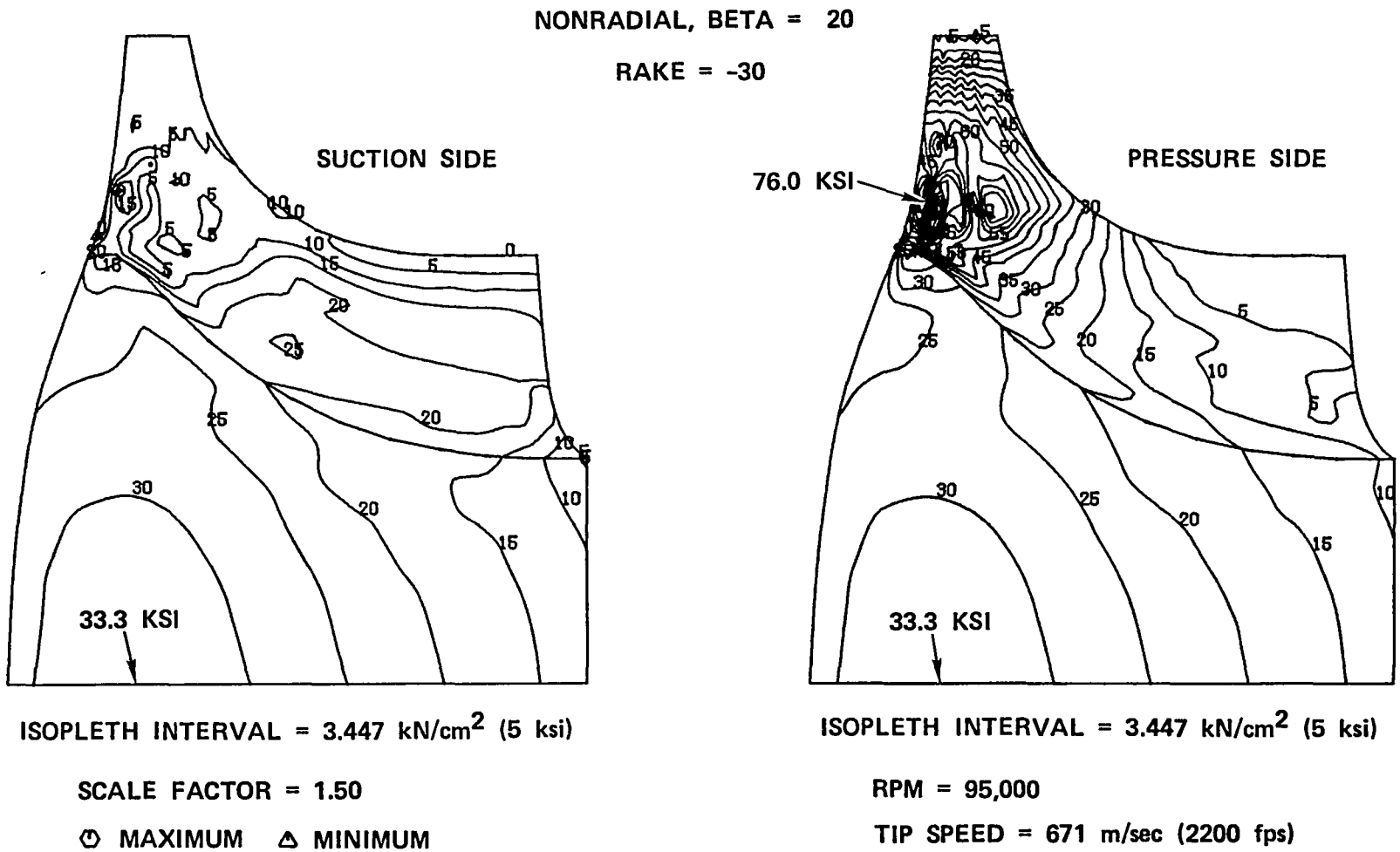

Figure 72. Maximum Principal Stresses, Modified Thickness (3).

TABLE VI. STRESS AND CUMULATIVE PROBABILITY OF SUCCESS SUMMARY AT 95,000 RPM

Configuration	Rake	Blade Inlet Tip Speed, m/sec (fps)	Max Blade Stress, kN/cm^2 (ksi)	Max Disk Stress, kN/cm^2 (ksi)	Cumulative Probability of Success		
					Contribution		Total
					from Blades	from Disk	
Radial Blade		701 (2300)	16.8 (24.4)	22.3 (32.4)	1.00000	0.99989	0.99989
10-Degree Inlet Radial Blade Thicknesses	0	686 (2250)	59.4 (86.1)	21.4 (31.0)	0.93950	0.99992	0.93942
	-30	↓	44.5 (64.5)	21.4 (31.0)	0.99862	0.99992	0.99855
Modified Thickness Distribution #1	↓	↓	33.8 (49.0)	22.0 (31.9)	0.99940	0.99987	0.99928
#2	↓	↓	31.4 (45.6)	22.5 (32.7)	0.99996	0.99981	0.99976
#3	↓	↓	28.1 (40.7)	23.0 (33.3)	0.99996	0.99972	0.99970
20-Degree Inlet Radial Blade Thickness	↓	671 (2200)	91.5 (132.7)	21.4 (31.1)	0.00006	0.99992	0.00006
Modified Thickness Distribution #3	↓	671 (2200)	52.4 (76.0)	23.0 (33.3)	0.71518	0.99972	0.71498

stresses at acceptable levels. Increased blade load increased disk stresses and caused disk survival rates to be lower than those for the radial blade design. With sufficient blade thickness and rake adjustments, moderate amounts of backsweep (10 degrees or less) can be tolerated with nearly the same cps as a radial bladed wheel.

The 10-degree inlet design that possessed the highest cumulative probability of survival (modified thickness No. 2) and the radial blade configuration were compared, using ceramic properties more representative of present day materials [a characteristic strength of 44.816 kN/cm^2 (65 ksi) and a Weibull modulus of 12]. With these lower values, the radial wheel again possessed a better survival rate--0.9686 versus 0.9359 for the nonradial design.

5.0 OFF-DESIGN PERFORMANCE EVALUATION

For a single-shaft configuration, turbine operating conditions will vary significantly from maximum power to idle. Therefore, the turbine design derived from the maximum power optimization study may not provide minimum SFC and maximum driveability over the entire duty cycle. Although the turbine design point could be selected at any power setting and then examined off-design, this approach is not necessary. Evaluating the off-design characteristics at different "simulated" power settings can be accomplished merely by selecting a range of vector diagrams at maximum power setting. For example, since turbine flow, speed, and pressure ratio will be reduced at idle, high positive swirl would be expected and, with the duct loss characteristics used in the parametric study, would result in decreased performance. Of course, turbine performance at idle is also dependent on a number of other parameters, such as work coefficient and reaction.

The point is that if the vector diagram at maximum power is changed (for example, from -10.0 to -40.0 degrees exit swirl), all off-design vector diagrams will shift, and new efficiency characteristics will be defined. In addition, the system efficiency envelope already provides alternate vector diagrams that would maintain maximum efficiency at the design-point.

The effect of design-point vector diagram selection on overall duty cycle performance will be illustrated based on the results of the current NASA-DOE Advanced Gas Turbine Power Train System Development Program (Contract No. DEN3-167). Since the cycle and selected design point parameters are very similar to the 701 m/sec^2 (2300 fps) tip speed radial-bladed configurations, the results are directly applicable to the present study.

Figure 73 shows three selected inlet work coefficients (and the corresponding rotor exit swirl levels) on the system efficiency envelope for 95,000 rpm and a tip speed of 701 m/sec (2300 fps). The three cases are designated low (-9.8 degrees) swirl, high (-27.0 degrees) swirl, and maximum (-37.0 degrees), and the low swirl case corresponds to peak system efficiency at maximum power.

Figure 74 shows the results of each vector diagram over the entire duty cycle. At idle, the maximum swirl design increased efficiency by approximately 6.0 points compared to the low-swirl design. At maximum throttle and cruise, the performance of the high-swirl and maximum-swirl designs was almost equivalent. At maximum power, the maximum swirl efficiency was reduced by approximately 2.5 points. Overall, the high-swirl design appeared to offer the best compromise between reduced maximum power and increased part-power characteristics. However, cycle studies will be required for each case before a final selection can be made. Not only were the off-design characteristics

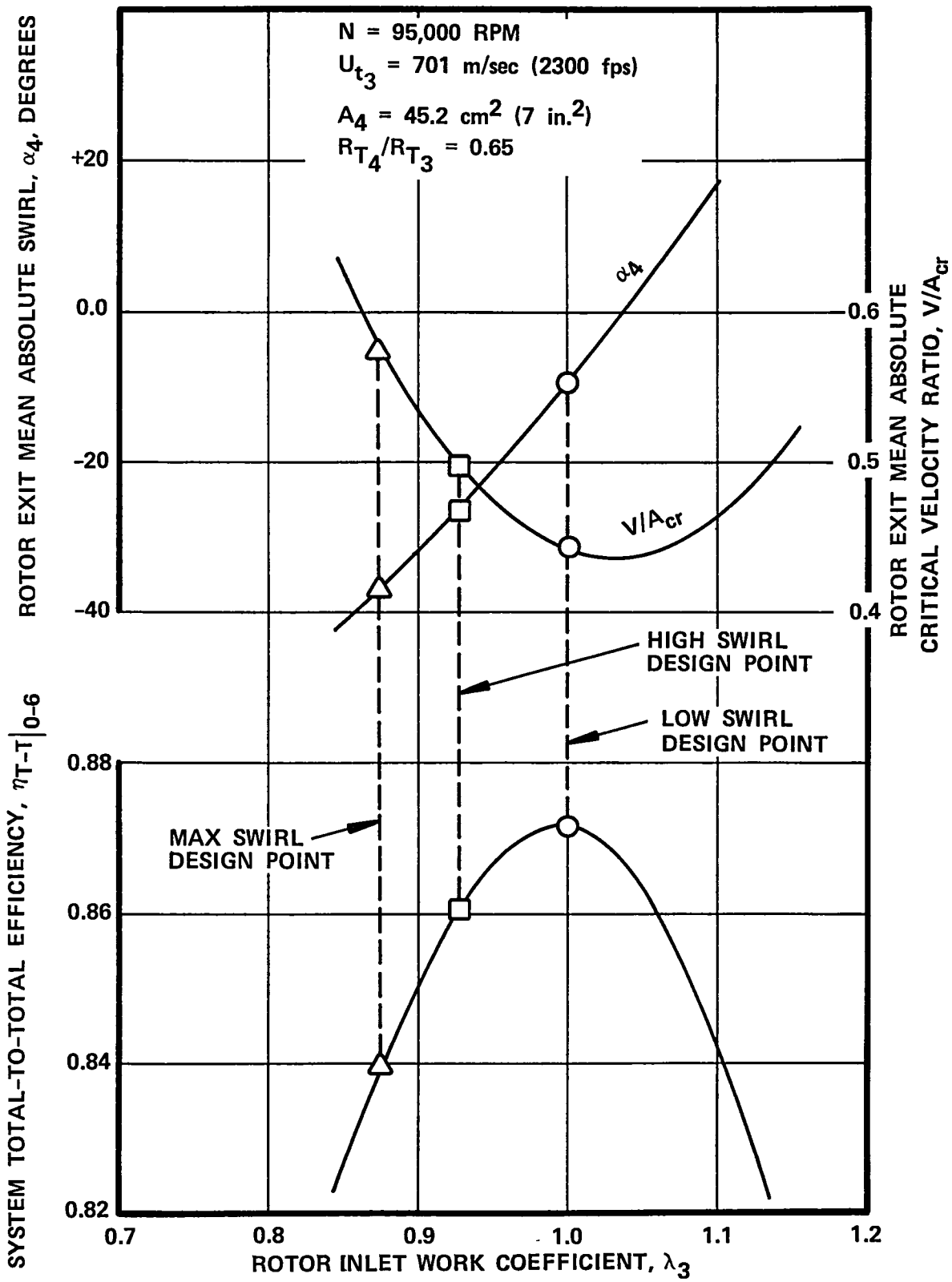

Figure 73. Maximum Power Design-Point Selection for Off-Design Performance Evaluation.

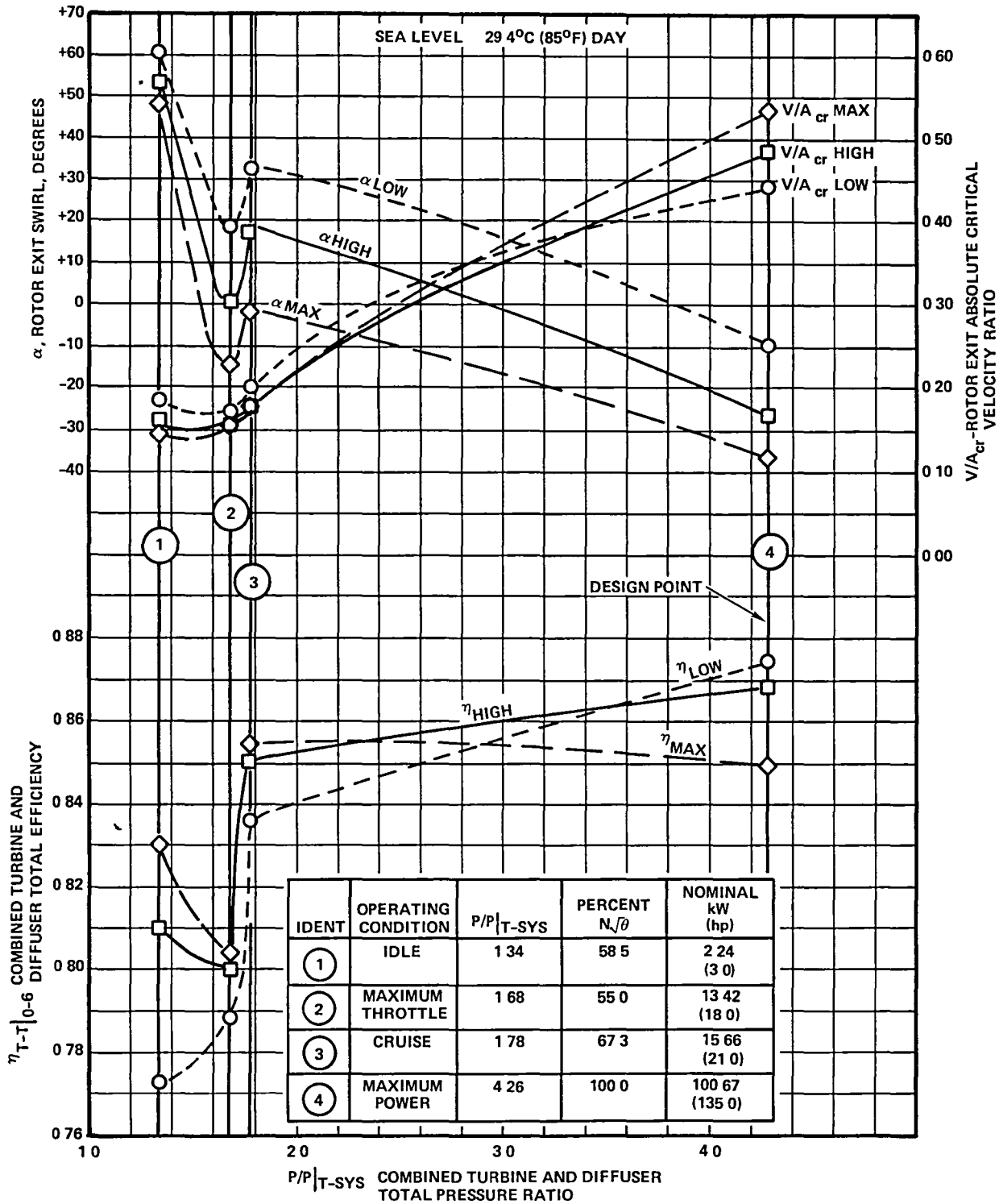

Figure 74. Off-Design Performance Characteristics as a Function of Design-Point Exit Swirl (from NASA-DOE Advanced Gas Turbine Power-Train System Development Program).

strongly dependent on the exhaust duct swirl loss characteristics (and, therefore, had to be known before a vector diagram was selected), but the turbine Reynolds number was reduced significantly at part-power and had to be accounted for in the off-design analysis.

The off-design analysis also confirms that the use of deswirl vanes is not viable for the single-shaft engine application due to the large rotor exit swirl excursion during the normal duty cycle operation. The parametric study has shown that deswirl vanes can significantly reduce downstream duct losses; therefore, deswirl vanes should not be ignored during the turbine optimization process.

6.0 CONCLUSIONS

The results of this program show that exceptionally high radial turbine tip speeds are feasible with the projected 1983 ceramic material properties (62.1 KN/cm^2 characteristic strength and a Weibull modulus of 15). These results indicate a high-work ceramic radial turbine with 0.076 cm (0.030 inch) thick blade tips could achieve both the cycle performance goal of 0.87 η_{T-T} and the rotor mechanical integrity goal of 0.9999 cumulative probability of success for a single-shaft automotive engine application.

Three-dimensional rotor analyses showed that viable high tip speed designs were derived from a design technique that combined the characteristic of low disk volume and relatively deep scallops with a blending of the blades and disk in the rotor back-face region. With radial blade element rotors, three-dimensional mechanical analysis showed that the cumulative probability of success (CPS) goal of 0.9999 was achieved at a tip speed of 701 m/sec (2300 fps).

With a rotor inlet blade angle of 10 degrees, the rotor tip speed requirement was reduced to 686 m/sec (2250 fps), and detailed mechanical optimization of this design showed that the CPS was reduced to 0.9998. At a tip speed of 671 m/sec (2200 fps) and a rotor inlet blade angle of 20 degrees, additional blade thickness was required to achieve tolerable blade stress levels. The increased loading from this additional blade material caused higher disk stresses that adversely effected the CPS value. Therefore, the conclusion is that although nonradial rotor blading allowed a reduction in tip speed, this advantage was offset by an increase in rotor blade stress levels. This conclusion also would apply with reduced ceramic material properties; that is, the unique ceramic characteristic of low ductility and density favors the lower global stress field associated with the radial bladed designs. Therefore, if the projected ceramic properties are not achieved, turbine performance potential would be reduced with both radial and nonradial blading, and fuel economy would suffer.

Additional observations, resulting from the advanced radial turbine program, are:

- The turbine system optimization technique more accurately identified peak system efficiency configurations compared to an analysis approach involving individual stage and exhaust duct optimization.

- The estimated effects of reaction and rotor exit blockage were relatively important for a large number of solutions examined. Additional work is desirable to more accurately refine/define performance correlations for these effects.

- For engine operation requiring only relatively small variations from turbine design-point operating conditions, the analysis showed that significant improvements in performance were provided with the application of deswirl vanes. However, for a single-shaft automotive engine, the large excursion in rotor exit swirl eliminated consideration of deswirl vanes for this application.

- The off-design analysis showed that the integrated duty cycle performance was highly dependent on the selected design-point vector diagram. This implies that either the effect of rotor exit swirl on duct performance must be accurately known in advance of the study analysis, or that several design-point vector diagram rotor configurations must be evaluated experimentally to arrive at the optimum duty cycle configuration.

APPENDIX A

ABBREVIATIONS AND SYMBOLS

APPENDIX A

ABBREVIATIONS AND SYMBOLS

a - Scroll inlet diameter, cm (in.)

b - Stator exit and rotor inlet passage width, cm (in.)

$b/\Delta R$ - Stator aspect ratio

c - $\ln(r_o + a)/r_o$

g - Force-mass conversion constant, 32.174 lbm-ft/ lbf-sec^2

q - Dynamic pressure, kN/m^2 (lb/in.^{2})

r_o - Scroll inside radius, cm (in.)

w - Stage mass flow, kg/sec (lb/sec)

$w\sqrt{\theta}/\delta$ - Stage inlet corrected flow, kg/sec (lb/sec)

A - Annular area, cm^2 (in.^{2})

J - Mechanical equivalent of heat, 778.0 ft-lbf/Btu

L - Rotor axial length, diffuser length, cm (in.)

M - Meridional length, cm (in.)/Rotor exit mean, cm (in.)

N - Rotational or shaft speed, rpm

R - Radius, cm (in.)

U - Blade speed, m/sec (ft/sec)

V - Absolute velocity, m/sec (ft/sec)

W - Relative velocity, m/sec (ft/sec)

Z - Axial dimension, cm (in.)

A_{cr} - Critical velocity $\left(\frac{2}{+1} gR_g T_T\right)^{1/2}$, m/sec (ft/sec)

AR - Deswirl vane aspect ratio

Ca - Axial rotor shroud clearance, cm (in.)

Cb - Rotor backface clearance, cm (in.)

Cr - Radial rotor shroud clearance, cm (in.)

D_H - Hydraulic diameter, m (ft)

Max - Maximum

MC - Midchannel

Min - Minimum loss coefficient

M_N - Absolute flow Mach number

$M_{N_{REL}}$ - Relative flow Mach number

$N/\sqrt{\theta}$ - Corrected speed, rpm

N_B - Rotor blade number

N_S - Specific speed $\frac{N\left(V_{x_4} A_4\right)^{1/2}}{\left(J\Delta H_{T_{ISEN}}\right)^{3/4}}$, rpm ($ft^{3/4}/sec^{1/2}$)

N_v - Number of stator vanes

$P_{R_{T-DE}}$ - Total-to-diffuser exit static pressure ratio

P_R - Pressure ratio

PS - Pressure surface

P_S - Static pressure, kN/m^2 ($lb/in.^2$)

P_{STD} - Standard atmospheric pressure, 1.01325 kN/m^2 (14.696 $lb/in.^2$)

P_T - Total pressure, kN/m^2 ($lb/in.^2$)

ABBREVIATIONS AND SYMBOLS (Contd)

R_D - Diffuser recovery $\left(P_{S_6} - P_{S_4}\right) / q_4$

Re - Reynolds number for turbine stage (w/R_T)

$\bar{R}e$ - Reynolds number for turbine scroll

R_g - Gas constant, J/kg K (ft-lb/lb-°R)

R_{STG} - Stage reaction

S.F. - Slip factor for radial blades

SS - Suction surface

T_{STD} - Standard atmospheric temperature, 288.2 K (518.7°R)

TPLP - Total pressure loss parameter

T_T - Absolute total temperature, K (°R)

U_t - Blade tip speed, m/sec (ft/sec)

V_R - Absolute radial velocity, m/sec (ft/sec)

V_u - Absolute tangential velocity, m/sec (ft/sec)

V_x - Absolute axial velocity, m/sec (ft/sec)

W - Relative velocity, m/sec (ft/sec)

W/A_{cr} - Relative critical velocity ratio

α - Rotor exit swirl angle, absolute flow angle, degrees (measured from axial direction)

β - Rotor blade angle, degrees

β_B - Rotor inlet blade angle, degrees

γ - Ratio of specific heats

δ - Ratio of turbine inlet total pressure to standard atmospheric pressure

$\Delta\alpha$ - Total stator turning, degrees

Δh - Static enthalpy change across rotor, kJ/kg (Btu/lb)

ΔH_T - Specific stage work, kJ/kg (Btu/lb) (based on total conditions)

$\Delta H_T/\theta$ - Specific stage corrected work, kJ/kg (Btu/lb) (based on total conditions)

$\Delta P/P$ - Total pressure loss

ΔR - Stator radial chord, rotor exit blade height, cm (in.)

$\Delta\eta$ - Change in efficiency

η - Efficiency

θ - Ratio of turbine inlet total temperature to standard atmospheric temperature

θ_{eq} - Equivalent cone angle defined in Appendix B

λ - Work coefficient (V_u/U)

$\overline{\lambda}$ - Friction resistance coefficient for scroll loss

STG - Stage work coefficient $\left(gJ\Delta H_T/U_{t_3}^2\right)$

$\lambda_{3,i}$ - Ideal rotor inlet work coefficient

$\lambda_{3,act}$ - Actual rotor inlet work coefficient from vector diagram

$\lambda_{4,M}$ - Rotor exit mean work coefficient

ν - Kinematic viscosity, m^2/sec (ft^2/sec)

μ - Absolute viscosity, N sec/m^2 ($lb\text{-}sec/ft^2$)

$\overline{\omega}$ - Loss coefficient $\left(P_{T_{in}} - P_{T_{out}}\right)\Big/q$

SUBSCRIPTS

base - Base turbine total efficiency from specific speed curve

blockage - Rotor exit blockage

D - Diffusion efficiency

i - Turbine stage total efficiency with incidence loss

final - Total system efficiency with blockage and reaction effects

ISEN - Isentropic

loss - Rotor relative total pressure loss

max - Maximum

min - Minimum

reaction - Stage reaction

T-DE - Total to diffuser exit static

T - Tip

T-sys - Inlet total to exhaust diffuser exit total

T-T - Stage or system total-to-total efficiency

Turbine System Station Nomenclature

o - Scroll inlet (combustor discharge)

1 - Stator inlet

2 - Stator exit

3 - Rotor inlet

4 - Rotor exit (deswirl vane inlet)

5 - Deswirl vane exit (exhaust diffuser inlet)

6 - Exhaust diffuser exit

APPENDIX B

DESWIRL VANE LOSS MODEL

APPENDIX B

DESWIRL VANE LOSS MODEL

For highly loaded radial turbine designs, Section 3.7 showed that system performance is significantly increased with the application of rotor exit deswirl vanes. The concept is to relieve the rotor inducer loading by increasing rotor exit work coefficient, which in turn increases rotor exit velocity and swirl levels. The deswirl vane is then utilized to reestablish axial flow and reduce velocity by the difference between the absolute and axial components.

A comprehensive evaluation of deswirl vane losses was conducted by Mitchell and Soileau (ref. 3) between 1974 and 1977 under Air Force sponsorship. From a preliminary design standpoint, the major results of this program are:

- o Non-series - Airfoils demonstrated a reduction in total pressure, higher diffusion efficiencies, and reduced tendencies for flow separation relative to series airfoils.
- o Conical angle - An equivalent conical angle correlation (θ_{eq}) was extended for diffusing cascades into a range of cone angles applicable to advanced engine turbine exit guide vanes. The correlation is used to define optimum diffusion efficiencies and was successfully demonstrated in 3-D annular cascade testing.

The correlation derived by Mitchell and Soileau (from diffusing cascade data) is presented in Figure 75. The correlation relates equivalent cone angle (the rate of diffusion) with diffusion efficiency (η_D) as a function of equivalent area ratio (amount of diffusion).

The equivalent cone angle is defined with the nomenclature of this report as:

$$\theta_{eq} = \tan^{-1}\left[0.564\left(\frac{AR}{\sigma}\right)^{1/2}\left(\cos \alpha_5^{1/2} - \cos \alpha_4\right)^{1/2}\right]$$

With parallel end-walls, the equivalent area ratio is:

$$A_5/A_4 = \frac{1}{\cos \alpha_4}$$

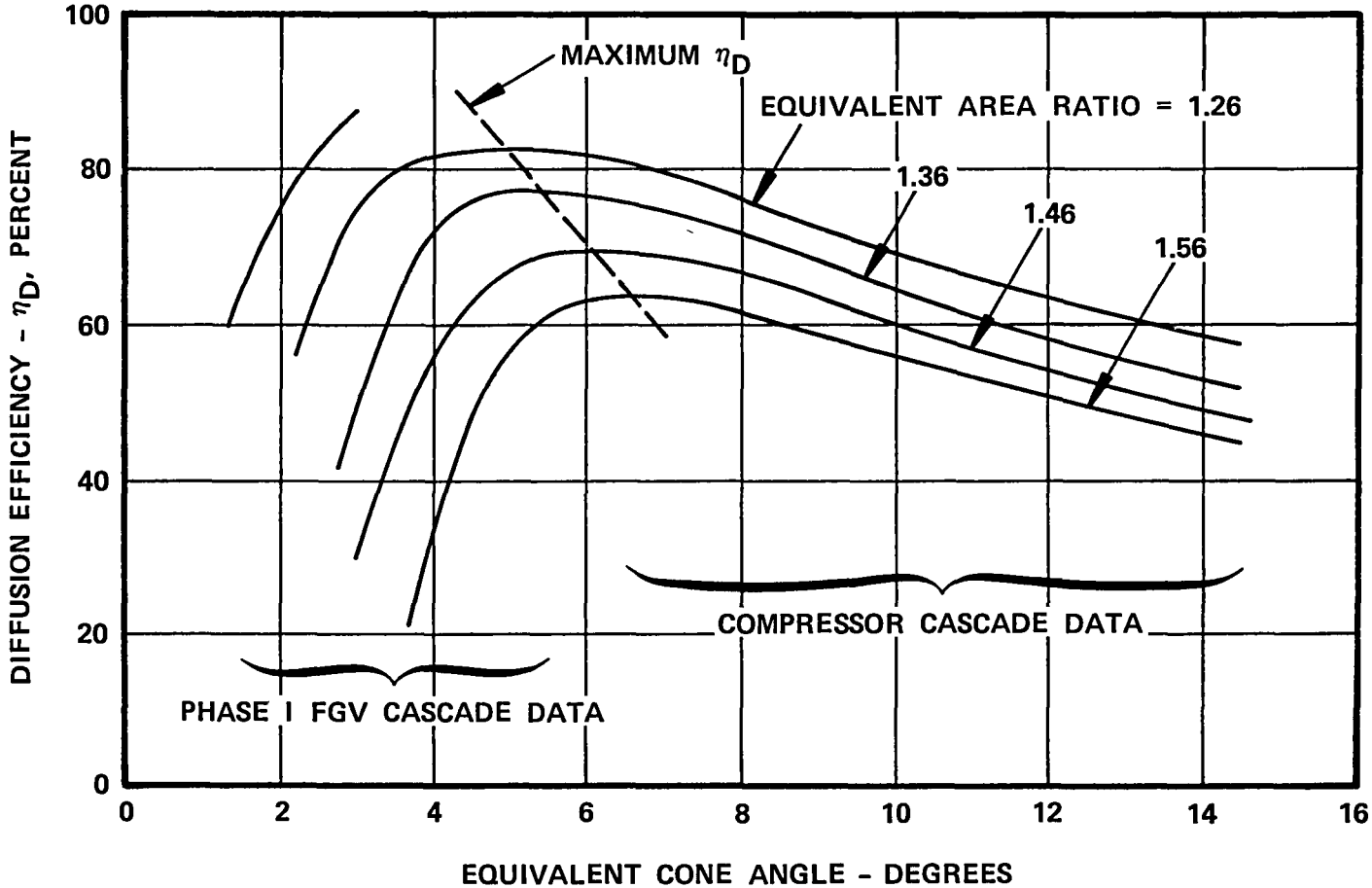

Figure 75. Equivalent Conical Angle Correlation of Diffusing Cascade Data (ref. 3).

The diffusion efficiency relates the actual-to-ideal recovery in the following manner:

$$\eta_D = \frac{(P_{S5} - P_{S4})/[P_{T4} - P_{S4(measured)}]}{(P_{S5} - P_{S4})/[P_{T4} - P_{S4(ideal)}]}$$

For the advanced radial turbine parametric study, the line of optimum diffuser efficiency shown in Figure 75 was used to define a relationship between equivalent area ratio and efficiency (Figure 76). Since parallel end-walls were assumed for the study (consistent with the selected diffuser geometry), the rotor exit swirl angle is shown as a function of area ratio. From the data of Figure 76, rotor exit swirl levels from 37.47 to 50 degrees can be evaluated. Fifty degrees appeared reasonable for the upper limit and, therefore, the maximum rotor exit angle considered with deswirl vanes was set at this value. However, at the lower swirl levels, the trade-off occurrence between deswirl and no deswirl vanes is not clear. Therefore, the data from Figure 76 was extrapolated to 30 degrees, and then conventional axial compressor cascade correlations were used to define the deswirl vane loss to 0-degree swirl.

The loss model for 0- to 30-degree exit swirls was based on an in-house correlation between a total loss parameter (TPLP) and diffusion factor (D_f) with corrections for end-wall effects. With representative values of solidity (σ) and diffusion factor of 1.4 and 0.4, respectively, a loss coefficient ($\bar{\omega}$) was calculated with the following relationship:

$$\bar{\omega} = \frac{2(TPLP)}{\cos \alpha_4}$$

For exit swirl levels from 30 to 50 degrees, nonseries airfoils were assumed to apply, and the total pressure loss for the deswirl vanes were calculated.

From the one-dimensional rotor vector exit mean-line vector diagram, the following quantities were known:

$$\frac{V}{A_{cr}} \quad , \quad \alpha_4 \quad , \quad P_{T4} \quad , \quad P_{S4} \quad , \quad \text{and} \quad \left.\frac{w\sqrt{T}}{A\ P_T}\right|_4$$

The deswirl vane ideal exit conditions can be obtained from the area ratio and continuity relationships. The equation is rearranged to solve for the deswirl vane exit static pressure (since diffusion efficiency is known):

$$P_{S5(measured)} = \eta_D \left(\frac{P_{S5} - P_{S4}}{P_{T4} - P_{S4}}\right)_{ideal} [P_{T4} - P_{S4(measured)}]$$

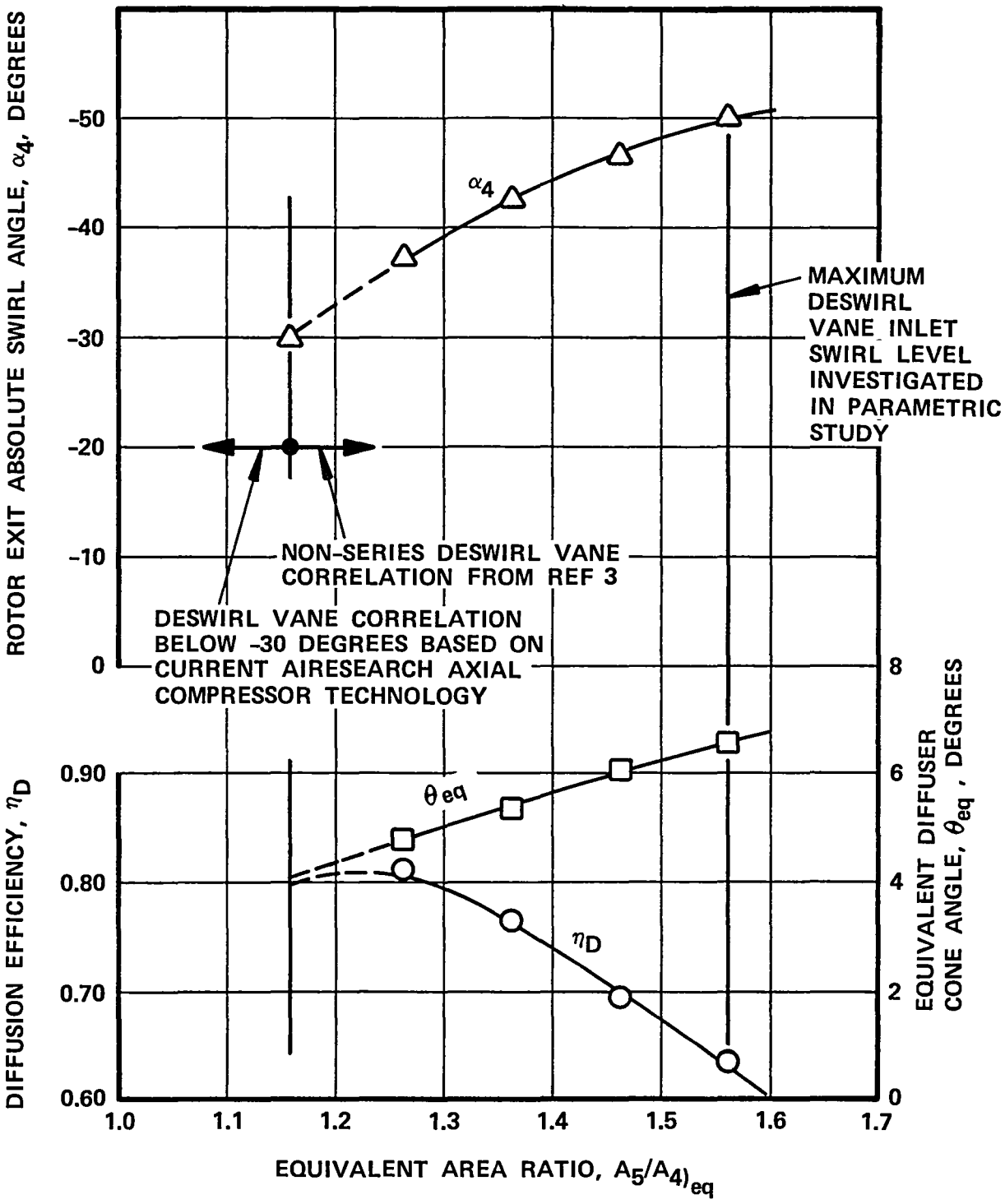

Figure 76. Deswirl Equivalent Area Ratio for Maximum Diffusion Efficiency (ref. 3).

The deswirl vane exit measured static pressure is used to solve for continuity, and an exit measured total pressure is defined.

The downstream diffuser loss is based on the axial velocity (zero swirl), total pressure, and loss coefficient established at the deswirl vane exit. The summation of the deswirl vane and diffuser losses are used with the stage efficiency to define the system efficiency for the particular configuration being examined in the parametric study.

APPENDIX C

ROTOR FLOW PATH AND BLADE GEOMETRY FOR β_B = 0, 10 AND 20°

APPENDIX C

ROTOR FLOW PATH AND BLADE GEOMETRY FOR β_B = 0, 10 AND 20°

The rotor flow path and blade geometry for the three rotor inlet blade angle configurations are presented in Tables I, II and III for β_B = 0, 10 and 20°, respectively. The data array included is for 7 equally-spaced modal points along a quasi-orthogonal station line. The first station point is on the shroud streamline and the last (seventh) point defines the hub streamline. The blade normal thickness is defined as the base-line distribution for β_B = 0°. The variables for each station line are defined below:

R - Local radius on station line (inches)

Z - Local axial dimension on station line (inches) (Z = 0 is defined at rotor trailing edge)

BETA - True blade angle ($\tan \beta = \frac{R d\phi}{dm}$)

where:

ϕ = Polar angle about the axis of rotation

m = Meridional distance along a streamline

DEV - DEVIATION; the difference between the rotor flow and blade angle in degrees. Rotor inlet and exit deviations were applied in the internal flow solution

THICK - Blade normal thickness (inches)

The final thickness array used to minimize the blade bending stresses for β_B = 10 and 20° is presented in Tables IV and V. Station data in these two tables starts at the blade inlet, instead of the exit, and contains tangential thickness in place of normal thickness. Beta distribution for these thickness distributions is similar to the distributions in Tables II and III. Dimensions are in inches.

Rot Number 4 = Blade Trailing Edge
Ind Number 19 = Blade Leading Edge

ST					
R					
Z					
BETA	1.59300	1.50300	1.41200	1.32100	1.23000
DEV	.70900	.79100	.87300	.95500	1.04000
THICK	10.67000	24.07000	17.47000	10.87000	4.27000
	-0.00000	-0.00000	-0.00000	-0.00000	-0.00000
S1	.03803	.05136	.07159	.09816	.15148
R					
Z					
BETA	1.65300	1.57900	1.50500	1.43200	1.35800
DEV	.83800	.93000	1.02200	1.11300	1.20500
THICK	14.18000	18.38000	12.58000	6.78000	.98500
	-0.00000	-0.00000	-0.00000	-0.00000	-0.00000
S1	.03816	.05302	.07266	.10703	.15825
R					
Z					
BETA	1.73100	1.67700	1.62200	1.56800	1.51300
DEV	.97800	1.07400	1.16900	1.26500	1.35780
THICK	6.43000	12.36000	8.29000	4.21000	.14000
	0.00000	-0.00000	-0.00000	-0.00000	-0.00000
S1	.04046	.05711	.08627	.12351	.17630
R					
Z					
BETA	1.85000	1.81250	1.77500	1.73750	1.70000
DEV	1.11500	1.20300	1.29000	1.37800	1.46500
THICK	8.49000	6.38000	4.26000	2.14000	.02000
	0.00000	-0.00000	-0.00000	-0.00000	-0.00000
S1	.04758	.06803	.10223	.13418	.18345
R					
Z					
BETA	2.01400	1.99300	1.97200	1.95100	1.93000
DEV	1.24300	1.31800	1.39200	1.46600	1.54000
THICK	3.20000	2.38000	1.56000	.74000	-.08000
	-0.00000	-0.00000	-0.00000	-0.00000	-0.00000
S1	.05690	.08034	.10276	.13592	.17514
R					
Z					
BETA	2.19000	2.18000	2.17000	2.16000	2.15000
DEV	1.33300	1.39500	1.45700	1.51800	1.58000
THICK	1.12000	.83000	.54000	.25000	-.04000
	0.00000	-0.00000	-0.00000	-0.00000	-0.00000
S	.05579	.06933	.08792	.09870	.11225
R					
Z					
BETA	2.39300	2.39000	2.38700	2.38300	2.38000
DEV	1.39300	1.44500	1.49700	1.54800	1.60000
THICK	.16300	.13000	.09700	.06300	.03000
	0.00000	-0.00000	-0.00000	-0.00000	-0.00000
S	.04252	.04704	.05687	.06238	.06696
R					
Z					
BETA	2.59300	2.59000	2.58700	2.58300	2.58000
DEV	1.42300	1.46800	1.51200	1.55600	1.60000
THICK	0.00000	-0.00000	-0.00000	-0.00000	-0.00000
	0.00000	-0.00000	-0.00000	-0.00000	-0.00000
S	.03498	.03515	.03535	.03554	.03601
R					
Z					
BETA	2.77430	2.77430	2.77430	2.77430	2.77430
DEV	1.43850	1.47890	1.51930	1.55960	1.60000
THICK	0.00000	0.00000	0.00000	0.00000	0.00000
	0.00000	-0.00000	-0.00000	-0.00000	-0.00000
S	.03013	.03010	.03008	.03008	.03009
R					
Z					
BETA	2.92390	2.92390	2.92390	2.92390	2.92390
DEV	1.43850	1.47890	1.51930	1.55960	1.60000
THICK	0.00000	-0.00000	-0.00000	-0.00000	-0.00000
	0.00000	-0.00000	-0.00000	-0.00000	-0.00000
	.03596	.03596	.03596	.03596	.03596

This Page Intentionally Left Blank

TABLE II. ROTOR FLOW PATH AND BLADE GEOMETRY
FOR β_B = 10.0 DEGREES

Rotational Speed = 95,000 rpm
Inducer Tip Speed = 2250 fps

Station Number 4 = Blade Trailing Edge
Station Number 19 = Blade Leading Edge

STATION NUMBER 1							
R	1.75300	1.61417	1.47533	1.33650	1.19767	1.05883	.92000
Z	-.20000	-.20000	-.20000	-.20000	-.20000	-.20000	-.20000
BETA	60.50000	57.70000	54.90000	52.10000	49.01700	45.93300	42.85000
DEV	-0.00000	-0.00000	-0.00000	-0.00000	-0.00000	-0.00000	-0.00000
THICK	.02781	.02781	.03532	.04771	.06448	.08341	.10701
STATION NUMBER 2							
R	1.75300	1.61417	1.47533	1.33650	1.19767	1.05883	.92000
Z	-.13330	-.13330	-.13330	-.13330	-.13330	-.13300	-.13300
BETA	60.45000	57.53300	54.61700	51.70000	48.68300	45.66700	42.65000
DEV	-0.00000	-0.00000	-0.00000	-0.00000	-0.00000	-0.00000	-0.00000
THICK	.02781	.02781	.03532	.04771	.06448	.08341	.10701
STATION NUMBER 3							
R	1.75300	1.61480	1.47670	1.33850	1.20030	1.06220	.92400
Z	-.06670	-.06670	-.06670	-.06670	-.06670	-.06670	-.06670
BETA	60.10000	57.13300	54.16700	51.20000	48.20000	45.20000	42.20000
DEV	-0.00000	-0.00000	-0.00000	-0.00000	-0.00000	-0.00000	-0.00000
THICK	.02781	.02781	.03532	.04771	.06448	.08341	.10701
STATION NUMBER 4							
R	1.75300	1.61530	1.47770	1.34000	1.20230	1.06470	.92700
Z	0.00000	0.00000	0.00000	0.00000	0.00000	0.00000	0.00000
BETA	59.40000	56.43300	53.46700	50.50000	47.50000	44.50000	41.50000
DEV	-0.00000	-0.00000	-0.00000	-0.00000	-0.00000	-0.00000	-0.00000
THICK	.02781	.02781	.03532	.04771	.06448	.08341	.09865
STATION NUMBER 5							
R	1.75300	1.61720	1.48130	1.34550	1.20970	1.07380	.93800
Z	.06700	.07550	.08400	.09250	.10100	.10950	.11800
BETA	58.45000	55.30000	52.15000	49.00000	46.00000	43.00000	40.00000
DEV	-0.00000	-0.00000	-0.00000	-0.00000	-0.00000	-0.00000	-0.00000
THICK	.02842	.02842	.03532	.04824	.06513	.08475	.10754
STATION NUMBER 6							
R	1.75300	1.61920	1.48530	1.35150	1.21770	1.08380	.95000
Z	.13600	.15450	.17300	.19150	.21000	.22850	.24700
BETA	56.90000	53.66700	50.43300	47.20000	43.96700	40.73300	37.50000
DEV	-0.00000	-0.00000	-0.00000	-0.00000	-0.00000	-0.00000	-0.00000
THICK	.02861	.02901	.03573	.04830	.06592	.08691	.10800
STATION NUMBER 7							
R	1.75300	1.62250	1.49200	1.36150	1.23100	1.10050	.97000
Z	.21000	.23800	.26700	.29500	.32300	.35170	.38000
BETA	54.67000	51.28000	47.89000	44.49000	41.10000	37.71000	34.32000
DEV	-0.00000	-0.00000	-0.00000	-0.00000	-0.00000	-0.00000	-0.00000
THICK	.02875	.02965	.03586	.04878	.06707	.08810	.11517
STATION NUMBER 8							
R	1.75300	1.62750	1.50200	1.37650	1.25100	1.12550	1.00000
Z	.28500	.32450	.36400	.40350	.44300	.48250	.52200
BETA	52.00000	48.41000	44.83000	41.24000	37.65000	34.07000	30.48000
DEV	-0.00000	-0.00000	-0.00000	-0.00000	-0.00000	-0.00000	-0.00000
THICK	.02885	.03002	.03645	.04937	.06734	.08860	.12580
STATION NUMBER 9							
R	1.75400	1.63670	1.51900	1.40200	1.28500	1.16700	1.05000
Z	.36000	.41500	.46900	.52400	.57900	.63300	.68800
BETA	48.85000	44.96000	41.07000	37.17000	33.28000	29.39000	25.50000
DEV	-0.00000	-0.00000	-0.00000	-0.00000	-0.00000	-0.00000	-0.00000
THICK	.02901	.03057	.03679	.04943	.06772	.09475	.12654
STATION NUMBER 10							
R	1.76000	1.65400	1.54800	1.44300	1.33700	1.23100	1.12500
Z	.44500	.51500	.58400	.65400	.72300	.79300	.86500
BETA	44.78000	40.60000	36.43000	32.25000	28.07000	23.90000	19.72000
DEV	-0.00000	-0.00000	-0.00000	-0.00000	-0.00000	-0.00000	-0.00000
THICK	.02927	.03080	.03798	.05086	.07156	.09593	.14224
STATION NUMBER 11							
R	1.77500	1.68400	1.59300	1.50300	1.41200	1.32100	1.23000
Z	.54500	.62700	.70900	.79100	.87300	.95500	1.04000
BETA	39.34000	35.09000	30.85000	26.60000	22.35000	18.11000	13.86000
DEV	-0.00000	-0.00000	-0.00000	-0.00000	-0.00000	-0.00000	-0.00000
THICK	.02931	.03107	.03803	.05136	.07159	.09816	.15148
STATION NUMBER 12							
R	1.80000	1.72600	1.65300	1.57900	1.50500	1.43200	1.35800
Z	.65500	.74700	.83800	.93000	1.02200	1.11300	1.20500
BETA	32.36000	28.35000	24.33000	20.32000	16.31000	12.29000	8.28000
DEV	-0.00000	-0.00000	-0.00000	-0.00000	-0.00000	-0.00000	-0.00000
THICK	.02947	.03124	.03816	.05302	.07266	.10703	.15825
STATION NUMBER 13							
R	1.84000	1.78600	1.73100	1.67700	1.62200	1.56800	1.51300
Z	.78700	.88300	.97800	1.07400	1.16900	1.26500	1.35780
BETA	23.48000	20.03000	16.58000	13.13000	9.68000	6.23000	2.78000
DEV	-0.00000	-0.00000	-0.00000	-0.00000	-0.00000	-0.00000	-0.00000
THICK	.02952	.03180	.04046	.05711	.08627	.12351	.17630
STATION NUMBER 14							
R	1.92500	1.88750	1.85000	1.81250	1.77500	1.73750	1.70000
Z	.94000	1.02800	1.11500	1.20300	1.29000	1.37800	1.46500
BETA	13.59000	11.03000	8.47000	5.91000	3.35000	.79000	-1.77000
DEV	-0.00000	-0.00000	-0.00000	-0.00000	-0.00000	-0.00000	-0.00000
THICK	.02981	.03454	.04758	.06803	.10223	.13418	.18345
STATION NUMBER 15							
R	2.05600	2.03500	2.01400	1.99300	1.97200	1.95100	1.93000
Z	1.09500	1.16900	1.24300	1.31800	1.39200	1.46600	1.54000
BETA	4.20000	2.50000	.80000	-.90000	-2.60000	-4.30000	-6.00000
DEV	-0.00000	-0.00000	-0.00000	-0.00000	-0.00000	-0.00000	-0.00000
THICK	.03299	.04162	.05690	.08034	.10276	.13592	.17514
STATION NUMBER 16							
R	2.21000	2.20000	2.19000	2.18000	2.17000	2.16000	2.15000
Z	1.21000	1.27200	1.33300	1.39500	1.45700	1.51800	1.58000
BETA	-2.50000	-3.48000	-4.45000	-5.43000	-6.40000	-7.38000	-8.35000
DEV	-0.00000	-0.00000	-0.00000	-0.00000	-0.00000	-0.00000	-0.00000
THICK	.03515	.04363	.05579	.06933	.08792	.09870	.11225
STATION NUMBER 17							
R	2.40000	2.39700	2.39300	2.39000	2.38700	2.38300	2.38000
Z	1.29000	1.34200	1.39300	1.44500	1.49700	1.54800	1.60000
BETA	-7.20000	-7.63000	-8.05000	-8.48000	-8.90000	-9.33000	-9.75000
DEV	-0.00000	-0.00000	-0.00000	-0.00000	-0.00000	-0.00000	-0.00000
THICK	.03482	.03794	.04252	.04704	.05687	.06238	.06696
STATION NUMBER 18							
R	2.60000	2.59700	2.59300	2.59000	2.58700	2.58300	2.58000
Z	1.33500	1.37900	1.42300	1.46800	1.51200	1.55600	1.60000
BETA	-9.70000	-9.75000	-9.80000	-9.85000	-9.90000	-9.95000	-10.00000
DEV	-0.00000	-0.00000	-0.00000	-0.00000	-0.00000	-0.00000	-0.00000
THICK	.03471	.03486	.03498	.03515	.03535	.03554	.03601
STATION NUMBER 19							
R	2.71400	2.71400	2.71400	2.71400	2.71400	2.71400	2.71400
Z	1.35120	1.39270	1.43410	1.47560	1.51710	1.55850	1.60000
BETA	-10.00000	-10.00000	-10.00000	-10.00000	-10.00000	-10.00000	-10.00000
DEV	-0.00000	-0.00000	-0.00000	-0.00000	-0.00000	-0.00000	-0.00000
THICK	.03038	.03025	.03013	.03010	.03008	.03008	.03009
STATION NUMBER 20							
R	2.86780	2.86780	2.86780	2.86780	2.86780	2.86780	2.86780
Z	1.35120	1.39270	1.43410	1.47560	1.51710	1.55850	1.60000
BETA	-10.00000	-10.00000	-10.00000	-10.00000	-10.00000	-10.00000	-10.00000
DEV	-0.00000	-0.00000	-0.00000	-0.00000	-0.00000	-0.00000	-0.00000
THICK	.03522	.03522	.03522	.03522	.03522	.03522	.03522

This Page Intentionally Left Blank

TABLE III. ROTOR FLOW PATH AND BLADE GEOMETRY
FOR β_B = 20.0 DEGREES

Rotational Speed = 95,000 rpm
Inducer Tip Speed = 2200 fps

Station Number 5 = Blade Trailing Edge
Station Number 20 = Blade Leading Edge

STATION NUMBER 1							
R	1.75300	1.61417	1.47533	1.33650	1.19767	1.05883	.92000
Z	-.30000	-.30000	-.30000	-.30000	-.30000	-.30000	-.30000
BETA	60.60000	58.54000	56.20000	53.53000	50.48600	46.99000	42.96600
DEV	-0.00000	-0.00000	-0.00000	-0.00000	-0.00000	-0.00000	-0.00000
THICK	.02781	.02781	.03532	.04771	.06448	.08341	.10701

STATION NUMBER 2							
R	1.75300	1.61417	1.47533	1.33650	1.19767	1.05883	.92000
Z	-.20000	-.20000	-.20000	-.20000	-.20000	-.20000	-.20000
BETA	60.50000	57.70000	54.90000	52.10000	49.01700	45.93300	42.85000
DEV	-0.00000	-0.00000	-0.00000	-0.00000	-0.00000	-0.00000	-0.00000
THICK	.02781	.02781	.03532	.04771	.06448	.08341	.10701

STATION NUMBER 3							
R	1.75300	1.61417	1.47533	1.33650	1.19767	1.05883	.92000
Z	-.13330	-.13330	-.13330	-.13330	-.13330	-.13300	-.13300
BETA	59.80000	56.88000	53.97000	51.05000	48.13000	45.22000	42.30000
DEV	-0.00000	-0.00000	-0.00000	-0.00000	-0.00000	-0.00000	-0.00000
THICK	.02781	.02781	.03532	.04771	.06448	.08341	.10701

STATION NUMBER 4							
R	1.75300	1.61480	1.47670	1.33850	1.20030	1.06220	.92400
Z	-.06670	-.06670	-.06670	-.06670	-.06670	-.06670	-.06670
BETA	59.18000	56.27000	53.35000	50.44000	47.53000	44.61000	41.70000
DEV	-0.00000	-0.00000	-0.00000	-0.00000	-0.00000	-0.00000	-0.00000
THICK	.02781	.02781	.03532	.04771	.06448	.08341	.10701

STATION NUMBER 5							
R	1.75300	1.61530	1.47770	1.34000	1.20230	1.06470	.92700
Z	0.00000	0.00000	0.00000	0.00000	0.00000	0.00000	0.00000
BETA	58.20000	55.30000	52.40000	49.50000	46.63000	43.76700	40.90000
DEV	-0.00000	-0.00000	-0.00000	-0.00000	-0.00000	-0.00000	-0.00000
THICK	.02781	.02781	.03532	.04771	.06448	.08341	.10701

STATION NUMBER 6							
R	1.75300	1.61720	1.48130	1.34550	1.20970	1.07380	.93800
Z	.06700	.07550	.08400	.09250	.10100	.10950	.11800
BETA	55.50000	52.75000	50.00000	47.25000	44.50000	41.75000	39.00000
DEV	-0.00000	-0.00000	-0.00000	-0.00000	-0.00000	-0.00000	-0.00000
THICK	.02842	.02842	.03532	.04824	.06513	.08475	.10754

STATION NUMBER 7							
R	1.75300	1.61920	1.48530	1.35150	1.21770	1.08380	.95000
Z	.13600	.15450	.17300	.19150	.21000	.22850	.24700
BETA	53.50000	50.55000	47.60000	44.65000	41.70000	38.75000	35.80000
DEV	-0.00000	-0.00000	-0.00000	-0.00000	-0.00000	-0.00000	-0.00000
THICK	.02861	.02901	.03573	.04830	.06592	.08691	.10800

STATION NUMBER 8							
R	1.75300	1.62250	1.49200	1.36150	1.23100	1.10050	.97000
Z	.21000	.23800	.26700	.29500	.32300	.35170	.38000
BETA	50.55000	47.46000	44.37000	41.27000	38.18000	35.09000	32.00000
DEV	-0.00000	-0.00000	-0.00000	-0.00000	-0.00000	-0.00000	-0.00000
THICK	.02875	.02965	.03586	.04878	.06707	.08810	.11517

STATION NUMBER 9							
R	1.75300	1.62750	1.50200	1.37650	1.25100	1.12550	1.00000
Z	.28500	.32450	.36400	.40350	.44300	.48250	.52200
BETA	47.70000	44.28000	40.87000	37.45000	34.03000	30.62000	27.20000
DEV	-0.00000	-0.00000	-0.00000	-0.00000	-0.00000	-0.00000	-0.00000
THICK	.02885	.03002	.03645	.04937	.06734	.08860	.12580

STATION NUMBER 10							
R	1.75400	1.63670	1.51900	1.40200	1.28500	1.16700	1.05000
Z	.36000	.41500	.46900	.52400	.57900	.63300	.68800
BETA	45.34000	41.25000	37.16000	33.07000	28.98000	24.89000	20.80000
DEV	-0.00000	-0.00000	-0.00000	-0.00000	-0.00000	-0.00000	-0.00000
THICK	.02901	.03057	.03679	.04943	.06772	.09475	.12654

STATION NUMBER 11							
R	1.76000	1.65400	1.54800	1.44300	1.33700	1.23100	1.12500
Z	.44500	.51500	.58400	.65400	.72300	.79300	.86500
BETA	39.50000	35.22000	30.93000	26.65000	22.37000	18.08000	13.80000
DEV	-0.00000	-0.00000	-0.00000	-0.00000	-0.00000	-0.00000	-0.00000
THICK	.02927	.03080	.03798	.05086	.07156	.09593	.14224

STATION NUMBER 12							
R	1.77500	1.68400	1.59300	1.50300	1.41200	1.32100	1.23000
Z	.54500	.62700	.70900	.79100	.87300	.95500	1.04000
BETA	33.00000	28.51000	24.02000	19.52000	15.03000	10.54000	6.05000
DEV	-0.00000	-0.00000	-0.00000	-0.00000	-0.00000	-0.00000	-0.00000
THICK	.02931	.03107	.03803	.05136	.07159	.09816	.15148

STATION NUMBER 13							
R	1.80000	1.72600	1.65300	1.57900	1.50500	1.43200	1.35800
Z	.65500	.74700	.83800	.93000	1.02200	1.11300	1.20500
BETA	25.75000	21.33000	16.90000	12.48000	8.05000	3.63000	-.80000
DEV	-0.00000	-0.00000	-0.00000	-0.00000	-0.00000	-0.00000	-0.00000
THICK	.02947	.03124	.03816	.05302	.07266	.10703	.15825

STATION NUMBER 14							
R	1.84000	1.78600	1.73100	1.67700	1.62200	1.56800	1.51300
Z	.78700	.88000	.97310	1.06610	1.15910	1.25220	1.34520
BETA	16.20000	12.46000	8.73000	4.99000	1.25000	-2.48000	-6.22000
DEV	-0.00000	-0.00000	-0.00000	-0.00000	-0.00000	-0.00000	-0.00000
THICK	.02952	.03180	.04046	.05711	.08627	.12351	.17630

STATION NUMBER 15							
R	1.92500	1.88750	1.85000	1.81250	1.77500	1.73750	1.70000
Z	.94000	1.02800	1.11500	1.20300	1.29000	1.37800	1.46500
BETA	5.44000	2.62000	-.19000	-3.01000	-5.83000	-8.64000	-11.46000
DEV	-0.00000	-0.00000	-0.00000	-0.00000	-0.00000	-0.00000	-0.00000
THICK	.02981	.03454	.04758	.06803	.10223	.13418	.18345

STATION NUMBER 16							
R	2.05600	2.03500	2.01400	1.99300	1.97200	1.95100	1.93000
Z	1.09500	1.16900	1.24300	1.31800	1.39200	1.46600	1.54000
BETA	-6.00000	-7.60000	-9.20000	-10.80000	-12.40000	-14.00000	-15.60000
DEV	-0.00000	-0.00000	-0.00000	-0.00000	-0.00000	-0.00000	-0.00000
THICK	.03299	.04162	.05690	.08034	.10276	.13592	.17514

STATION NUMBER 17							
R	2.21000	2.20000	2.19000	2.18000	2.17000	2.16000	2.15000
Z	1.21000	1.27200	1.33300	1.39500	1.45700	1.51800	1.58000
BETA	-13.30000	-14.12000	-14.93000	-15.75000	-16.57000	-17.38000	-18.20000
DEV	-0.00000	-0.00000	-0.00000	-0.00000	-0.00000	-0.00000	-0.00000
THICK	.03515	.04363	.05579	.06933	.08792	.09870	.11225

STATION NUMBER 18							
R	2.40000	2.39700	2.39300	2.39000	2.38700	2.38300	2.38000
Z	1.29000	1.34200	1.39300	1.44500	1.49700	1.54800	1.60000
BETA	-18.00000	-18.30000	-18.60000	-18.90000	-19.20000	-19.50000	-19.80000
DEV	-0.00000	-0.00000	-0.00000	-0.00000	-0.00000	-0.00000	-0.00000
THICK	.03482	.03794	.04252	.04704	.05687	.06238	.06696

STATION NUMBER 19							
R	2.60000	2.59700	2.59300	2.59000	2.58700	2.58300	2.58000
Z	1.33500	1.37900	1.42300	1.46800	1.51200	1.55600	1.60000
BETA	-20.00000	-20.00000	-20.00000	-20.00000	-20.00000	-20.00000	-20.00000
DEV	-0.00000	-0.00000	-0.00000	-0.00000	-0.00000	-0.00000	-0.00000
THICK	.03471	.03486	.03498	.03515	.03535	.03554	.03601

STATION NUMBER 20							
R	2.65370	2.65370	2.65370	2.65370	2.65370	2.65370	2.65370
Z	1.34520	1.38770	1.43010	1.47260	1.51510	1.55750	1.60000
BETA	-20.00000	-20.00000	-20.00000	-20.00000	-20.00000	-20.00000	-20.00000
DEV	-0.00000	-0.00000	-0.00000	-0.00000	-0.00000	-0.00000	-0.00000
THICK	.03038	.03025	.03013	.03010	.03008	.03008	.03009

STATION NUMBER 21							
R	2.81110	2.81110	2.81110	2.81110	2.81110	2.81110	2.81110
Z	1.34520	1.38770	1.43010	1.47260	1.51510	1.55750	1.60000
BETA	-20.00000	-20.00000	-20.00000	-20.00000	-20.00000	-20.00000	-20.00000
DEV	-0.00000	-0.00000	-0.00000	-0.00000	-0.00000	-0.00000	-0.00000
THICK	.03458	.03458	.03458	.03458	.03458	.03458	.03458

This Page Intentionally Left Blank

Rotational Speed = 95,000 rpm
Inducer Tip Speed = 2250 fps

NOTE:
X = Axial distance (inches)
T = Tangential thickness (inches)

STATION NO. 1

STREAMLINE	X	R	T
1	.2488	2.7140	.0417
2	.2281	2.7140	.0427
3	.2073	2.7140	.0433
4	.1866	2.7140	.0492
5	.1659	2.7139	.0494
6	.1451	2.7140	.0498
7	.1244	2.7140	.0548
8	.1037	2.7140	.0539
9	.0829	2.7140	.0542
10	.0622	2.7140	.0575
11	.0415	2.7140	.0560
12	.0207	2.7140	.0560
13	0.0000	2.7140	.0587

STATION NO. 2

STREAMLINE	X	R	T
1	.2613	2.6235	.0484
2	.2388	2.6228	.0541
3	.2163	2.6223	.0562
4	.1938	2.6217	.0588
5	.1713	2.6211	.0637
6	.1489	2.6205	.0659
7	.1264	2.6199	.0699
8	.1039	2.6193	.0705
9	.0814	2.6187	.0718
10	.0589	2.6181	.0746
11	.0364	2.6175	.0736
12	.0139	2.6169	.0743
13	-.0086	2.6163	.0748

STATION NO. 3

STREAMLINE	X	R	T
1	.2771	2.5331	.0565
2	.2525	2.5318	.0628
3	.2280	2.5306	.0660
4	.2035	2.5294	.0704
5	.1790	2.5282	.0776
6	.1544	2.5270	.0822
7	.1299	2.5258	.0857
8	.1054	2.5246	.0908
9	.0809	2.5234	.0917
10	.0563	2.5221	.0925
11	.0318	2.5210	.0950
12	.0073	2.5198	.0958
13	-.0172	2.5185	.0958

STATION NO. 4

STREAMLINE	X	R	T
1	.2977	2.4435	.0621
2	.2707	2.4415	.0668
3	.2437	2.4397	.0746
4	.2166	2.4378	.0823
5	.1896	2.4359	.0894
6	.1626	2.4340	.0979
7	.1356	2.4322	.1007
8	.1086	2.4303	.1092
9	.0816	2.4284	.1106
10	.0546	2.4265	.1145
11	.0276	2.4247	.1148
12	.0006	2.4228	.1134
13	-.0264	2.4209	.1151

STATION NO. 5

STREAMLINE	X	R	T
1	.3248	2.3552	.0627
2	.2947	2.3525	.0741
3	.2646	2.3498	.0775
4	.2345	2.3472	.0936
5	.2044	2.3445	.0976
6	.1743	2.3419	.1137
7	.1442	2.3393	.1171
8	.1141	2.3366	.1279
9	.0841	2.3340	.1299
10	.0540	2.3313	.1344
11	.0239	2.3287	.1350
12	-.0062	2.3260	.1355
13	-.0363	2.3233	.1357

STATION NO. 6

STREAMLINE	X	R	T
1	.3597	2.2692	.0673
2	.3258	2.2657	.0701
3	.2918	2.2621	.0840
4	.2579	2.2584	.0948
5	.2240	2.2548	.1087
6	.1900	2.2512	.1197
7	.1561	2.2476	.1328
8	.1221	2.2440	.1459
9	.0882	2.2403	.1487
10	.0542	2.2367	.1547
11	.0203	2.2331	.1561
12	-.0136	2.2295	.1582
13	-.0476	2.2259	.1589

STATION NO. 7

STREAMLINE	X	R	T
1	.4035	2.1876	.0630
2	.3649	2.1827	.0740
3	.3261	2.1778	.0780
4	.2874	2.1729	.0956
5	.2487	2.1680	.1094
6	.2100	2.1631	.1253
7	.1713	2.1582	.1469
8	.1326	2.1532	.1523
9	.0939	2.1483	.1669
10	.0552	2.1434	.1746
11	.0165	2.1386	.1779
12	-.0222	2.1336	.1835
13	-.0609	2.1287	.1873

STATION NO. 8

STREAMLINE	X	R	T
1	.4572	2.1116	.0607
2	.4127	2.1049	.0679
3	.3682	2.0983	.0776
4	.3237	2.0916	.0869
5	.2792	2.0850	.1084
6	.2348	2.0783	.1348
7	.1903	2.0717	.1436
8	.1458	2.0650	.1672
9	.1013	2.0584	.1850
10	.0568	2.0518	.1946
11	.0123	2.0451	.2048
12	-.0322	2.0385	.2146
13	-.0767	2.0318	.2223

STATION NO. 9

STREAMLINE	X	R	T
1	.5187	2.0419	.0591
2	.4673	2.0331	.0649
3	.4160	2.0243	.0734
4	.3647	2.0154	.0865
5	.3133	2.0066	.1045
6	.2620	1.9977	.1238
7	.2107	1.9890	.1543
8	.1593	1.9802	.1824
9	.1080	1.9714	.2029
10	.0567	1.9625	.2157
11	.0053	1.9537	.2285
12	-.0460	1.9449	.2481
13	-.0973	1.9361	.2633

STATION NO. 10

STREAMLINE	X	R	T
1	.5869	1.9797	.0577
2	.5276	1.9682	.0637
3	.4683	1.9568	.0706
4	.4091	1.9453	.0781
5	.3498	1.9338	.0978
6	.2905	1.9223	.1275
7	.2312	1.9108	.1641
8	.1719	1.8993	.1982
9	.1126	1.8878	.2205
10	.0533	1.8764	.2429
11	-.0060	1.8649	.2631
12	-.0653	1.8534	.2867
13	-.1246	1.8420	.2997

TABLE IV. OPTIMIZED TANGENTIAL THICKNESSES FOR β_B = 10 DEGREES

STATION NO. 11

STREAMLINE	X	R	T
1	.6600	1.9749	.0535
2	.5893	1.9084	.0614
3	.5185	1.8918	.0693
4	.4478	1.8752	.0832
5	.3770	1.8586	.0985
6	.3063	1.8421	.1264
7	.2355	1.8254	.1803
8	.1648	1.8089	.2180
9	.0941	1.7923	.2441
10	.0233	1.7757	.2743
11	-.0474	1.7591	.3051
12	-.1046	1.7594	.3282
13	-.1600	1.7500	.3424

STATION NO. 12

STREAMLINE	X	R	T
1	.7730	1.8584	.0519
2	.7033	1.8390	.0573
3	.6337	1.8195	.0618
4	.5641	1.8001	.0716
5	.4945	1.7808	.0805
6	.4248	1.7613	.1011
7	.3552	1.7419	.1290
8	.2856	1.7225	.1733
9	.2159	1.7031	.2149
10	.1463	1.6837	.2500
11	.0767	1.6643	.2822

STATION NO. 13

STREAMLINE	X	R	T
1	.8890	1.8147	.0507
2	.8201	1.7868	.0569
3	.7511	1.7588	.0591
4	.6822	1.7308	.0658
5	.6133	1.7029	.0768
6	.5444	1.6749	.0859
7	.4755	1.6470	.1005
8	.4066	1.6190	.1306
9	.3377	1.9340	.3527
10	.2687	1.5632	.2231
11	.1998	1.5352	.2018

STATION NO. 14

STREAMLINE	X	R	T
1	1.0012	1.7863	.0527
2	.9352	1.7478	.0554
3	.8692	1.7095	.0621
4	.8032	1.6711	.0654
5	.7372	1.6327	.0757
6	.6712	1.5944	.0866
7	.6052	1.5560	.1097
8	.5392	1.5176	.1213
9	.4732	1.4792	.1504
10	.4072	1.4408	.1876
11	.3412	1.4025	.2376

STATION NO. 15

STREAMLINE	X	R	T
1	1.1057	1.7664	.0527
2	1.0452	1.7172	.0625
3	.9847	1.6681	.0651
4	.9241	1.6188	.0718
5	.8636	1.5697	.0776
6	.8031	1.5206	.0902
7	.7426	1.4714	.1054
8	.6820	1.4222	.1283
9	.6215	1.3730	.1583
10	.5610	1.3238	.1785
11	.5004	1.2747	.2226

STATION NO. 16

STREAMLINE	X	R	T
1	1.2025	1.7559	.0529
2	1.1501	1.6967	.0641
3	1.0978	1.6375	.0700
4	1.0454	1.5783	.0749
5	.9930	1.5190	.0826
6	.9406	1.4598	.1008
7	.8883	1.4006	.1156
8	.8359	1.3413	.1352
9	.7835	1.2822	.1668
10	.7311	1.2229	.1899
11	.6788	1.1637	.2245

STATION NO. 17

STREAMLINE	X	R	T
1	1.2920	1.7530	.0534
2	1.2498	1.6849	.0655
3	1.2076	1.6166	.0760
4	1.1654	1.5484	.0865
5	1.1232	1.4802	.0941
6	1.0810	1.4120	.1035
7	1.0389	1.3438	.1262
8	.9967	1.2756	.1520
9	.9545	1.2072	.1754
10	.9123	1.1392	.1972
11	.8701	1.0710	.2386

STATION NO. 18

STREAMLINE	X	R	T
1	1.3750	1.7529	.0550
2	1.3443	1.6778	.0679
3	1.3136	1.6028	.0781
4	1.2829	1.5276	.0903
5	1.2522	1.4526	.1027
6	1.2215	1.3774	.1181
7	1.1908	1.3024	.1412
8	1.1601	1.2273	.1593
9	1.1294	1.1522	.1980
10	1.0987	1.0771	.2231
11	1.0680	1.0020	.2572

STATION NO. 19

STREAMLINE	X	R	T
1	1.4529	1.7530	.0542
2	1.4287	1.6747	.0677
3	1.4067	1.5964	.0794
4	1.3854	1.5182	.0922
5	1.3645	1.4399	.1075
6	1.3446	1.3619	.1275
7	1.3254	1.2839	.1543
8	1.3083	1.2063	.1831
9	1.2907	1.1279	.2140
10	1.2766	1.0483	.2360
11	1.2668	.9585	.2601

STATION NO. 20

STREAMLINE	X	R	T
1	1.5268	1.7531	.0549
2	1.5119	1.6716	.0687
3	1.4987	1.5901	.0804
4	1.4866	1.5087	.0927
5	1.4758	1.4273	.1117
6	1.4660	1.3460	.1332
7	1.4588	1.2654	.1585
8	1.4536	1.1848	.1858
9	1.4539	1.1053	.2157
10	1.4504	1.0225	.2472
11	1.4553	.9334	.2649

STATION NO. 21

STREAMLINE	X	R	T
1	1.5978	1.7530	.0565
2	1.5928	1.6684	.0705
3	1.5890	1.5837	.0805
4	1.5864	1.4991	.0937
5	1.5847	1.4146	.1125
6	1.5853	1.3303	.1358
7	1.5882	1.2461	.1607
8	1.5965	1.1634	.1872
9	1.6097	1.0817	.2134
10	1.6339	1.0036	.2403
11	1.6344	.9221	.2631

STATION NO. 22

STREAMLINE	X	R	T
1	1.6670	1.7530	.0554
2	1.6722	1.6651	.0693
3	1.6778	1.5774	.0805
4	1.6843	1.4895	.0938
5	1.6922	1.4020	.1130
6	1.7009	1.3141	.1439
7	1.7138	1.2271	.1679
8	1.7317	1.1396	.1920
9	1.7595	1.0556	.2153
10	1.8030	.9798	.2316
11	1.8670	.9200	.2517

This Page Intentionally Left Blank

TABLE V. OPTIMIZED TANGENTIAL THICKNESSES FOR β_B = 20 DEGREES

Rotational Speed = 95,000 rpm
Inducer Tip Speed = 2200 fps

NOTE:
X = Axial distance (inches)
T = Tangential thickness (inches

STATION NO. 1

STREAMLINE	X	R	T
1	.2548	2.6537	.0449
2	.2336	2.6537	.0496
3	.2123	2.6537	.0504
4	.1911	2.6537	.0560
5	.1699	2.6537	.0592
6	.1486	2.6537	.0602
7	.1274	2.6537	.0648
8	.1062	2.6536	.0655
9	.0849	2.6537	.0660
10	.0637	2.6537	.0696
11	.0425	2.6537	.0688
12	.0212	2.6537	.0691
13	0.0000	2.6537	.0725

STATION NO. 2

STREAMLINE	X	R	T
1	.2703	2.5720	.0482
2	.2471	2.5712	.0552
3	.2239	2.5703	.0616
4	.2007	2.5696	.0650
5	.1774	2.5688	.0724
6	.1542	2.5679	.0746
7	.1310	2.5670	.0771
8	.1078	2.5661	.0814
9	.0845	2.5653	.0830
10	.0613	2.5645	.0845
11	.0381	2.5637	.0873
12	.0149	2.5628	.0891
13	-.0084	2.5620	.0916

STATION NO. 3

STREAMLINE	X	R	T
1	.2872	2.4900	.9673
2	.2618	2.4883	.9640
3	.2364	2.4867	.9581
4	.2110	2.4850	.9561
5	.1856	2.4835	.9515
6	.1602	2.4818	.9509
7	.1348	2.4802	.9490
8	.1094	2.4785	.9465
9	.0840	2.4769	.9452
10	.0586	2.4753	.9433
11	.0332	2.4736	.9414
12	.0078	2.4720	.1083
13	-.0176	2.4704	.1150

STATION NO. 4

STREAMLINE	X	R	T
1	.3074	2.4083	.0626
2	.2797	2.4059	.0687
3	.2517	2.4034	.0777
4	.2238	2.4009	.0866
5	.1958	2.3984	.0922
6	.1679	2.3961	.1015
7	.1399	2.3936	.1060
8	.1120	2.3911	.1136
9	.0840	2.3886	.1189
10	.0561	2.3863	.1228
11	.0281	2.3838	.1286
12	.0002	2.3813	.1314
13	-.0278	2.3788	.1372

STATION NO. 5

STREAMLINE	X	R	T
1	.3349	2.3276	.0606
2	.3038	2.3243	.0753
3	.2727	2.3208	.0838
4	.2415	2.3175	.0981
5	.2104	2.3142	.1040
6	.1792	2.3109	.1161
7	.1481	2.3075	.1227
8	.1170	2.3041	.1303
9	.0858	2.3008	.1372
10	.0547	2.2974	.1484
11	.0235	2.2941	.1510
12	-.0076	2.2907	.1612
13	-.0387	2.2874	.1638

STATION NO. 6

STREAMLINE	X	R	T
1	.3694	2.2490	.0662
2	.3344	2.2446	.0731
3	.2993	2.2402	.0919
4	.2643	2.2358	.0999
5	.2293	2.2314	.1150
6	.1943	2.2269	.1228
7	.1592	2.2226	.1387
8	.1242	2.2182	.1471
9	.0892	2.2137	.1583
10	.0541	2.2093	.1737
11	.0191	2.2049	.1780
12	-.0159	2.2005	.1904
13	-.0509	2.1961	.1936

STATION NO. 7

STREAMLINE	X	R	T
1	.4124	2.1738	.0642
2	.3726	2.1681	.0780
3	.3329	2.1624	.0871
4	.2932	2.1566	.1076
5	.2534	2.1509	.1179
6	.2137	2.1451	.1360
7	.1739	2.1394	.1568
8	.1342	2.1337	.1632
9	.0945	2.1279	.1827
10	.0547	2.1222	.2015
11	.0150	2.1164	.2049
12	-.0247	2.1107	.2221
13	-.0645	2.1050	.2337

STATION NO. 8

STREAMLINE	X	R	T
1	.4641	2.1030	.0645
2	.4187	2.0956	.0766
3	.3734	2.0881	.0918
4	.3280	2.0808	.1029
5	.2827	2.0734	.1265
6	.2373	2.0660	.1470
7	.1920	2.0587	.1653
8	.1466	2.0512	.1829
9	.1013	2.0438	.2074
10	.0559	2.0364	.2298
11	.0106	2.0290	.2372
12	-.0348	2.0216	.2590
13	-.0801	2.0142	.2785

STATION NO. 9

STREAMLINE	X	R	T
1	.5232	2.0374	.0611
2	.4712	2.0280	.0743
3	.4193	2.0186	.0856
4	.3674	2.0092	.1088
5	.3154	1.9998	.1292
6	.2635	1.9903	.1489
7	.2115	1.9809	.1730
8	.1596	1.9715	.2023
9	.1076	1.9621	.2311
10	.0556	1.9526	.2587
11	.0037	1.9433	.2697
12	-.0482	1.9338	.2966
13	-.1002	1.9245	.3179

STATION NO. 10

STREAMLINE	X	R	T
1	.5891	1.9779	.0563
2	.5295	1.9661	.0648
3	.4699	1.9543	.0820
4	.4103	1.9425	.1017
5	.3507	1.9307	.1279
6	.2910	1.9188	.1558
7	.2314	1.9070	.1854
8	.1718	1.8952	.2156
9	.1122	1.8835	.2547
10	.0526	1.8717	.2889
11	-.0070	1.8598	.3184
12	-.0667	1.8480	.3388
13	-.1263	1.8362	.3564

STATION NO. 11

STREAMLINE	X	R	T
1	.6600	1.9250	.0542
2	.5891	1.9085	.0624
3	.5182	1.8920	.0756
4	.4473	1.8754	.1099
5	.3764	1.8588	.1390
6	.3055	1.8423	.1699
7	.2346	1.8258	.2055
8	.1637	1.8093	.2465
9	.0928	1.7928	.2857
10	.0219	1.7762	.3258
11	-.0490	1.7596	.3662
12	-.1054	1.7593	.3874
13	-.1600	1.7500	.4088

STATION NO. 12

STREAMLINE	X	R	T
1	.7706	1.8595	.0512
2	.7008	1.8403	.0591
3	.6310	1.8212	.0674
4	.5612	1.8021	.0786
5	.4914	1.7830	.1019
6	.4216	1.7639	.1429
7	.3518	1.7448	.1694
8	.2820	1.7257	.2057
9	.2122	1.7066	.2424
10	.1424	1.6874	.2815
11	.0726	1.6683	.3297

STATION NO. 13

STREAMLINE	X	R	T
1	.8855	1.8157	.0497
2	.8163	1.7884	.0555
3	.7470	1.7611	.0609
4	.6778	1.7338	.0699
5	.6085	1.7064	.0866
6	.5392	1.6790	.1092
7	.4700	1.6517	.1414
8	.4007	1.6244	.1735
9	.3315	1.5970	.2132
10	.2622	1.5697	.2513
11	.1929	1.5424	.2914

STATION NO. 14

STREAMLINE	X	R	T
1	.9984	1.7868	.0516
2	.9317	1.7493	.0573
3	.8650	1.7117	.0612
4	.7983	1.6741	.0681
5	.7317	1.6365	.0741
6	.6650	1.5989	.0955
7	.5983	1.5614	.1160
8	.5316	1.5237	.1533
9	.4649	1.4861	.1840
10	.3982	1.4486	.2251
11	.3315	1.4110	.2598

STATION NO. 15

STREAMLINE	X	R	T
1	1.1048	1.7666	.0547
2	1.0433	1.7182	.0578
3	.9818	1.6698	.0660
4	.9203	1.6214	.0702
5	.8588	1.5730	.0753
6	.7973	1.5379	.1043
7	.7358	1.4761	.1039
8	.6743	1.4278	.1323
9	.6127	1.3793	.1608
10	.5512	1.3310	.1957
11	.4897	1.2825	.2347

STATION NO. 16

STREAMLINE	X	R	T
1	1.2038	1.7559	.0558
2	1.1504	1.6972	.0624
3	1.0970	1.6385	.0690
4	1.0436	1.5799	.0764
5	.9902	1.5212	.0849
6	.9368	1.4625	.0962
7	.8834	1.4038	.1080
8	.8300	1.3451	.1376
9	.7766	1.2865	.1540
10	.7232	1.2277	.1818
11	.6698	1.1691	.2274

STATION NO. 17

STREAMLINE	X	R	T
1	1.2948	1.7531	.0566
2	1.2518	1.6851	.0650
3	1.2088	1.6172	.0744
4	1.1658	1.5492	.0805
5	1.1228	1.4812	.0912
6	1.0798	1.4133	.1055
7	1.0368	1.3454	.1291
8	.9938	1.2775	.1475
9	.9508	1.2095	.1731
10	.9078	1.1416	.1559
11	.8648	1.0736	.2373

STATION NO. 18

STREAMLINE	X	R	T
1	1.3782	1.7529	.0573
2	1.3470	1.6779	.0691
3	1.3159	1.6028	.0803
4	1.2847	1.5278	.0924
5	1.2536	1.4527	.1023
6	1.2224	1.3776	.1187
7	1.1912	1.3026	.1340
8	1.1601	1.2275	.1611
9	1.1289	1.1525	.1908
10	1.0978	1.0774	.2240
11	1.0666	1.0023	.2577

STATION NO. 19

STREAMLINE	X	R	T
1	1.4558	1.7530	.0576
2	1.4310	1.6747	.0705
3	1.4085	1.5964	.0817
4	1.3868	1.5183	.0946
5	1.3657	1.4400	.1095
6	1.3454	1.3620	.1257
7	1.3259	1.2841	.1484
8	1.3085	1.2065	.1755
9	1.2908	1.1281	.2052
10	1.2769	1.0484	.2367
11	1.2682	.9582	.2605

STATION NO. 20

STREAMLINE	X	R	T
1	1.5289	1.7530	.0583
2	1.5136	1.6716	.0716
3	1.5000	1.5901	.0813
4	1.4877	1.5086	.0946
5	1.4766	1.4274	.1126
6	1.4666	1.3461	.1360
7	1.4592	1.2655	.1607
8	1.4539	1.1850	.1877
9	1.4542	1.1055	.2170
10	1.4515	1.0225	.2479
11	1.4579	.9331	.2655

STATION NO. 21

STREAMLINE	X	R	T
1	1.5989	1.7530	.0580
2	1.5936	1.6683	.0724
3	1.5897	1.5837	.0825
4	1.5870	1.4992	.0960
5	1.5852	1.4146	.1153
6	1.5857	1.3304	.1385
7	1.5884	1.2461	.1629
8	1.5967	1.1634	.1873
9	1.6101	1.0817	.2140
10	1.6347	1.0035	.2410
11	1.6369	.9220	.2600

STATION NO. 22

STREAMLINE	X	R	T
1	1.6670	1.7530	.0587
2	1.6722	1.6652	.0718
3	1.6778	1.5773	.0825
4	1.6843	1.4896	.0959
5	1.6922	1.4020	.1157
6	1.7009	1.3141	.1394
7	1.7138	1.2271	.1692
8	1.7317	1.1396	.1923
9	1.7595	1.0556	.2156
10	1.8030	.9798	.2322
11	1.8670	.9200	.2517

This Page Intentionally Left Blank

REFERENCES

1. Stanitz, J. D., "Some Theoretical Aerodynamic Investigations of Impellers in Radial and Mixed Flow Centrifugal Compressors," Trans. ASME Vol. 74, No. 4, May 1952.

2. Dovzhik, S. A. and V. M. Kartavenko, "Measurement of the Effect of Flow Swirl on the Efficiency of Annular Ducts and Exhaust Nozzles of Axial Turbomachines," Fluid Mechanics Soviet Research. Vol. 4, No. 4, July-August 1975.

3. Mitchell, W. S. and J. F. Soileau, "Turbine Exit Guide Vane Program," AFAPL-TR-77-75, November 1977.

4. Rogo, C., "Development of a High Tip Speed Radial Turbine System for a Small Turboalternator," SAE Paper 710552, Presented at SAE Mid-Year Meeting, Montreal, Quebec, Canada, June 1971.

5. Eckert, B., "Axial Kompressoren and Radial Kompressoren," Berlin/Bottingen/Heidelberg: Springer-Yerlag, 1953.

6. Kofskey, M. G. and W. M. Nusbaum, "Effects of Specific Speed on Experimental Performance of a Radial-Inflow Turbine," NASA TN D-6605, February 1972.

7. Nusbaum, W. J. and C. A. Wassenhauer, "Experimental Performance Evaluation of a 4.59-Inch Radial Inflow Turbine Over a Range of Reynolds Numbers," NASA TN D-3835, February 1967.

8. Penny, N., "Rover Case History of Small Gas Turbines," SAE Paper No. 634A, January 1, 1963.

9. Futral, Jr., W. M. and D. E. Holeski, "Experimental Results of Varying the Blade-Shroud Clearance in a 6.02-Inch Radial-Inflow Turbine," NASA TN D-5513, 1970.

10. Kidwell, J. R. and G. D. Large, "Advanced Technology Components for Model GTP305-2 Aircraft Auxiliary Power System," AFAPL-TR-2106, February 1980.

11. Calvert, G. S. and U. Opapuu, "Design and Evaluation of a High-Temperature Radial Turbine," USAAVLABS Technical Report 68-69, Phase I - Final Report, January 1969.

12. Daily, J. W. and R. E. Nece, "Chamber Dimensions Effects on Induced Flow and Frictional Resistance of Enclosed Rotating Disks," Journal of Basic Engineering, Vol. 82, No. 1, March 1960, pp. 217-232.

This Page Intentionally Left Blank

26. Weibull, W. A., "Statistical Distribution Function of Wide Applicability," Journal of Applied Mechanics, 18[3], 1951, pp. 293-297.

27. Evans, A. G., "A General Approach for the Statistical Analysis of Multiaxial Fracture," Journal of The American Ceramic Society, Vol. 61, No. 7-8, July-August 1978.

This Page Intentionally Left Blank

DISTRIBUTION LIST

NASA-Lewis
21000 Brookpark Road
Cleveland, OH 44135

Kerry L. McLallin, MS 77-2
Project Manager (10 copies)

George Virosteck, MS 501-11
Contracting Officer

Norman T. Musial, MS 500-318
Patent Counsel

Library, MS 60-3
(2 copies)

Robert Y. Wong, MS 77-2

Report Control Office, MS 5-5

Harold E. Rohlik, MS 77-2

Richard A. Rudey, MS 86-5

Morton H. Krasner, MS 500-210

Melvin J. Hartmann, MS 3-7

William E. Goette, MS 500-210

David G. Evans, MS 500-210

Harry W. Davison, MS 500-210

Stanley M. Nosek, MS 501-11

Paul T. Kerwin, MS 500-210

Roger S. Palmer, MS 500-210

James N. Deyo, MS 500-210

William E. B. Mason, MS 500-211

Harold H. Valentine, MS 500-125

Charles Wagner
CIMS 418-37-18
Chrysler Corporation
P.O. Box 1118
Detroit, MI 48288

E. E. Bailey
AF APL/DO
Wright Patterson Air Force Base, OH 45433

NASA Scientific and Technical Information Facility
Attn: Accessioning Department
P.O. Box 8757
Baltimore/Washington International Airport 21240
(50 copies)

NASA Headquarters
Attn: REC-1/J. F. Slomski
Washington, DC 20546

Jet Propulsion Lab.
4800 Oak Grove Drive
Pasadena, CA 91103
Attn: R. C. Heft

Robert B. Schulz
U. S. Department of Energy
MS 5H-039
20 Massachusetts Avenue
Washington, DC 20585
(6 copies)

USDOE TIC
Attn: T. Laughlin
Building 1916-T-1
Oak Ridge Turnpike at Athens Road
Oak Ridge, TN 37830
(154 copies for distribution under DOE Category UC-96)

H. E. Helms T-15
General Motors Corporation
Detroit Diesel Allison Division
P.O. Box 894
Indianapolis, IN 46206

Edwin E. Strain
Garrett Turbine Engine Company
Division of Garrett Corporation
P.O. Box 5217
Phoenix, AZ 85010

William I. Chapman
Williams Research Corporation
2280 West Maple Road
Walled Lake, MI 48088

1 Report No DOE/NASA/0106-1 NASA CR-165170	2 Government Accession No	3 Recipient's Catalog No
4 Title and Subtitle ANALYTICAL DESIGN OF AN ADVANCED RADIAL TURBINE		5 Report Date February 1981 6 Performing Organization Code
7 Author(s) G. D. Large, D. G. Finger, C. G. Linder		8 Performing Organization Report No 31-3653 10 Work Unit No
9 Performing Organization Name and Address Garrett Turbine Engine Company A Division of The Garrett Corporation 111 S. 34th Street Phoenix, Arizona 85034		11 Contract or Grant No DEN3-106 13 Type of Report and Period Covered Contractor Report - 2-1-79 to 8-1-80
12 Sponsoring Agency Name and Address U.S. Department of Energy Office of Transportation Programs Washington, DC 20545		14 Sponsoring Agency Code DOE/NASA/0106-1

15 Supplementary Notes

Project Manager, Kerry McLallin
NASA-Lewis Research Center
Cleveland, OH 44135

Final Report prepared under
Interagency Agreement
No. DEAI 01-77CS51040

16 Abstract

The aerodynamic and mechanical potential of a single-stage ceramic radial inflow turbine was evaluated for a high-temperature single-stage automotive engine. The aerodynamic analysis utilized a turbine system optimization technique to evaluate both radial and non-radial rotor blading. Selected turbine rotor configurations were evaluated mechanically with 3-D finite element techniques. The analysis showed that exceptionally high rotor tip speeds (2300 ft/sec) and performance potential are feasible with radial-bladed rotors if the projected ceramic material properties are realized. Non-radial rotors reduced tip speed requirements (at constant turbine efficiency) but resulted in a lower cumulative probability of success due to higher blade and disk stresses.

17 Key Words (Suggested by Author(s))	18 Distribution Statement
Advanced Radial Turbine Ceramic Engine Automotive Gas Turbine	Unclassified - Unlimited STAR Category - 85 DOE Category - UC-96

19 Security Classif (of this report)	20 Security Classif (of this page)	21 No of Pages	22 Price*
Unclassified	Unclassified		

* For sale by the National Technical Information Service, Springfield, Virginia 22161

End of Document